UCLA
UCLA Electronic Theses and Dissertations

Title
Nucleoside Salvage Kinases Regulate Hematopoiesis by Linking Nucleotide Metabolism with DNA Replication Stress

Permalink
https://escholarship.org/uc/item/5rx091t7

Author
Austin, Wayne Robert

Publication Date
2012

Peer reviewed|Thesis/dissertation

eScholarship.org Powered by the California Digital Library
University of California

UNIVERSITY OF CALIFORNIA

Los Angeles

Nucleoside Salvage Kinases Regulate Hematopoiesis by Linking Nucleotide Metabolism with DNA Replication Stress

A dissertation submitted in partial satisfaction of the requirements for the degree

Doctor of Philosophy in Molecular and Medical Pharmacology

by

Wayne Robert Austin

2012

© Copyright by

Wayne Robert Austin

2012

ABSTRACT OF THE DISSERTATION

Nucleoside Salvage Kinases Regulate Hematopoiesis by Linking Nucleotide Metabolism with DNA Replication Stress

by

Wayne Robert Austin

Doctor of Philosophy in Molecular and Medical Pharmacology

University of California, Los Angeles, 2012

Professor Caius G. Radu, Co-Chair

Professor Johannes Czernin, Co-Chair

Deoxycytidine kinase (dCK) is a rate-limiting enzyme in the salvage pathway of deoxribonucleotide triphosphate (dNTP) biosynthesis. dCK is highly expressed in hematopoietic tissues such as the bone marrow and thymus, indicating that the enzyme is important for the generation of a normal hematopoietic system. However, it has never been determined as to why dCK is highly expressed in these proliferating cell types versus others in the body. To begin answering this fundamental biological question, we generated mice that were globally deficient for dCK activity (*dCK*$^{-/-}$) using genetic knockout technology. We found that inactivation of dCK activity results in severely inhibited differentiation of major hematopoietic lineages consisting of T cells, B cells,

and erythroid cells. Examination of the cell cycle kinetics in *dCK*$^{-/-}$ cells from these distinct lineages revealed that these cells undergo cell cycle arrest early during the process of DNA replication *in vivo*. This arrest is associated with the presence of active DNA damage response, thus indicating that hematopoietic progenitor cells are subject to significant DNA replication stress *in vivo*. We found that induction of DNA replication stress in *dCK*$^{-/-}$ hematopoietic progenitors was dependent upon the salvage of thymidine by the nucleoside salvage enzyme thymidine kinase 1 (TK1). We subsequently demonstrated that simultaneous inactivation of both dCK and TK1 in mice greatly ameliorated the proliferation and differentiation defects that were present in hematopoietic progenitor cells from *dCK*$^{-/-}$ mice. The results from our studies thus demonstrate that dCK functions to counteract the DNA replication stress-inducing activity of TK1 that occurs during *in vivo* proliferation of murine hematopoietic progenitors.

The dissertation of Wayne Robert Austin is approved.

Steven J. Bensinger

Harvey R. Herschman

Michael A. Teitell

Johannes Czernin, Committee Co-Chair

Caius G. Radu, Committee Co-Chair

University of California, Los Angeles

2012

DEDICATION

I would like to dedicate this dissertation to my parents, Dr. Shirley Suiling Chan, and Dr. Robert Hamilton Austin, for all the love and support they have given me throughout the years. Mom and Dad, your hard work, perseverance, and scholastic achievement have inspired me at every stage of my scientific training. Thank you always for raising me to be the man that I am today.

TABLE OF CONTENTS

Abstract of the Dissertation		ii
Committee Page		iv
Dedication Page		v
List of Figures		viii
Acknowledgements		x
Vita		xi
Chapter 1	Introduction: The Biochemical Role of Deoxycytidine Kinase in Deoxyribonucleotide Metabolism	1
	References	12
Chapter 2	Requirement for Deoxycytidine Kinase for Normal Hematopoietic Development	15
	Abstract	16
	Introduction	17
	Materials and Methods	20
	Results	24
	Discussion	30
	References	42
Chapter 3	Deletion of Deoxycytidine Kinase Causes dCTP Pool Deficiency, DNA Replication Stress, and Cell Cycle Arrest in Murine Hematopoietic Progenitors	46
	Abstract	47
	Introduction	48
	Materials and Methods	50
	Results	53
	Discussion	64
	References	75

Chapter 4	Deoxycytidine Kinase Counteracts DNA Replication Stress Induced by Thymidine Kinase 1 Activity *In Vivo*	79
	Abstract	80
	Introduction	81
	Materials and Methods	84
	Results	86
	Discussion	99
	References	118
Chapter 5	Conclusions	123
	References	127

LIST OF FIGURES AND TABLES

Chapter 1

Figure 1.1	*De novo* and salvage synthesis of pyrimidine dNTPs	8
Figure 1.2	dCK regulates a rate-limiting step in the nucleoside salvage pathway	10
Figure 1.3	General structure and allosteric control of the ribonucleotide reductase (RNR) complex	11

Chapter 2

Figure 2.1	Targeting vector strategy to genetically eliminate dCK activity	34
Figure 2.2	Validation of complete inactivation of dCK activity	36
Figure 2.3	Defective T cell development in the *dCK*$^{-/-}$ mice	37
Figure 2.4	Defective B cell development in the *dCK*$^{-/-}$ mice	39
Figure 2.5	*dCK*$^{-/-}$ mice display abnormal erythroid population distributions in the bone marrow and spleen	40

Chapter 3

Figure 3.1	*dCK*$^{-/-}$ hematopoietic defects are transplantable into WT mice	65
Figure 3.2	*dCK*$^{-/-}$ hematopoietic defects are rescued by bone marrow transplantation with WT cells	66
Figure 3.3	Expression of a transgenic TCR fails to rescue *dCK*$^{-/-}$ thymocyte development	67
Figure 3.4	dCTP pool deficiency in *dCK*$^{-/-}$ lymphoid and erythroid progenitor populations	68
Figure 3.5	Abnormal S-phase profiles in *dCK*$^{-/-}$ hematopoietic progenitors	69
Figure 3.6	*dCK*$^{-/-}$ hematopoietic progenitors are arrested in early S-phase *in vivo*	71

Figure 3.7 *dCK*$^{-/-}$ hematopoietic progenitors undergo replication stress responses *in vivo* 72

Figure 3.8 Conditional deletion of dCK in adult mice recapitulates the cell cycle defects and RSR pathway activation phenotypes characteristic of germline *dCK*$^{-/-}$ mice 73

Chapter 4

Figure 4.1 High thymidine concentrations in hematopoietic and lymphopoietic tissues in mice 104

Figure 4.2 *In vitro* thymidine salvage selectively blocks the proliferation of *dCK*$^{-/-}$ thymocytes 105

Figure 4.3 *In vitro* thymidine salvage selectively induces RS and cell death in *dCK*$^{-/-}$ thymocytes 107

Figure 4.4 Lymphoid and erythroid development in *TK1*$^{-/-}$ mice 108

Figure 4.5 *TK1*$^{-/-}$ hematopoietic progenitors from the bone marrow have dTTP pool depletions 109

Figure 4.6 *TK1*$^{-/-}$ hematopoietic progenitors undergo replication stress *in vivo* 110

Figure 4.7 Gross sizes and pyrimidine dNTP pools from dCK/TK1 double-knockout (DKO) mice 111

Figure 4.8 TK1 inactivation largely rescues thymic T cell development in *dCK*$^{-/-}$ mice 112

Figure 4.9 DKO thymocytes are resistant to thymidine-induced proliferation block *in vitro* 113

Figure 4.10 TK1 deletion largely recues bone marrow B cell development in *dCK*$^{-/-}$ mice 114

Figure 4.11 TK1 inactivation relieves the early S-phase arrest observed in erythroid precursors from *dCK*$^{-/-}$ mice 115

Figure 4.12 Deoxyribonucleoside salvage kinases induce and resolve replication stress (RS) during hematopoiesis 116

ACKNOWLEDGEMENTS

I would first like to thank Dr. Caius Radu and Dr. Johannes Czernin for their continued support throughout my graduate career. Thank you for entrusting the dCK knockout project to me and guiding me through this complex journey. I will always be grateful for the opportunity that you two gave me.

I would like to thank the members of my doctoral committee: Dr. Harvey Herschman, Dr. Michael Teitell, and Dr. Steven Bensinger, for their valuable insight and advice regarding the dCK knockout project.

I would like to thank all the members of the Radu/Czernin laboratory for their incredible assistance over the years. I am especially indebted to the efforts of Dr. Dean Campbell, Amanda Armijo, Dr. Arun Singh, Dr. David Nathanson, Gerald Toy, and Terry Hsieh, for their help in generating and analyzing *dCK*$^{-/-}$, *TK1*$^{-/-}$, and DKO mice. Without all of your dedicated efforts, none of the data presented in this dissertation would have been possible to generate.

I would like to thank Dr. Liu Wei, Larry Pang, Dr. Jason Lee, and the staff of the Crump Institute of Molecular Imaging for their help in executing the mPET/CT imaging studies.

I would like to thank Dr. Hearn Cho, Dr. Donghui Cheng, Felicia Codrea, and Jessica Scholes, for their help in teaching me the principles of flow cytometry. This powerful analytical technique has had a profound impact upon my doctoral training and I consider myself lucky to have learned it from you all.

Chapter 2 is a version of Toy, G., Austin, W.R., Liao, H.I., Cheng, D., Singh, A., Campbell, D.O., Ishikawa, T.O., Lehmann, L.W., Satyamurthy, N., Phelps, M.E., Herschman, H.R., Czernin, J., Witte, O.N., and Radu, C.G. (2010). Requirement for deoxycytidine kinase in T and B lymphocyte development. *Proceedings of the National Academy of Sciences of the United States of America,* **107**(12): 5551-5556.

Chapters 3 and 4 are versions of Austin, W.R., Armijo, A.L., Campbell, D.O., Singh, A.S., Hsieh, T., Nathanson, D., Herschman, H.R., Phelps, M.E., Witte, O.N., Czernin, J., and Radu, C.G. (2012). Nucleoside salvage pathway kinases regulate hematopoiesis by linking nucleotide metabolism with replication stress. Submitted to the *Journal of Experimental Medicine* for review on May 18, 2012.

Finally, I would like to acknowledge the funding from a career development award though the *In vivo* Cellular and Molecular Imaging Center (ICMIC) grant at UCLA (NIH/NCI P50 CA86306 to H.R. Herschman).

VITA

2005	B.A., Molecular Biology Princeton University Princeton, New Jersey
2005-06	Laboratory Research Assistant Weill Cornell Medical College New York, New York
2006-07	Laboratory Research Assistant NYU Cancer Institute New York, New York
2009	Teaching Assistant Department of Microbiology, Immunology, and Molecular Genetics University of California, Los Angeles
2010	Teaching Assistant Department of Microbiology, Immunology, and Molecular Genetics University of California, Los Angeles
2011	Spring Travel Grant Awardee Department of Molecular and Medical Pharmacology University of California, Los Angeles
2011-2012	*In vivo* Cellular and Molecular Imaging Center (ICMIC) Career Development Training Grant Awardee University of California, Los Angeles

PUBLICATIONS AND PRESENTATIONS

Lendvai N, Gnjatic S, Ritter E, Mangone M, **Austin W**, Reyner K, Jayabalan D, Niesvizky R, Jagannath S, Bhardwaj N, Chen-Kiang S, Old LJ, Cho HJ. (2010). Cellular immune responses against CT7 (MAGE-C1) and humoral responses against other cancer-testis antigens in multiple myeloma patients. *Cancer Immunity,* **10**:4.

Toy, G.*, **Austin, W.R.***, Liao, H.I., Cheng, D., Singh, A., Campbell, D.O., Ishikawa, T.O., Lehmann, L.W., Satyamurthy, N., Phelps, M.E., Herschman, H.R., Czernin, J., Witte, O.N., and Radu, C.G. (2010). Requirement for deoxycytidine kinase in T and B lymphocyte development. *Proceedings of the National Academy of Sciences of the United States of America,* **107**(12): 5551-5556. (*denotes equal contribution)

Austin, W.R., Toy, G., Liao, H.I., Armijo, A., Singh, A., Campbell, D.O., Czernin, J., and Radu, C.G. Requirement for deoxycytidine kinase in thymocyte development. Poster presentation. Keystone Symposia: Lymphocyte Activation and Gene Expression. Breckinridge, Colorado. March, 2010.

Austin, W.R., Campbell, D.O., Armijo, A., Singh, A., Liao, H.I., Czernin, J., and Radu, C.G. Deoxyribonucleoside recycling is required to maintain genomic integrity during lymphopoiesis and erythropoiesis. Poster presentation. Keystone Symposia: Hematopoiesis. Big Sky, Montana. March, 2011.

CHAPTER 1:

Introduction

The Biochemical Role of Deoxycytidine Kinase

in Deoxyribonucleotide Metabolism

Nucleotides for DNA synthesis are generated by two interrelated pathways

It is a fundamental fact of biology that a cell must generate a balanced supply of DNA precursors in order to support DNA replication and minimize the errors associated with this process (1). However, underneath this seemingly trivial statement lies a complex biosynthetic network that must produce and maintain the fundamental building blocks of the genome. Nucleotide biosynthesis is traditionally thought of as consisting of two pathways: the *de novo* pathway that generates nucleotides from essential precursors such as glucose and amino acids; and the salvage pathway that recycles previously formed nucleosides (2) (Figure 1.1). Often, the *de novo* and salvage pathways are studied individually. This may be problematic, since it is inaccurate to think of these two pathways as being independent from one another; they are inextricably linked via shared intermediates and products, and the activity of one pathway can drastically influence the other (2).

Deoxycytidine kinase, a multi-substrate salvage enzyme

The focus of this dissertation is to understand the role that the deoxyribonucleoside (dN) salvage enzyme deoxycytidine kinase (dCK) plays in the overall regulation of DNA replication in hematopoietic cells. dCK is highly expressed in hematopoietic tissues and it functions biochemically to help generate deoxyribonucleotide triphosphates (dNTPs), the direct precursors of DNA synthesis (3). The dCK enzyme has wide substrate capacity that naturally includes deoxycytidine (dC), deoxyadenosine (dA), and deoxyguanosine (dG) (2). However, dCK can also phosphorylate many synthetic nucleoside analog prodrugs (4). The clinical utilization of

dCK to activate various antineoplastic drugs makes understanding dCK's fundamental biological role a clinically important goal; a better understanding of this enzyme can lead to improved or novel therapeutic strategies in the future.

The various dNs and related prodrugs that dCK phosphorylates enter a cell through facilitated transport mediated by equilibrative and concentrative nucleoside transporters (ENTs, CNTs) (Figure 1.2) (5, 6). dNs can freely efflux out of the cell until dCK's enzymatic activity covalently adds an electronegative phosphate group to the 5'-OH position of the deoxyribose sugar ring, thus converting the dNs into monophosphate nucleotides (dNMPs) (4). The electronegative phosphate group prevents the dNMPs from exiting the cytoplasm via the ENTs, causing them to be trapped intracellularly (5). These dNMPs are then quickly phosphorylated twice more by cytoplasmic nucleotide kinases to become dNTPs (2). Through these mechanisms dCK can directly contribute to intracellular deoxycytidine-, deoxyadenosine-, and deoxyguanosine- triphosphate (dCTP, dATP, and dGTP, respectively) pools. dCK can also indirectly contribute to thymidine triphosphate (dTTP) pools by way of the conversion of its product deoxycytidine monophosphate (dCMP) into deoxyuridine monophosphate (dUMP) by dCMP deaminase (DCTD) (7). The enzyme thymidylate synthase (TYMS) can then convert dUMP into thymidine monophosphate (dTMP) for use in generating dTTP (8).

Ribonucleotide reductase regulates the de novo synthesis pathway

The *de novo* pathway can also generate dCTP (2). *De novo* synthesis of pyrimidine dNTPs starts with glucose and amino acid metabolism to generate the central pyrimidine precursor uridine monophosphate (UMP) (9). UMP can then be

phosphorylated by uridine-cytidine kinase 2 (UCK2) to generate the product uridine diphosphate (UDP) (10). UDP is a substrate for the rate-limiting *de novo* pathway enzyme complex called ribonucleotide reductase (RNR) (Figure 1.1) (2).

RNR is a multi-component complex comprised of a regulatory subunit and an enzymatic subunit. The regulatory subunit is called ribonucleotide reductase M1 (RRM1); it is expressed throughout the cell cycle (11). The enzymatic subunit is called ribonucleotide reductase M2 (RRM2); its transcription and translation are activated upon entry into S-phase of the cell cycle (11). Following completion of S-phase RRM2 is rapidly eliminated through ubiquitination-mediated proteosomal degradation (12). An alternative M2 subunit of RNR is the p53-inducible ribonucleotide reductase M2 B gene (RRM2B), whose transcription is not cell cycle dependent but instead is induced by p53 activation in response to DNA damage (13). RRM1 pairs with either RRM2 or RRM2B to form a complete RNR complex that is capable of reducing ribonucleoside diphosphates (NDPs) into deoxyribonucleotide diphosphates (dNDPs) (Figure 1.3, A) (14).

The enzymatic activity of RNR is allosterically controlled by the concentrations of the triphosphate products of nucleotide synthesis (2) (Figure 1.3, B). RRM1 contains an activity regulation site that binds either adenosine triphosphate (ATP) or deoxyadenosine triphosphate (dATP), depending on relative concentrations of either nucleotide in the cell (14). The binding of ATP to RRM1's activity regulation site activates the enzyme to reduce NDPs into dNDPs; conversely, the binding of dATP to the activity regulation site turns off RNR's enzymatic activity (14). The generation of

dATP through RNR is therefore a negative feedback mechanism to control the overall generation of dNTPs through the *de novo* pathway (11).

RNR has the ability to reduce four separate NDPs into dNDPs, thereby allowing it to generate the precursors for all four dNTPs (2). However, RNR cannot reduce all four nucleotides simultaneously; its specific nucleotide substrate is dictated by other nucleotides that occupy a substrate specificity regulation site located on RRM1 (11). For example, the binding of ATP or dATP to RRM1's substrate specificity site promotes the binding of either cytidine diphosphate (CDP) or UDP to the M2 subunit's enzymatic activity site. In another case, the binding of deoxyguanosine triphosphate (dGTP) to the specificity site promotes the binding of adenosine diphosphate (ADP) to the enzymatic activity site. Lastly, the binding of dTTP to the specificity site promotes the binding of guanosine diphosphate (GDP) to the enzymatic activity site. Intriguingly, dCTP is the only dNTP that does not regulate RNR's overall enzymatic activity (15).

Regulation of dCTP pool size through various mechanisms

Of the four dNTPs produced by the *de novo* pathway, dCTP appears to be the most susceptible to pool depletions due to allosteric regulation of RNR's substrate specificity. The generation of dCTP by *de novo* synthesis requires that 1) ATP binds the *activity regulatory site*, and that 2) ATP or dATP binds the *substrate specificity site*. In such conditions of high available energy (i.e. sufficient ATP concentration), and relatively high purine nucleotide availability (dATP bound to the specificity site), RNR will preferentially generate dCTP over other possible products. However, dCTP generation via *de novo* synthesis can be shut down through the action of dTTP binding

to RNR's specificity site (16). This mechanism is commonly employed in the laboratory to synchronize immortalized cell lines at the G_1/S border in a method called a thymidine block (17).

The thymidine block method to synchronize cells depends upon the activity of another dN salvage enzyme: thymidine kinase 1 (TK1) (18). TK1's substrate specificity is distinct from that of dCK's; TK1 can only phosphorylate the pyrimidine dNs of thymidine (dT) and deoxyuridine (dU) (Figure 1.2) (3). Like RRM2, TK1 gene expression is subject to S-phase activation (19). TK1's salvage of both dT and dU converts these dNs into dTMP and dUMP, respectively. dTMP can be phosphorylated twice more to generate dTTP directly, while dUMP requires conversion into dTMP by the action of TYMS in order to feed into dTTP pools (Figure 1.2) (2).

Regulation of dCK activity through various mechanisms

dCK is both transcribed and translated during the non-DNA replicating phases of the cell cycle (i.e. G_0/G_1, G_2 and M phases), making it unlike several key components of the dNTP biosynthetic pathway, such as RRM2, TK1, and TYMS (19-23). The fact that dCK is expressed and active at times when dNTPs are not required to support DNA synthesis has led to the speculation that dCK plays a role in supplying dNTPs to enable DNA repair (24, 25). Recently, dCK was identified as a potential phosphorylation target for the key DNA damage response (DDR) sensor kinases of ataxia-telangiectasia mutated (ATM) and ataxia-telangiectasia mutated Rad3-related (ATR) (26). In that phosphoproteomic study, Stephen Elledge's group identified dCK's serine 74 (Ser74) as residing in a conserved amino acid sequence motif that is the recognition target for the

ATM/ATR kinases. This Ser74 residue is particularly significant in the post-translational control of dCK activity. It is believed that phosphorylation of the Ser74 residue increases dCK's enzymatic activity by locking the enzyme in an open confirmation that more readily accepts dC substrate and the ATP/UTP phosphate donor molecules (4, 27, 28). Because this Ser74 occupies a conserved ATM/ATR kinase target motif, it has been postulated that dCK activity may increase via ATM/ATR activation in response to DNA damage (26).

Concluding remarks about dCK's role in development

Although dCK expression and activity has been studied for decades, it has never been determined what function, if any, that dCK has in supporting normal development. Neither has it been shown if dCK functionally contributes to dNTP pools *in vivo*. To address these questions, we generated mice globally and conditionally deficient for dCK activity (*dCK*$^{-/-}$ mice). Chapter 2 will describe the profound defects in hematopoietic development we observed in *dCK*$^{-/-}$ mice. In Chapter 3, we will document the cell cycle defects and the presence of active DNA damage responses in *dCK*$^{-/-}$ hematopoietic progenitors. Chapter 4 will describe the underlying mechanisms that we believe cause the cell cycle and differentiation defects present in *dCK*$^{-/-}$ mice. Lastly, Chapter 5 will include a discussion of the potential clinical applicability of the fundamental biological insights revealed by studying the *dCK*$^{-/-}$ mouse model.

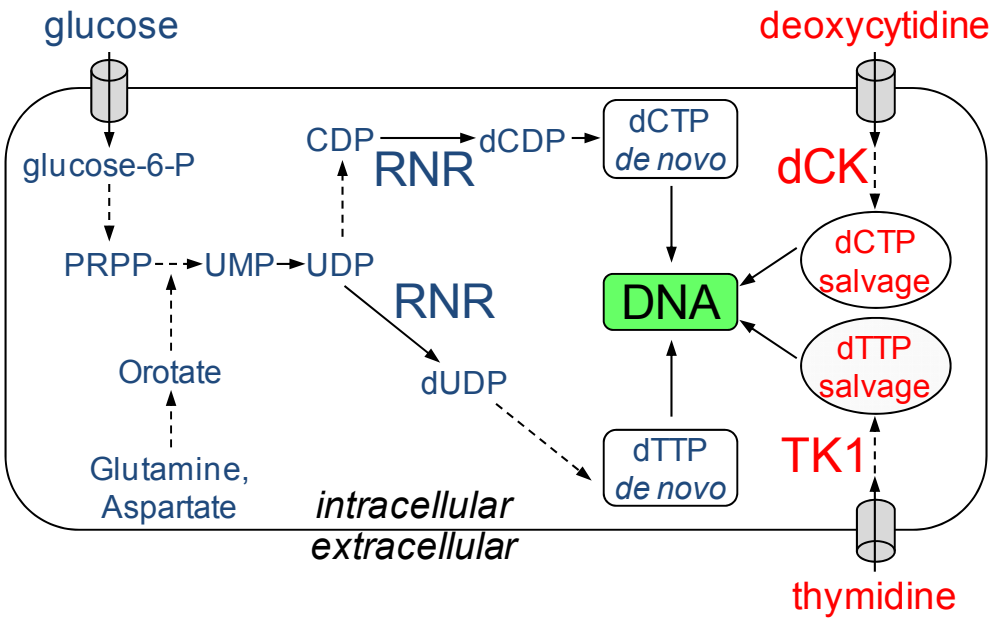


Figure 1.1. ***De novo* and salvage synthesis of pyrimidine dNTPs.** Schematic of *de novo* (blue) and salvage pyrimidine nucleotide (red) synthesis inputs into pyrimidine dNTP pools for DNA synthesis. Solid arrows indicate single step processes; dashed arrows indicate multi-step processes with intermediates not named/depicted in the schematic. Glucose is transported and phosphorylated into glucose-6-phosphate (glucose-6-P), which can be converted into 5-phosphoribosyl-1-pyrophosphate (PRPP). Glutamine and aspartate contribute to the formation of the pyrimidine base orotate, which is reacted with PRPP to later form uridine monophosphate (UMP). UMP is phosphorylated once more to become uridine diphosphate (UDP), a substrate of ribonucleotide reductase (RNR). RNR converts UDP into deoxyuridine diphosphate (dUDP), which can later be converted into thymidine triphosphate (dTTP). UDP can also be converted into cytidine diphosphate (CDP), another substrate of RNR. RNR converts CDP into deoxycytidine diphosphate (dCDP), which is then phosphorylated once more to contribute to deoxycytidine triphosphate (dCTP) pools. dCK contributes to dCTP

pools by phosphorylating deoxycytidine to generate deoxycytidine monophosphate (dCMP), an intermediate that is rapidly phosphorylated twice more to generate dCTP. Thymidine kinase 1 (TK1) contributes to dTTP pools by phosphorylating thymidine to generate thymidine monophosphate (dTMP), an intermediate that is rapidly phosphorylated twice more to generate dTTP.

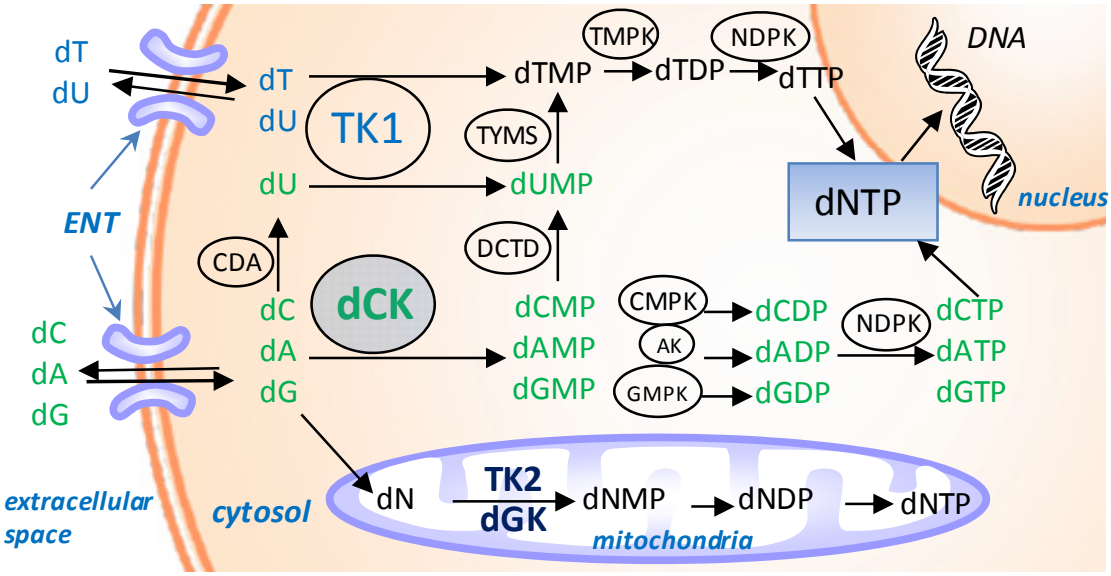


Figure 1.2. dCK regulates a rate-limiting step in the nucleoside salvage pathway. dCK is the only salvage enzyme that can supply cells with all 4 precursors of DNA, 3 of them through direct phosphorylation and trapping of dC, dA and dG and the fourth through metabolic processing of dCMP to dTMP. ENT, equilibrative nucleoside transporter; CDA, cytidine deaminase; DCTD, dCMP deaminase; TYMS, thymidylate synthase; AK, adenylate kinase; GMPK, guanylate kinase; CMPK, cytidylate kinase; TMPK, thymidylate kinase; NDPK, nucleotide diphosphate kinase; TK2, thymidine kinase 2; dGK, deoxyguanosine kinase.

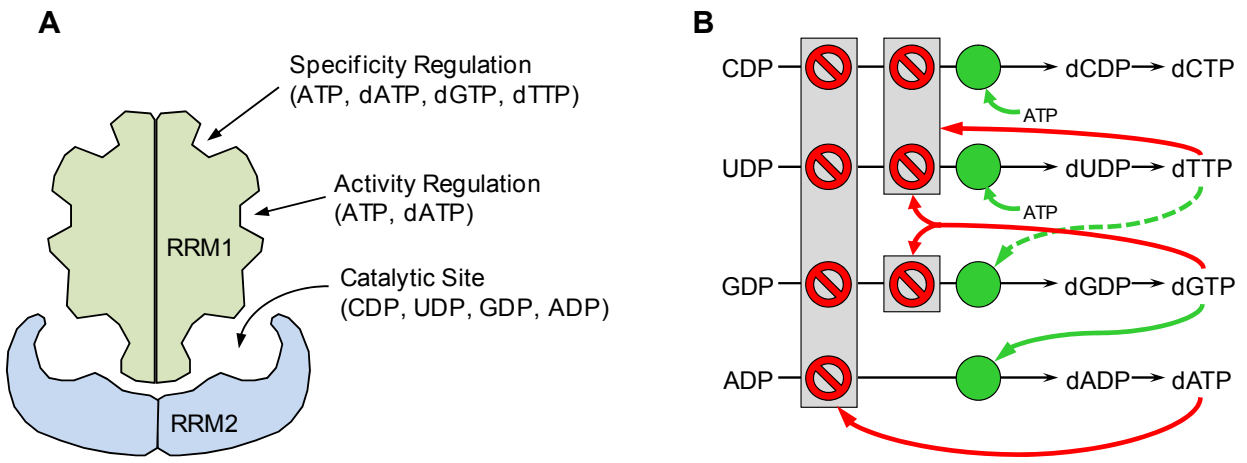


Figure 1.3. General structure and allosteric control of the ribonucleotide reductase (RNR) complex. (**A**) RNR is composed of 2 RRM1 and 2 RRM2 subunits. RRM1 contains activity and specificity regulation sites. The catalytic activity of RNR is present at the interface between RRM1 and RRM2. The activity regulation site binds either ATP (activating) or dATP (inactivating). The specificity regulation site binds ATP (promotes pyrimidine reduction), dATP (promotes pyrimidine reduction), dGTP (promotes ADP reduction), or dTTP (promotes GDP reduction). The catalytic activity site binds UDP, CDP, ADP and GDP to reduce these RNA precursors into the DNA precursors of dUDP, dCDP, dADP and dGDP, respectively. (**B**) Graphical representation of allosteric control of RNR output as determined by nucleotide binding to activity regulatory and specificity regulatory sites of RNR. (Figures adapted from Voet and Voet, *Biochemistry, 2nd Ed.,* J. Wiley & Sons, with permission.)

References

1. Bryant, J.A., and S.J. Aves. 2011. Initiation of DNA replication: functional and evolutionary aspects. *Annals of botany* 107:1119-1126.

2. Reichard, P. 1988. Interactions between deoxyribonucleotide and DNA synthesis. *Annual review of biochemistry* 57:349-374.

3. Arner, E.S., and S. Eriksson. 1995. Mammalian deoxyribonucleoside kinases. *Pharmacology & therapeutics* 67:155-186.

4. Sabini, E., S. Hazra, S. Ort, M. Konrad, and A. Lavie. 2008. Structural basis for substrate promiscuity of dCK. *Journal of molecular biology* 378:607-621.

5. Baldwin, S.A., P.R. Beal, S.Y. Yao, A.E. King, C.E. Cass, and J.D. Young. 2004. The equilibrative nucleoside transporter family, SLC29. *Pflugers Arch* 447:735-743.

6. Gray, J.H., R.P. Owen, and K.M. Giacomini. 2004. The concentrative nucleoside transporter family, SLC28. *Pflugers Arch* 447:728-734.

7. Heinemann, V., and W. Plunkett. 1989. Modulation of deoxynucleotide metabolism by the deoxycytidylate deaminase inhibitor 3,4,5,6-tetrahydrodeoxyuridine. *Biochemical pharmacology* 38:4115-4121.

8. Carreras, C.W., and D.V. Santi. 1995. The catalytic mechanism and structure of thymidylate synthase. *Annual review of biochemistry* 64:721-762.

9. Evans, D.R., and H.I. Guy. 2004. Mammalian pyrimidine biosynthesis: fresh insights into an ancient pathway. *The Journal of biological chemistry* 279:33035-33038.

10. Van Rompay, A.R., A. Norda, K. Linden, M. Johansson, and A. Karlsson. 2001. Phosphorylation of uridine and cytidine nucleoside analogs by two human uridine-cytidine kinases. *Molecular pharmacology* 59:1181-1186.

11. Fairman, J.W., S.R. Wijerathna, M.F. Ahmad, H. Xu, R. Nakano, S. Jha, J. Prendergast, R.M. Welin, S. Flodin, A. Roos, P. Nordlund, Z. Li, T. Walz, and C.G. Dealwis. 2011. Structural basis for allosteric regulation of human ribonucleotide reductase by nucleotide-induced oligomerization. *Nature structural & molecular biology* 18:316-322.

12. D'Angiolella, V., V. Donato, F.M. Forrester, Y.T. Jeong, C. Pellacani, Y. Kudo, A. Saraf, L. Florens, M.P. Washburn, and M. Pagano. 2012. Cyclin F-Mediated Degradation of Ribonucleotide Reductase M2 Controls Genome Integrity and DNA Repair. *Cell* 149:1023-1034.

13. Kimura, T., S. Takeda, Y. Sagiya, M. Gotoh, Y. Nakamura, and H. Arakawa. 2003. Impaired function of p53R2 in Rrm2b-null mice causes severe renal failure through attenuation of dNTP pools. *Nature genetics* 34:440-445.

14. Jordan, A., and P. Reichard. 1998. Ribonucleotide reductases. *Annual review of biochemistry* 67:71-98.

15. Chimploy, K., and C.K. Mathews. 2001. Mouse ribonucleotide reductase control: influence of substrate binding upon interactions with allosteric effectors. *The Journal of biological chemistry* 276:7093-7100.

16. Larsson, K.M., A. Jordan, R. Eliasson, P. Reichard, D.T. Logan, and P. Nordlund. 2004. Structural mechanism of allosteric substrate specificity regulation in a ribonucleotide reductase. *Nature structural & molecular biology* 11:1142-1149.

17. Bjursell, G., and P. Reichard. 1973. Effects of thymidine on deoxyribonucleoside triphosphate pools and deoxyribonucleic acid synthesis in Chinese hamster ovary cells. *The Journal of biological chemistry* 248:3904-3909.

18. Ke, P.Y., C.M. Hu, Y.C. Chang, and Z.F. Chang. 2007. Hiding human thymidine kinase 1 from APC/C-mediated destruction by thymidine binding. *Faseb J* 21:1276-1284.

19. Sherley, J.L., and T.J. Kelly. 1988. Regulation of human thymidine kinase during the cell cycle. *The Journal of biological chemistry* 263:8350-8358.

20. Hengstschlager, M., C. Denk, and E. Wawra. 1993. Cell cycle regulation of deoxycytidine kinase. Evidence for post-transcriptional control. *FEBS letters* 321:237-240.

21. Fyrberg, A., F. Albertioni, and K. Lotfi. 2007. Cell cycle effect on the activity of deoxynucleoside analogue metabolising enzymes. *Biochemical and biophysical research communications* 357:847-853.

22. Chabes, A.L., S. Bjorklund, and L. Thelander. 2004. S Phase-specific transcription of the mouse ribonucleotide reductase R2 gene requires both a proximal repressive E2F-binding site and an upstream promoter activating region. *The Journal of biological chemistry* 279:10796-10807.

23. Feder, J.N., C.J. Guidos, B. Kusler, C. Carswell, D. Lewis, and R.T. Schimke. 1990. A cell cycle analysis of growth-related genes expressed during T lymphocyte maturation. *The Journal of cell biology* 111:2693-2701.

24. Csapo, Z., G. Keszler, G. Safrany, T. Spasokoukotskaja, I. Talianidis, M. Staub, and M. Sasvari-Szekely. 2003. Activation of deoxycytidine kinase by gamma-irradiation and inactivation by hyperosmotic shock in human lymphocytes. *Biochemical pharmacology* 65:2031-2039.

25. Xu, Y.Z., P. Huang, and W. Plunkett. 1995. Functional compartmentation of dCTP pools. Preferential utilization of salvaged deoxycytidine for DNA repair in human lymphoblasts. *The Journal of biological chemistry* 270:631-637.

26. Matsuoka, S., B.A. Ballif, A. Smogorzewska, E.R. McDonald, 3rd, K.E. Hurov, J. Luo, C.E. Bakalarski, Z. Zhao, N. Solimini, Y. Lerenthal, Y. Shiloh, S.P. Gygi, and S.J. Elledge. 2007. ATM and ATR substrate analysis reveals extensive protein networks responsive to DNA damage. *Science (New York, N.Y* 316:1160-1166.

27. Hazra, S., A. Szewczak, S. Ort, M. Konrad, and A. Lavie. 2011. Post-translational phosphorylation of serine 74 of human deoxycytidine kinase favors the enzyme adopting the open conformation making it competent for nucleoside binding and release. *Biochemistry* 50:2870-2880.

28. Smal, C., D. Vertommen, L. Bertrand, S. Ntamashimikiro, M.H. Rider, E. Van Den Neste, and F. Bontemps. 2006. Identification of in vivo phosphorylation sites on human deoxycytidine kinase. Role of Ser-74 in the control of enzyme activity. *The Journal of biological chemistry* 281:4887-4893.

CHAPTER 2

Requirement for Deoxycytidine Kinase

for Normal Hematopoietic Development

Abstract

Deoxycytidine kinase (dCK) is a rate-limiting enzyme in deoxyribonucleoside salvage, a metabolic pathway that recycles products of DNA degradation. dCK phosphorylates and therefore activates nucleoside analog pro-drugs frequently used to treat various cancers, autoimmune diseases, and viral infections. While its therapeutic relevance is well established, the biological function of dCK remains enigmatic. Highest levels of dCK expression are found in thymus and bone marrow, indicating that dCK may play a role in hemato- and lymphopoiesis. To test this hypothesis we generated dCK knockout (*dCK*$^{-/-}$) mice. dCK inactivation selectively and profoundly affected T cell, B cell, and erythroid development. A 20-fold decrease in thymic cellularity was observed in the *dCK*$^{-/-}$ mice; this deficit in cellularity was associated with a differentiation block at the CD4/CD8 double-negative stage of T cell development. Analogous blocks in B cell development in the bone marrow of *dCK*$^{-/-}$ mice were observed. Additionally, abnormalities in erythroid development were observed in the bone marrow and the spleens of *dCK*$^{-/-}$ mice. The severe impact of dCK inactivation on lymphoid and erythroid development were unexpected given that nucleoside salvage has been thought to play a limited, 'fine tuning' role in regulating deoxyribonucleotide triphosphate (dNTP) pools produced by the *de novo* pathway. The *dCK*$^{-/-}$ phenotype challenges this view and indicates that, in contrast to the great majority of other somatic cells, normal hematopoietic development critically requires the deoxyribonucleoside salvage pathway.

Introduction

T cell, B cell, and erythroid development are each characterized by stages of massive, clonal proliferation of immature progenitors (1-3). It is currently poorly understood how T cell, B cell, and erythroid progenitors meet the deoxyribonucleotide triphosphate (dNTP) synthesis requirements to support DNA replication during these phases of massive proliferation. Genetic deficiencies in purine and pyrimidine metabolism are responsible for at least 14 different disorders, with a broad spectrum of clinical manifestations (4). Of these documented clinical disorders of nucleotide metabolism, mutations in the adenosine deaminase and purine nucleoside phosphorylase genes lead to human immunodeficiency syndromes (5, 6). Increased susceptibility to infections also accompanies disorders of pyrimidine metabolism such as orotic aciduria and the pyrimidine nucleotide depletion syndrome (4). Therefore, lymphocytes appear to be very sensitive to defects in nucleotide metabolism.

In theory, lymphocytes and other cells can rely on two pathways to produce dNTPs for DNA replication and repair: the *de novo* synthesis pathway and the deoxyribonucleoside (dN) salvage synthesis pathway. These pathways converge at the level of deoxyribonucleotide diphosphates (dNDP) and are further connected by complex feedback mechanisms (7). Ribonucleotide reductase (RNR), the most important enzyme in the *de novo* pathway, produces all four dNDP precursors for DNA synthesis by converting ribonucleotide diphosphates into dNDPs. Models explaining the production and maintenance of dNTP pools by the *de novo* pathway alone, *without* input from the dN salvage pathway, have been proposed (8). However, in tissues with active

nucleoside salvage, recycling of extracellular dNs via the salvage pathway may also contribute to cellular dNTP pools (9).

The dN flux through the salvage pathway is controlled by specialized kinases (7). Mammalian genomes encode two cytosolic dN kinases with non-overlapping substrate specificities: thymidine kinase 1 (TK1), and deoxycytidine kinase (dCK) (10). TK1 phosphorylates thymidine (dT) and deoxyuridine (dU), while dCK phosphorylates deoxycytidine (dC), deoxyadenosine (dA) and deoxyguanosine (dG); dCK can also contribute to dTTP pools since its product, dCMP, can be converted to dTMP by dCMP deaminase and thymidylate synthase (11). While dCK resembles RNR in terms of its ability to produce all four dNTPs, the biological function of this kinase is not yet defined. Several hypotheses have been formulated including potential roles for dCK in DNA repair, in synthesis of liponucleotide precursors of membrane phospholipids and in programmed cell death (12). The evidence in favor or against these hypotheses is circumstantial. According to a model proposed by Reichard and colleagues, dCK may be responsible for “fine tuning” dNTP pools in dividing cells through its involvement in a substrate (futile) cycle (13-16). The cycle consists of a phosphorylation reaction catalyzed by dCK and a dephosphorylation reaction catalyzed by 5’-nucleotidase (5’-NT). The rates of these opposing reactions are influenced by the rates of dNTP synthesis through the *de novo* pathway and by other factors. For example, in rapidly dividing cells, a decrease in the dCTP pool due to incorporation into DNA poises the substrate cycle towards anabolism by attenuating a dCTP-dependent negative feedback mechanism. dCK may be involved in a similar substrate cycle for deoxyadenosine (17).

While the existence of salvage substrate cycles has been confirmed by biochemical studies in cultured cancer cells (13-16), its *in vivo* significance has not been tested experimentally. The enzymatic activities of dCK and nucleotidases vary widely in different cell types (18). Lymphocytes and erythroid progenitors express high levels of dCK (12, 19) and their nucleoside substrate cycles are geared towards anabolism (20). Furthermore, the importance of the dN substrate cycles may increase during developmental and functional events associated with proliferative stress, such as rapid clonal expansion of T cell, B cell, and erythroid precursors in thymus and bone marrow.

To elucidate the function of the dN salvage pathway a genetic animal model of dCK deficiency would be of considerable interest. In this chapter, we describe the generation and characterization of hematopoietic development in dCK knockout (*dCK*$^{-/-}$) mice. The analysis of this new genetic model demonstrates that deletion of dCK has a selective developmental impact. Embryogenesis and development of most organs and systems are not affected. However, dCK inactivation significantly impaired T cell, B cell, and erythroid development. In addition to establishing the immunological relevance of an ancillary dNTP biosynthetic mechanism, the genetic model of dCK deficiency described herein may improve our understanding of the differential “wiring” of dNTP metabolic pathways in various cell types. In turn, this may lead to the identification of new therapeutic targets for immune disorders and lymphoid malignancies.

Materials and Methods

Generation of the dCK targeting vector.

A recombineering-based approach (21) was used that employed the temperature sensitive λ prophage Red Recombinase and Arabinose inducible Cre recombinase in *E. coli.* This approach used 2 types of recombination sites: *loxP* sites (recognized by the bacteriophage P1-derived Cre recombinase) and *FRT* sites (recognized by the flippase recombinase - FLP). All reagents for recombineering were obtained from NCI-Frederick (http://recombineering.ncifcrf.gov). A genomic DNA sequence containing dCK retrieved from a BAC clone was transferred by homologous recombination into the pL253 vector to generate the pL253/dCK plasmid. A mini-targeting vector containing a *loxP* flanked *Neo* cassette surrounded by regions homologous to an intronic site upstream of dCK exon 3 was electroporated into pL253/dCK-containing EL350 cells induced for λ prophage Red Recombinase. The *Neo* cassette was excised as described (21), resulting in a single *loxP* site upstream of exon 3. A second targeting step was then performed using a vector containing a *FRT* flanked *Neo* gene with an upstream *loxP* site. This final step yielded a genomic targeting construct containing *dCK* exon 3 flanked by loxP sites.

Generation of the global dCK$^{-/-}$ mice.

Upon sequencing verification of targeting construct integrity, the construct was linearized and electroporated into LW-1 (129Sv/J) embryonic stem cells for integration by homologous recombination. Neomycin resistant clones were selected (the HSV1-tk-based selection was not used) and subjected to Southern blot analysis using probes

specific for exons 2 and 5 of the dCK gene to verify insertion of the targeting construct. The probes were generated by PCR using the following primers: Exon 2 probe - E2-left (5'-GAG AAA GGT CTC AGT GTT TCT GC-3') and E2-Right (5'-GGC CAT GGA GAC CAG ACG-3'); Exon 5 probe - E5-Left (5'-TCT GGC TAA AAT AAC TAC TGA TAG GG-3') and E5-Right (5'-TTG GGA AAA TGA GCA AAT CC-3'). Two positive clones were selected and expanded for blastocyst injection followed by implantation into a pseudo-pregnant female. Chimeric pups were selected and crossed with C57Bl/6 mice. Agouti pups were selected and subjected to Southern blot (performed as previously described (22)) and PCR genotyping to verify germline transmission of the targeted allele. For PCR-based genotyping, genomic DNA was isolated from mouse tail lysates using the PureLink Genomic DNA kit (Invitrogen). Touchdown PCR for *dCK* alleles was performed as described (23) using the following primers: P1 (5'-AAC TGC TGA GCC ATC TCT CC-3'); P2 (5'-AAA AAT AAT ACA GGT TTC TCT GCA TC-3'); and P3 (5'-GGG CTC TAT GGC TTC TGA GG-3').

Agouti mice with verified germline transmission of the targeting construct were then crossed with *B6.C-Tg(CMV-cre)1Cgn/J* mice (Jackson Laboratories, Bar Harbor ME), which express Cre recombinase under the control of a CMV promoter in all cell types, to generate $dCK^{+/flox}$ Cre^{Tg} mice. $dCK^{+/flox}$ Cre^{Tg} mice were then crossed with C57Bl/6 mice to obtain heterozygous knockout ($dCK^{+/-}$) mice without the Cre transgene. $dCK^{+/-}$ mice lacking the Cre transgene were identified by PCR genotyping and were subsequently intercrossed to yield the $dCK^{+/+}$, $dCK^{+/-}$ and $dCK^{-/-}$ littermates.

MicroPET/CT Imaging

Mice were kept warm, under gas anesthesia (2% isoflourane) and intravenously injected with 200 µCi of ^{18}F-FAC. 1 hr interval for uptake was allowed between probe administration and microPET/CT scanning. MicroPET data were acquired for 10 min using Siemens Preclinical Solutions (Knoxville, TN) Focus 220 or Inveon microPET scanners. CT scans were performed using MicroCAT II CT instruments. Images were analyzed using OsiriX software, an open access DICOM compatible image viewing, analysis and fusion software (http://www.osirix-viewer.com). Color scale is proportional to tissue concentration with red being the highest and lower values in yellow, green & blue.

Immunophenotyping antibodies

The following antibodies from eBioscience were used for B cell and erythroid phenotyping from whole bone marrow: B220 (Clone RA3-6B2) PE-Cy7 and APC-eFluor780; IgM (Clone II/41) FITC, PerCP-eFluor710; CD43 (Clone eBioR2/60) PE; CD19 (Clone 1D3) APC and PE-Cy7; Ter119 (Clone TER-119) PerCP-Cy5.5 and PE-Cy7; CD71 (Clone R17217) APC and PE.

The following antibodies from eBioscience were used for thymocyte phenotyping: CD4 (Clone L3T4) FITC, PE, Alexa700, and PE-Cy7; CD8a (Clone 53-6.7) PE, PE-Cy7, and PerCP-eFluor710; CD25 (Clone PC61.5) APC and PE-Cy7; CD44 (Clone IM7) APC-eFluor780; CD27 (Clone LG.7F9) PE; CD45 (Clone 30-F11) PE-Cy7; CD45.1 (Ly5.2) (Clone A20) PerCP-Cy5.5; and CD45.2 (Ly5.1) (Clone 104).

Flow cytometry analyses

All flow cytometry data were acquired on 4- and 5-laser LSRII cytometers (BD Biosciences) for analysis, and FACS-purification of cells was performed on 4-laser BD FACSAriaII cell sorters running BD FACSDiva6 software (BD Biosciences). All cytometry data were analyzed using FlowJo software (TreeStar, Inc.).

In vitro and in vivo assays to measure the enzymatic activity of dCK

Splenocytes and bone marrow cells were lysed and dCK kinase activity was determined using selective binding of phosphorylated products of ^{3}H-FAC (Moravek Biochemicals) to DE81 Whatman filter paper as previously described (24). ^{18}F-FAC was synthesized and used for microPET/CT imaging studies as previously described (25).

Statistical Analyses

Data are presented as means ± SEM. Group comparisons were performed using the One Sample T test function in column statistics in Prism 5 software (GraphPad Software, La Jolla, CA) using the observed mean value of wild-type samples as the theoretical mean of comparison. All *P* values are two-tailed and *P* values of <0.05 are considered to be statistically significant. Graphs were generated using the Prism 5 software.

Results

Generation of the dCK$^{-/-}$ mice

Given the lack of evidence in favor or against dCK being critically required during embryogenesis, organogenesis or other essential developmental processes, we decided to use a conditional gene targeting strategy to avoid a lethal phenotype. A recombineering-based cloning approach (21) was used to generate a dCK targeting construct in which exon 3 was flanked by *loxP* sites (*dCK^{flox}*) (Figure 2.1, A). Exon 3 deletion by Cre recombinase eliminates the dCK catalytic domain and also causes a frame shift mutation and early termination of dCK protein synthesis.

Targeting vectors encoding the *dCK^{flox}* allele were transfected into 129/Sv embryonic stem cells and integration by homologous recombination was selected for through G418 antibiotic resistance. Several G418-resistant clones were counter-screened for proper integration of the targeting vector using southern blotting techniques (Figure 2.1, B). Two clones were chosen and subsequently injected into C57Bl/6 blastocysts that were implanted into pseudopregnant C57Bl/6 females. Chimeric pups were selected and backcrossed to C57Bl/6 mice to confirm germline transmission of the *dCK^{flox}* allele. *dCK$^{+/flox}$* mice were then crossed to C57Bl/6 mice transgenically expressing Cre recombinase (*Cre^{Tg}*) under the control of a ubiquitous cytomegalovirus (CMV) promoter in order to generate *dCK$^{+/-}$ Cre^{Tg}* mice. These heterozygous mice were then backcrossed to C57Bl/6 again to eliminate the Cre transgene and subsequent *dCK$^{+/-}$ Cre^{neg}* mice were intercrossed together to generate *dCK$^{+/+}$* (wild-type, WT), *dCK$^{+/-}$*, and *dCK$^{-/-}$* progeny that were identified by PCR genotyping (Figure 2.1, C). Intercrossing *dCK$^{+/-}$* mice yielded 1:2:1 ratios of WT, *dCK$^{+/-}$*,

and *dCK*$^{-/-}$ pups as the first 93 genotyped progeny produced 24.7% WT, 47.3% *dCK*$^{+/-}$, and 28% *dCK*$^{-/-}$ mice (Figure 2.1, D). This normal Mendelian distribution indicated that the gene targeting strategy did not result in embryonic/perinatal lethality. Moreover, the developmental growth rates of *dCK*$^{-/-}$ mice were comparable to WT littermates (Figure 2.1, E).

Deletion of exon 3 from dCK abolishes enzymatic activity

We employed two biochemical assays to validate that *dCK*$^{-/-}$ mice did in fact lack dCK activity. These assays used radiolabeled 1-(2'-deoxy-2'-fluoroarabinofuranosyl) cytosine (FAC), a high affinity substrate for dCK that closely resembles the endogenous dCK substrate deoxycytidine (24, 25). We first performed an *in vitro* kinase assay using tritiated-FAC (^{3}H-FAC) as a substrate to assay dCK activity in lysates from bone marrow and spleen tissues. This assay demonstrated that *dCK*$^{-/-}$ lysates did not have measureable dCK activity (Figure 2.2, A).

As a corollary to the *in vitro* kinase assay, we imaged the *dCK*$^{-/-}$ mice by Micro Positron Emission Tomography (mPET) and computed tomography (CT) using fluorine-18 labeled FAC (^{18}F-FAC) (25). ^{18}F-FAC mPET/CT imaging allows non-invasive measurements of dCK activity throughout the body. There was a striking contrast between the ^{18}F-FAC biodistribution in the WT mice compared to the *dCK*$^{-/-}$ animals (Figure 2.2, B). In the WT mice, ^{18}F-FAC accumulated in hematopoietic and lymphoid tissues such as bone marrow, thymus, and spleen reflecting the normal high dCK activity present in these tissues. None of these signals were visible in the *dCK*$^{-/-}$ mice.

The ^{18}F-FAC uptake in the gastrointestinal tract observed in the WT mice was absent in *dCK*$^{-/-}$ mice, indicating that probe accumulation in this tissue is also dCK-specific.

Defective T cell development in the dCK*$^{-/-}$ *mice

dCK$^{-/-}$ mice at 6-8 weeks of age were severely microthymic with *dCK*$^{-/-}$ mice averaging 20-fold fewer cells than those from the WT littermates (average of 155 x 10^6 cells for WT, 8 x 10^6 cells for *dCK*$^{-/-}$; $P<0.0001$) (Figure 2.3, A). Histologically, the *dCK*$^{-/-}$ thymi lacked the normal corticomedullary organization and appeared less basophilic than WT thymi (Figure 2.3, B).

Discrete stages of T cell development have been well defined by the expression of cell surface markers (1). We therefore immunophenotyped *dCK*$^{-/-}$ thymocytes to determine if they were blocked at any particular stage of T cell development. We first analyzed WT and *dCK*$^{-/-}$ thymocytes for their expression of the prototypical T cell surface markers of CD4 and CD8. *dCK*$^{-/-}$ thymocytes were significantly reduced in CD4/CD8 double-positive cells (DP) (average of 86% for WT, 33% for *dCK*$^{-/-}$; $P<0.01$), and, in turn, displayed significantly greater proportions of CD4/CD8 double-negative (DN) cells (average of 5% for WT, 58% for *dCK*$^{-/-}$; $P<0.002$) (Figure 2.3, C). This observation was particularly interesting since it is known that first waves of proliferation that immature T cells execute in the thymus occur when they are the DN stage (26).

The significant skewing of *dCK*$^{-/-}$ thymocyte cells to the DN population warranted higher resolution immunophenotyping. The heterogeneous DN population can be further subdivided based on the expression of CD44 and CD25 into four stages: DN1 (CD44$^+$, CD25$^-$), DN2 (CD44$^+$, CD25$^+$), DN3 (CD44^{lo}, CD25$^+$), and DN4 (CD44$^-$, CD25$^-$) with

DN1 stage being the most immature and the DN4 stage immediately preceding the DP stage (1). Analysis of the DN1-DN4 distribution of cells showed that *dCK*$^{-/-}$ DN thymocytes have significantly more DN3 cells (average of 45% for WT, 78% for *dCK*$^{-/-}$; *P*<0.0001), and significantly fewer DN4 cells than WT DN thymocytes (average of 34% for WT, 6% for *dCK*$^{-/-}$; *P*<0.0001) (Figure 2.3, D).

The DN3 stage at which *dCK*$^{-/-}$ thymocytes are apparently blocked in development can be further subdivided into two distinct differentiation stages known as DN3a and DN3b thymocytes (27). DN3a and DN3b cells differ from each another based on the expression of CD25 and CD27: DN3a cells are CD25^{Hi} CD27^{Lo}, and DN3b cells are CD25^{Med-Lo} CD27^{Hi} (27). Analyzing WT and *dCK*$^{-/-}$ DN3 thymocytes for CD25 and CD27 expression revealed that *dCK*$^{-/-}$ DN3 thymocytes were blocked in their transition from DN3a cells into DN3b cells (Figure 2.3, E). WT mice average 55% of DN3 cells in the DN3a stage, while *dCK*$^{-/-}$ mice averaged 84% of DN3 cells in the DN3a stage (*P*=0.0002). Concurrently, fewer *dCK*$^{-/-}$ DN3 cells were found in the DN3b stage (average 11%) versus WT DN3 cells in the DN3b stage (average 40%) (*P*<0.0001).

This block in development corresponds to a critical stage in T cell development. It is during the DN3a stage that developing T cells rearrange the β chain of their T cell receptor (TCRβ) gene (27, 28). Expression of a successfully rearranged TCRβ gene paired with a non-rearranged α chain of the TCR creates DN3b thymocytes that express a pre-TCR complex on their cell surface (27). Pre-TCR signaling stimulates proliferation of DN3b thymocytes as they differentiate into DN4 and ultimately DP thymocytes (26).

Defective B lymphocyte development in the dCK$^{-/-}$ mice

The defects in T lymphocyte development prompted us to probe for potential analogous defects in B lymphocyte development. Similar to the discrete stages of T cell development, B cell development has also been mapped by expression of established cell surface markers at various stages, as classified by Hardy and colleagues (29). Analysis of Hardy Fraction E-F (B220^{+}, IgM^{+}) cells revealed that *dCK*$^{-/-}$ mice have 7-fold fewer Hardy E-F cells (average 0.9%) than WT mice (average 6.5%) (P<0.0001) (Figure 2.4, A). Consistent with the deficit in Hardy E-F cells was a 3-fold reduction in Hardy A-D cells (B220^{+}, IgM^{-}) in *dCK*$^{-/-}$ mice (average 4.3%) versus WT mice (13.4%) (P<0.001) (Figure 2.4, A).

Further sub-fractionation of the general Hardy A-D population using the CD43 and CD19 markers revealed another significant block in B cell development in *dCK*$^{-/-}$ mice. The most primitive of B cell-restricted progenitors are named Hardy Fraction A and are identified as being CD19^{-} and CD43^{Hi} (30). We found an average of 16% of WT Hardy A-D cells being specifically in the Hardy A stage, while *dCK*$^{-/-}$ mice had an average of 68% of Hardy A-D cells being in the Hardy A stage (P<0.003) (Figure 2.4, B). We did not observe a statistical difference in the percentage of WT and *dCK*$^{-/-}$ cells in the Hardy B-C stages (CD43^{Hi}, CD19^{Hi}). However, we did identify a significant decrease in Hardy Fraction D cells (CD43^{Lo}, CD19^{+}) amongst *dCK*$^{-/-}$ cells with WT Hardy D cells averaging 64% of Hardy A-D cells, and *dCK*$^{-/-}$ Hardy D cells averaging 13% of Hardy A-D cells (P=0.0001) (Figure 2.4, B). The apparent block in differentiation in *dCK*$^{-/-}$ mice from the highly proliferative Hardy B-C cells (2, 29) to the Hardy Fraction

D indicate that inactivation of dCK may reduce the proliferative capacity of these B lymphocyte progenitors.

Abnormal proportions of erythroid progenitors in the bone marrow and spleens of dCK$^{-/-}$ mice

dCK is also highly expressed in developing erythroid cells (19) prompting us to determine if dCK inactivation affects this hematopoietic lineage. We profiled erythroid development in the bone marrow based on expression of Ter119 and CD71. In conjunction with the Forward Scatter (FSC) measurement of general cell size by flow cytometry, erythroid development is be categorized into basophilic erythroblasts (EryA; Ter119^{+} CD71^{+} FSC^{Hi}), late basophilic/polychromatic erythroblasts (EryB; Ter119^{+} CD71^{+} FSC^{Hi}), and orthochromatic erythroblasts/reticulocytes (EryC; Ter119^{+} CD71^{-} FSC^{Hi}) (31). Performing this analysis to investigate EryA, EryB, and EryC stages of erythroid development in WT and *dCK*$^{-/-}$ mice revealed several significant differences.

dCK$^{-/-}$ mice averaged twice as many EryA cells (44% of Ter119^{+} cells) as EryA cells in WT mice (22% of Ter119^{+} cells) (P<0.0001) (Figure 2.5, A). This population corresponds to the highly proliferative erythroid progenitors that are in their final nucleated stage prior to differentiation into reticulocytes (31, 32). The increase in EryA cells was associated with a significant decrease in *dCK*$^{-/-}$ EryB cells (average 13%) relative to WT EryB cells (average 34%) (P<0.001) (Figure 2.5, A), thereby suggesting a potential block in differentiation from the EryA to the EryB stage in *dCK*$^{-/-}$ mice. Lastly, *dCK*$^{-/-}$ mice demonstrated a statistically significant decrease in EryC cells (36%) versus

WT EryC cells (41%) (P<0.03), although this difference was much less pronounced than the differences exhibited in the earlier stages of erythroid differentiation.

Abnormalities in erythroid development in the bone marrow of *dCK*$^{-/-}$ mice were accompanied by similar manifestations in the spleen. *dCK*$^{-/-}$ mice displayed splenomegaly characterized by a 2.5-fold increase in spleen size by weight (Figure 2.4, B). Histological analysis of *dCK*$^{-/-}$ spleens revealed an absence of normal red and white pulp architecture, typified by a distinct lack of white pulp (Figure 2.5, C), thus indicating that these spleens contain excess erythroid progenitors resulting from potential extramedullary hematopoiesis. Staining single cell suspensions of whole splenocytes from WT and *dCK*$^{-/-}$ mice for the erythroid development markers revealed a significant increase in the percentage of the EryA progenitor population in Ter119^{+} *dCK*$^{-/-}$ splenocytes (average 29%) versus Ter119^{+} WT splenocytes (average 6%) (P<0.002) (Figure 2.5, D), indicating the presence of abnormal red blood cell generation in *dCK*$^{-/-}$ spleens.

Discussion

Deoxycytidine kinase plays a selective role in hematopoietic development

The *de novo* and salvage deoxyribonucleotide synthesis pathways have been studied extensively. Recent *in vivo* studies of purine dNTP metabolism in various organs and cell types (33-35) and older studies in cell culture (7) support a model in which the *de novo* pathway plays the dominant role in dNTP synthesis (7). While the general applicability of this model awaits experimental confirmation, it is possible that

dNTP metabolism in developing hematopoietic cells follows a distinct set of rules (9). To unequivocally determine the biological significance of the dN salvage pathway we generated and analyzed mice deficient for dCK, the salvage enzyme that phosphorylates pyrimidine and purine dNs. *dCK*$^{-/-}$ mice develop normally and are born at the expected Mendelian ratio. In mice, dCK is therefore dispensable for dNTP metabolism and DNA synthesis during embryogenesis, organogenesis and other essential developmental processes. Since no other dN salvage enzyme can compensate for the loss of dCK function, it is likely that *de novo* dNTP production is sufficient to support rapid cell division during most developmental processes. The exceptions are lymphocyte and erythroid development, which are affected by dCK inactivation. The severity of the defects in these hematopoietic cell types were surprising to us, given the functional redundancy of dNTP biosynthetic pathways, and the 'fine tuning' role in dNTP metabolism assigned to the dN salvage pathway by previous studies (7). Our data suggest that, unlike other developmental programs, normal lymphopoiesis and erythropoiesis require dN salvage via dCK and that defects in this pathway cannot be compensated by endogenously increased output of *de novo* synthesis.

Hematopoietic development defects in dCK$^{-/-}$ mice occur at stages of massive clonal proliferation

Thymocytes from the *dCK*$^{-/-}$ mice display a partial block at the transition from the DN stage to the DP stage of development (Figure 2.3). A partial block is also present in B cell development in the bone marrow between the Hardy B-C to Hardy D stages of

development (Figure 2.4). These T and B cell developmental stages follow critical checkpoints in lymphopoiesis at stages of recombination of Variable, Diverse, and Joining (V(D)J) gene segments to generate pre-TCR and pre-BCR cell receptor complexes (26, 36). Signaling through these receptors halts further V(D)J recombination, induces differentiation and directs intense waves of clonal expansion. The correlation of defective lymphocyte development in *dCK*$^{-/-}$ mice at stages of V(D)J recombination indicate that dCK may be involved in this programmed DNA damage and repair process similar to the way that various other genes involved in V(D)J recombination (e.g. *RAG1*, *RAG2*, *DNA-PKcs*, *Ku70*, *Ku80*, *XRCC4* and *ligase 4*) quantitatively and qualitatively affect T cell and B cell development (37). However, an argument against defective V(D)J recombination as being the primary reason for defective hematopoietic development in *dCK*$^{-/-}$ mice lies in the fact that *dCK*$^{-/-}$ erythroid cells have differentiation abnormalities (Figure 2.5). Developing erythroid cells do not engage in V(D)J recombination, but deletion of dCK in these cells still induced severe blocks in differentiation at stages of massive proliferation similar to the developing T and B cells.

The rapid rate of cell division that occur during T cell, B cell, and erythroid development may be a proliferative stress that overwhelms the *de novo* dNTP biosynthetic machinery; it is estimated that immature T cell clones may expand 200-500 fold at this step (38). It is possible that the absence of dCK may create a “bottleneck” in dNTP production that impairs the proliferation of DN thymocytes during their differentiation into DP cells. An analogous mechanism may explain the defects in the B

cell lineage. This hypothesis merits further study by quantitative measurements of dNTP pools in *dCK*$^{-/-}$ lymphocyte precursors.

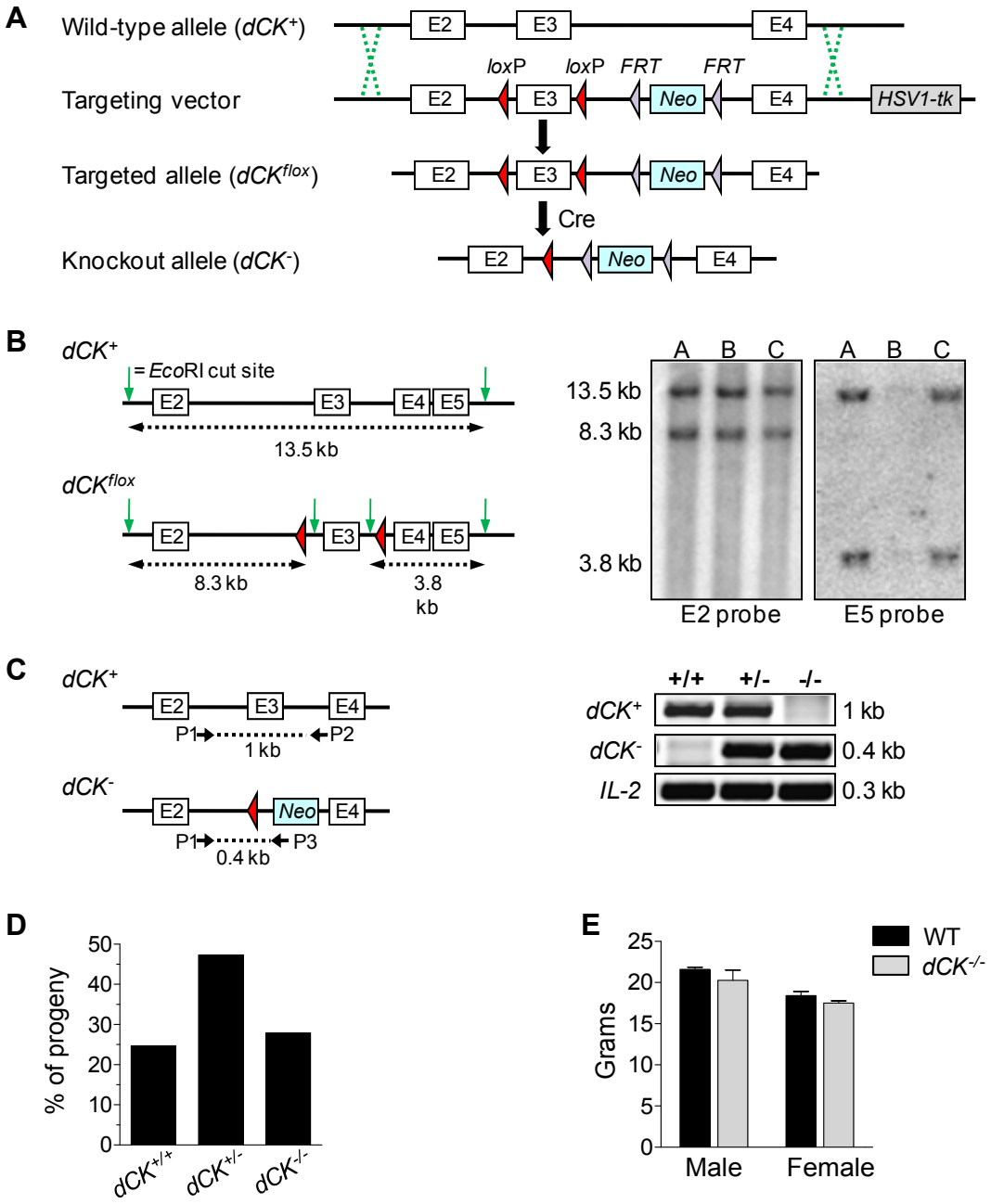


Figure 2.1. Targeting vector strategy to genetically eliminate dCK activity. (**A**) A targeting vector was designed to replace endogenous exons 2-4 (E2, E3, E4) of *dCK* allele with *loxP*-flanked (*flox*) version of *dCK* exon 3 (E3). Crossing mice with dCK^{flox} allele to mice transgenic for Cre recombinase will yield progeny containing a knockout

allele of *dCK* that retains the Neomycin-resistance cassette (*Neo*). (**B**) Genomic DNA from G418-resistant 129/SvJ embryonic stem cell lines (A, B, C) were probed for integration of the targeting vector by *Eco*RI digestion followed by southern blotting using probes specific for exons 2 or 5 of *dCK*. Stem cell lines A and C were selected for injection into C57Bl/6 blastocysts for implantation into pseudopregnant females. (**C**) PCR genotyping strategy and representative DNA gel used to identify $dCK^{+/+}$, $dCK^{+/-}$, and $dCK^{-/-}$ littermates. (**D**) Percentages of $dCK^{+/+}$, $dCK^{+/-}$, and $dCK^{-/-}$ mice generated from the first 93 genotyped progeny from $dCK^{+/-}$ intercrosses. (**E**) Weights of male and female WT (Black bars) and $dCK^{-/-}$ (Grey bars) mice at 6 weeks of age. Graphs are average values + SEM (N=4 mice per genotype and gender).

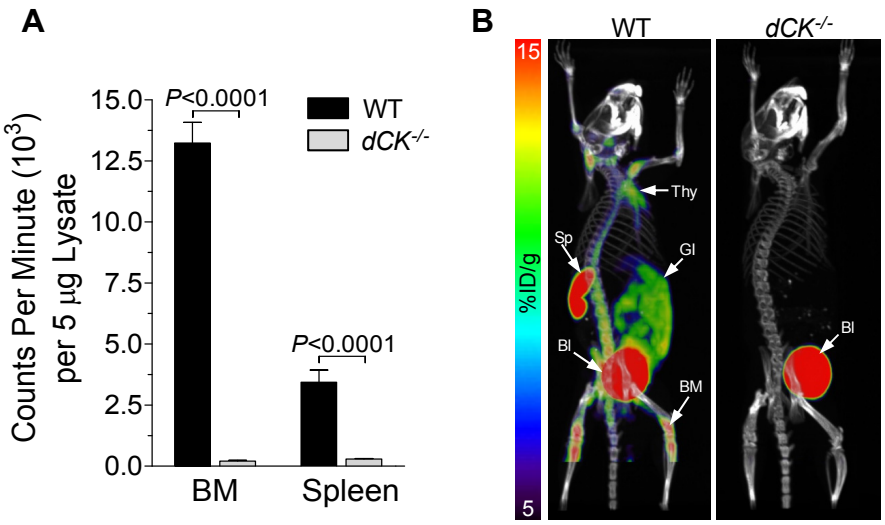


Figure 2.2. Validation of complete inactivation of dCK activity. (**A**) *In vitro* ^{3}H-FAC kinase assay using 5 µg of lysates from bone marrow (BM) and spleen cells from WT (Black bars) and *dCK*$^{-/-}$ (Grey bars) mice. Graphs are average values + SEM (N=6 samples per genotype and tissues). (**B**) *In vivo* ^{18}F-FAC mPET/CT imaging of WT and *dCK*$^{-/-}$ mice. Images scaled 5-15% of injected dose/gram (%ID/g) of tissue. Thy-thymus; Sp-spleen; BM-bone marrow; GI-gastrointestinal tract; Bl-bladder.

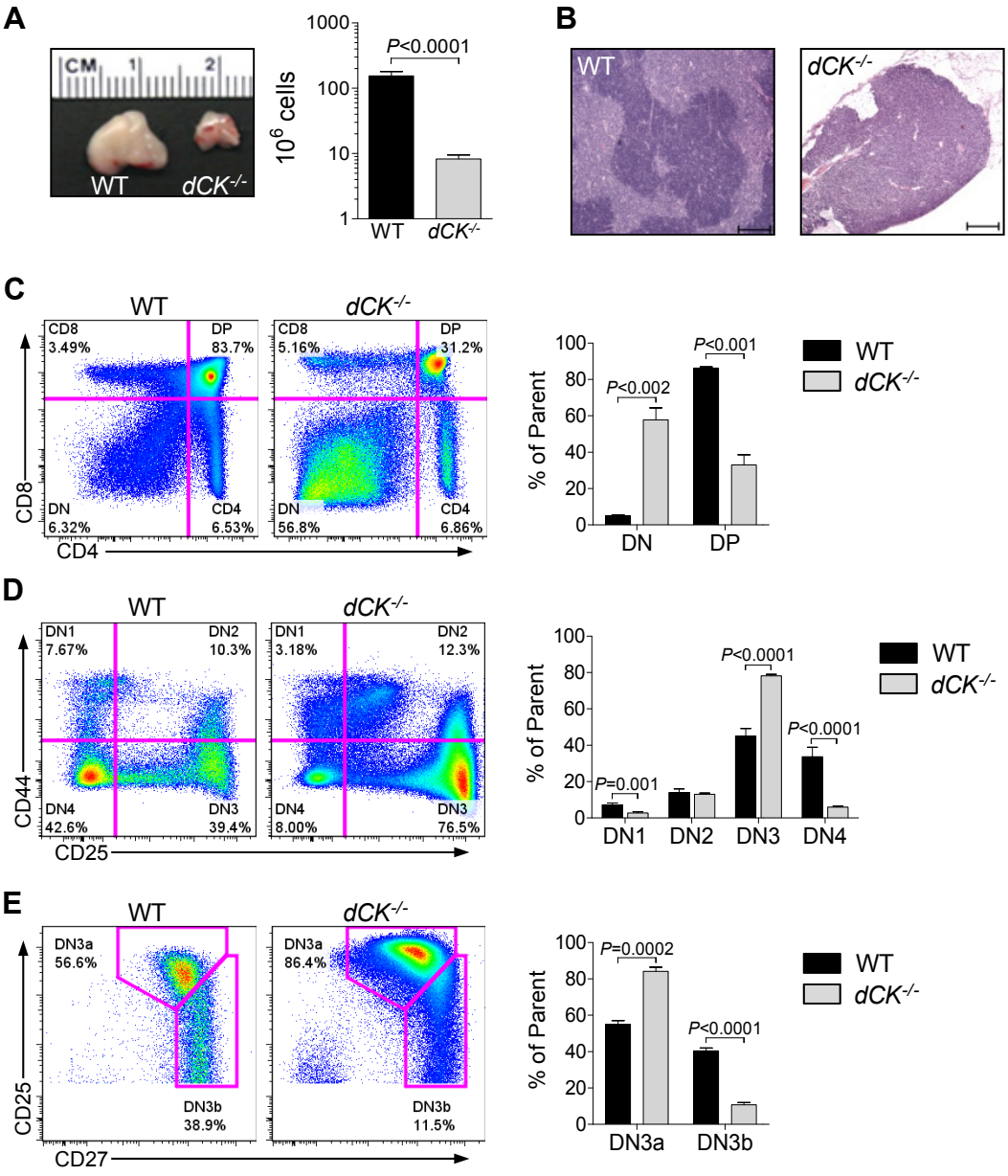


Figure 2.3. Defective T cell development in the *dCK*$^{-/-}$ mice. (**A**) Gross size and average cellularity of WT and *dCK*$^{-/-}$ thymi. Graphs are average values + SEM (N=6 mice/genotype; *P*<0.0001). (**B**) Hematoxylin and eosin staining of WT and *dCK*$^{-/-}$ thymi. Scale bar = 250 μm. (**C**) CD4 and CD8 staining of whole thymocytes to identify CD4^{-} /CD8^{-} thymocytes (DN cells), CD4^{+}/CD8^{+} thymocytes (DP cells), and CD4 and CD8 single-positive cells. Quantification of DN and DP subpopulations amongst whole

thymocytes from WT (Black bars) and *dCK*$^{-/-}$ (Grey bars) mice. Graphs are average values + SEM (N=5 mice/genotype; *P*<0.001 to 0.002). (**D**) CD25 and CD44 staining of DN cells to identify DN1-DN4 populations. Quantification of relative DN1-DN4 subpopulations in the DN population. Graphs are average values + SEM (N=5 mice/genotype; *P*<0.0001 to 0.001). (**E**) CD25 and CD27 staining of DN3 cells to identify DN3a and DN3b cells. Quantification of relative DN3a and DN3b populations in the DN3 population. Graphs are average values + SEM (N=5 mice/genotype; *P*<0.0001 to 0.0002).

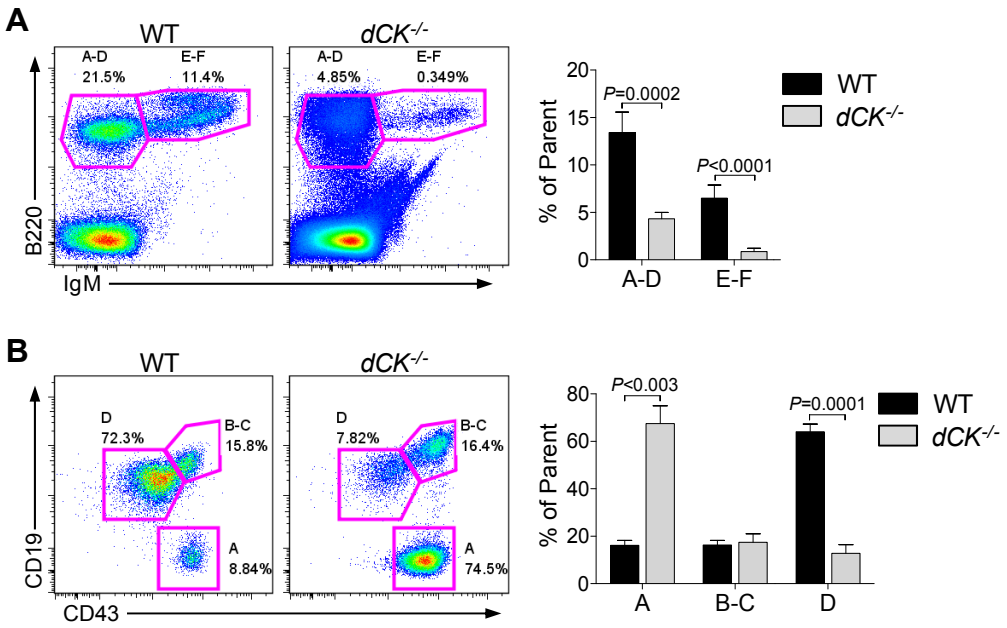


Figure 2.4. Defective B cell development in the *dCK*$^{-/-}$ mice. (**A**) IgM and B220 staining of whole bone marrow cells from WT and *dCK*$^{-/-}$ mice to identify Hardy Fraction A-D and E-F populations. Quantification of Hardy A-D and Hardy E-F subpopulations amongst whole bone marrow cells from WT (Black bars) and *dCK*$^{-/-}$ (Grey bars) mice. Graphs are average values + SEM (N=5 mice/genotype; *P*<0.0001 to 0.0002). (**B**) CD43 and CD19 staining of Hardy Fraction A-D cells to identify Hardy Fraction A, B-C, and D populations. Quantification of Hardy A, Hardy B-C, and Hardy D subpopulations. Graphs are average values + SEM (N=5 mice/genotype; *P*<0.0001 to 0.003).

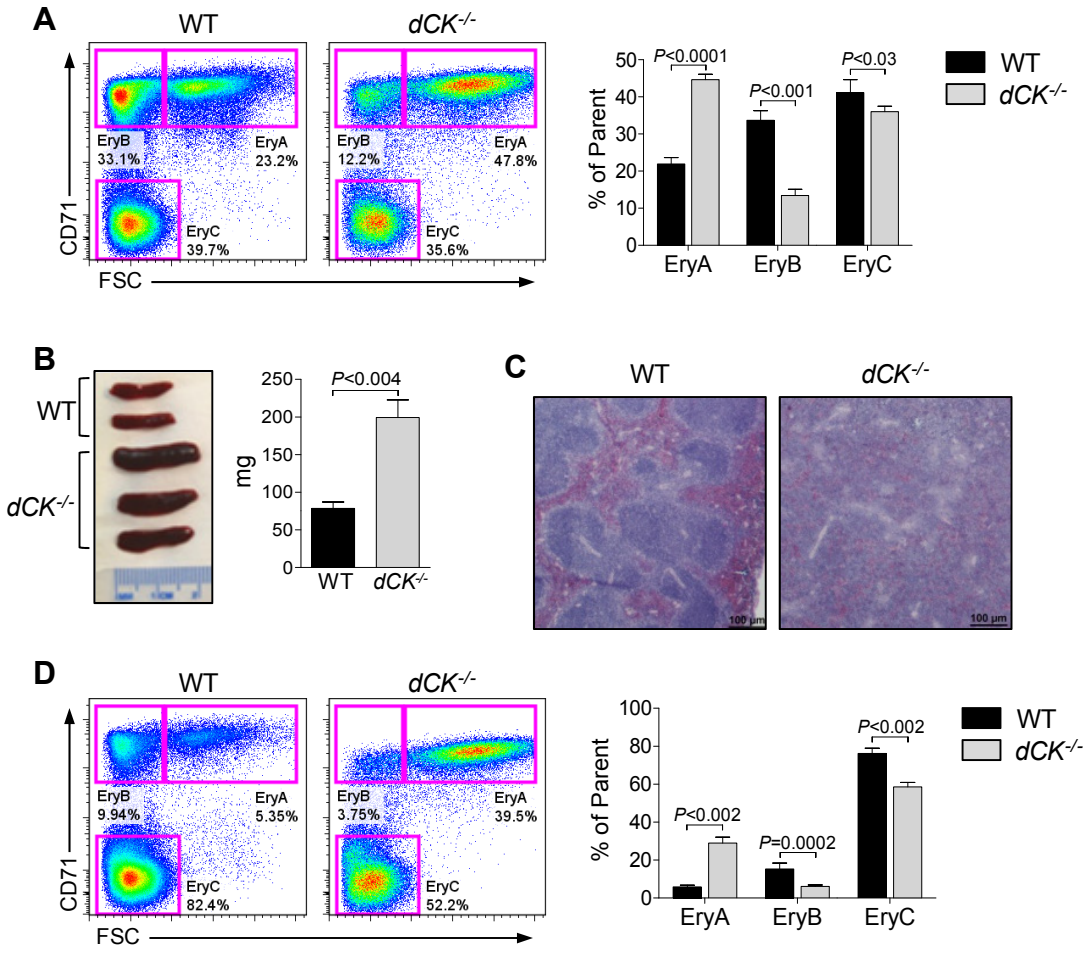


Figure 2.5. *dCK*$^{-/-}$ mice display abnormal erythroid population distributions in the bone marrow and spleen. (**A**) FSC and CD71 characteristics of Ter119^{+} cells from whole bone marrow cells from WT and *dCK*$^{-/-}$ mice to identify EryA, EryB and EryC stages of erythroid development. Quantification of erythroid subpopulations from WT (Black bars) and *dCK*$^{-/-}$ (Grey bars) Ter119^{+} bone marrow. Graphs are average values + SEM (N=5 mice/genotype; *P*<0.0001 to 0.03). (**B**) Gross sizes and quantification of weights (in mg) of spleens from WT and *dCK*$^{-/-}$ mice. Graphs are average values + SEM (N=6 mice/genotype; *P*<0.0004). (**C**) Hematoxylin and eosin staining of spleen sections from WT and *dCK*$^{-/-}$ mice to identify white pulp and red pulp morphological structures.

Scale bar = 100 μm. (**D**) FSC and CD71 characteristics of Ter119^{+} cells from whole spleen cells from WT and *dCK*$^{-/-}$ mice to identify EryA, EryB and EryC stages of erythroid development. Quantification of erythroid subpopulations from Ter119^{+} spleen cells from WT and *dCK*$^{-/-}$ mice. Graphs are average values + SEM (N=5 mice/genotype; $P<0.0002$ to 0.002).

References

1. Ciofani, M., and J.C. Zuniga-Pflucker. 2010. Determining gammadelta versus alphass T cell development. *Nat Rev Immunol* 10:657-663.

2. Kline, G.H., T.A. Hayden, and P. Riegert. 2001. The initiation of B cell clonal expansion occurs independently of pre-B cell receptor formation. *J Immunol* 167:5136-5142.

3. Pop, R., J.R. Shearstone, Q. Shen, Y. Liu, K. Hallstrom, M. Koulnis, J. Gribnau, and M. Socolovsky. 2010. A key commitment step in erythropoiesis is synchronized with the cell cycle clock through mutual inhibition between PU.1 and S-phase progression. *PLoS biology* 8:

4. Nyhan, W.L. 2005. Disorders of purine and pyrimidine metabolism. *Mol Genet Metab* 86:25-33.

5. Giblett, E.R., J.E. Anderson, F. Cohen, B. Pollara, and H.J. Meuwissen. 1972. Adenosine-deaminase deficiency in two patients with severely impaired cellular immunity. *Lancet* 2:1067-1069.

6. Giblett, E.R. 1985. ADA and PNP deficiencies: how it all began. *Ann N Y Acad Sci* 451:1-8.

7. Reichard, P. 1988. Interactions between deoxyribonucleotide and DNA synthesis. *Annu Rev Biochem* 57:349-374.

8. Thelander, L., and P. Reichard. 1979. Reduction of ribonucleotides. *Annu Rev Biochem* 48:133-158.

9. Cohen, A., J. Barankiewicz, H.M. Lederman, and E.W. Gelfand. 1983. Purine and pyrimidine metabolism in human T lymphocytes. Regulation of deoxyribonucleotide metabolism. *J Biol Chem* 258:12334-12340.

10. Eriksson, S., B. Munch-Petersen, K. Johansson, and H. Eklund. 2002. Structure and function of cellular deoxyribonucleoside kinases. *Cell Mol Life Sci* 59:1327-1346.

11. Staub, M., T. Spasokukotskaja, M. Benczur, and F. Antoni. 1988. DNA synthesis and nucleoside metabolism in human tonsillar lymphocyte subpopulations. *Acta Otolaryngol Suppl* 454:118-124.

12. Staub, M., and S. Eriksson. 2006. The Role of Deoxycytidine Kinase in DNA synthesis and Nucleoside Analog Synthesis. In Cancer Drug Discovery and Development: Deoxynucleoside Analogs in Cancer Therapy. G.J. Peters, editor Humana Press Inc., Totowa, NJ. 29-52.

13. Nicander, B., and P. Reichard. 1985. Evidence for the involvement of substrate cycles in the regulation of deoxyribonucleoside triphosphate pools in 3T6 cells. *J Biol Chem* 260:9216-9222.

14. Bianchi, V., E. Pontis, and P. Reichard. 1987. Regulation of pyrimidine deoxyribonucleotide metabolism by substrate cycles in dCMP deaminase-deficient V79 hamster cells. *Mol Cell Biol* 7:4218-4224.

15. Bianchi, V., E. Pontis, and P. Reichard. 1986. Interrelations between substrate cycles and de novo synthesis of pyrimidine deoxyribonucleoside triphosphates in 3T6 cells. *Proceedings of the National Academy of Sciences of the United States of America* 83:986-990.

16. Hoglund, L., E. Pontis, and P. Reichard. 1988. Effects of deoxycytidine and thymidine kinase deficiency on substrate cycles between deoxyribonucleosides and their 5'-phosphates. *Cancer Res* 48:3681-3687.

17. Bianchi, V., P. Ferraro, S. Borella, P. Bonvini, and P. Reichard. 1994. Effects of mutational loss of nucleoside kinases on deoxyadenosine 5'-phosphate/deoxyadenosine substrate cycle in cultured CEM and V79 cells. *J Biol Chem* 269:16677-16683.

18. Carson, D.A., J. Kaye, and J.E. Seegmiller. 1977. Lymphospecific toxicity in adenosine deaminase deficiency and purine nucleoside phosphorylase deficiency: possible role of nucleoside kinase(s). *Proceedings of the National Academy of Sciences of the United States of America* 74:5677-5681.

19. BioGPS. Accessed April 15, 2011. Deoxycytidine Kinase GeneAtlas U133A, gcrma, 203302_at Microarray. In.

20. Carson, D.A., J. Kaye, and D.B. Wasson. 1981. The potential importance of soluble deoxynucleotidase activity in mediating deoxyadenosine toxicity in human lymphoblasts. *J Immunol* 126:348-352.

21. Liu, P., N.A. Jenkins, and N.G. Copeland. 2003. A highly efficient recombineering-based method for generating conditional knockout mutations. *Genome research* 13:476-484.

22. Brown, T. 1993. Southern Blotting. *Current Protocols in Immunology* 10.6:1-9.

23. Korbie, D.J., and J.S. Mattick. 2008. Touchdown PCR for increased specificity and sensitivity in PCR amplification. *Nature protocols* 3:1452-1456.

24. Laing, R.E., M.A. Walter, D.O. Campbell, H.R. Herschman, N. Satyamurthy, M.E. Phelps, J. Czernin, O.N. Witte, and C.G. Radu. 2009. Noninvasive prediction of tumor responses to gemcitabine using positron emission tomography. *Proceedings of the National Academy of Sciences of the United States of America* 106:2847-2852.

25. Radu, C.G., C.J. Shu, E. Nair-Gill, S.M. Shelly, J.R. Barrio, N. Satyamurthy, M.E. Phelps, and O.N. Witte. 2008. Molecular imaging of lymphoid organs and immune activation by positron emission tomography with a new [18F]-labeled 2'-deoxycytidine analog. *Nature medicine* 14:783-788.

26. Ciofani, M., and J.C. Zuniga-Pflucker. 2007. The thymus as an inductive site for T lymphopoiesis. *Annual review of cell and developmental biology* 23:463-493.

27. Taghon, T., M.A. Yui, R. Pant, R.A. Diamond, and E.V. Rothenberg. 2006. Developmental and molecular characterization of emerging beta- and gammadelta-selected pre-T cells in the adult mouse thymus. *Immunity* 24:53-64.

28. Kreslavsky, T., A.I. Garbe, A. Krueger, and H. von Boehmer. 2008. T cell receptor-instructed alphabeta versus gammadelta lineage commitment revealed by single-cell analysis. *The Journal of experimental medicine* 205:1173-1186.

29. Hardy, R.R., C.E. Carmack, S.A. Shinton, J.D. Kemp, and K. Hayakawa. 1991. Resolution and characterization of pro-B and pre-pro-B cell stages in normal mouse bone marrow. *The Journal of experimental medicine* 173:1213-1225.

30. Hardy, R.R., P.W. Kincade, and K. Dorshkind. 2007. The protean nature of cells in the B lymphocyte lineage. *Immunity* 26:703-714.

31. Liu, Y., R. Pop, C. Sadegh, C. Brugnara, V.H. Haase, and M. Socolovsky. 2006. Suppression of Fas-FasL coexpression by erythropoietin mediates erythroblast expansion during the erythropoietic stress response in vivo. *Blood* 108:123-133.

32. Koulnis, M., R. Pop, E. Porpiglia, J.R. Shearstone, D. Hidalgo, and M. Socolovsky. 2011. Identification and analysis of mouse erythroid progenitors using the CD71/TER119 flow-cytometric assay. *J Vis Exp*

33. Macallan, D.C., C.A. Fullerton, R.A. Neese, K. Haddock, S.S. Park, and M.K. Hellerstein. 1998. Measurement of cell proliferation by labeling of DNA with stable isotope-labeled glucose: studies in vitro, in animals, and in humans. *Proc Natl Acad Sci U S A* 95:708-713.

34. Neese, R.A., L.M. Misell, S. Turner, A. Chu, J. Kim, D. Cesar, R. Hoh, F. Antelo, A. Strawford, J.M. McCune, M. Christiansen, and M.K. Hellerstein. 2002. Measurement in vivo of proliferation rates of slow turnover cells by 2H2O labeling of the deoxyribose moiety of DNA. *Proc Natl Acad Sci U S A* 99:15345-15350.

35. Busch, R., R.A. Neese, M. Awada, G.M. Hayes, and M.K. Hellerstein. 2007. Measurement of cell proliferation by heavy water labeling. *Nature protocols* 2:3045-3057.

36. Herzog, S., M. Reth, and H. Jumaa. 2009. Regulation of B-cell proliferation and differentiation by pre-B-cell receptor signalling. *Nature reviews* 9:195-205.

37. Bassing, C.H., W. Swat, and F.W. Alt. 2002. The mechanism and regulation of chromosomal V(D)J recombination. *Cell* 109 Suppl:S45-55.

38. Falk, I., J. Biro, H. Kohler, and K. Eichmann. 1996. Proliferation kinetics associated with T cell receptor-beta chain selection of fetal murine thymocytes. *The Journal of experimental medicine* 184:2327-2339.

39. Joachims, M.L., P.A. Marble, A.B. Laurent, P. Pastuszko, M. Paliotta, M.R. Blackburn, and L.F. Thompson. 2008. Restoration of adenosine deaminase-deficient human thymocyte development in vitro by inhibition of deoxynucleoside kinases. *J Immunol* 181:8153-8161.

CHAPTER 3

Deletion of Deoxycytidine Kinase Causes dCTP pool Deficiency, DNA Replication Stress, and Cell Cycle Arrest in Murine Hematopoietic Progenitors

Abstract

Mice deficient for deoxycytidine kinase activity display abnormal lymphopoiesis and erythropoiesis. The differentiation blocks experienced by dCK deficient hematopoietic cells coincide with developmental stages characterized by massive clonal expansions. Prior to the work presented in this Chapter, the cellular and molecular mechanisms underlying the differentiation blocks associated with dCK deletion were unknown Here we demonstrate that the *dCK*$^{-/-}$ hematopoietic phenotype is cell-autonomous to bone marrow derived cells. We then investigate a potential requirement for dCK during V(D)J recombination by engineering the expression of a rearranged T cell receptor (TCR) on the *dCK*$^{-/-}$ genetic background. Next, we show that intracellular dCTP pools are severely depleted in developing *dCK*$^{-/-}$ T cells, B cells, and erythroid cells. *In vivo*, actively proliferating lymphoid and erythroid subpopulations which experience dCTP deficiency display early S-phase arrest, and biomarkers indicative of the activation of the replication stress response pathway. Lastly, using a tamoxifen-inducible conditional knockout mouse model we demonstrate that the S-phase arrest and replication stress phenotypes observed in *dCK*$^{-/-}$ mice are specifically caused by the absence of dCK activity in adult lymphoid and erythroid progenitor populations. Collectively, these data indicate that deletion of dCK depletes dCTP pools in dividing lymphoid and erythroid progenitors in the thymus and bone marrow. In turn, dCTP deficiency triggers the activation of the replication stress response pathway, thus causing both S-phase arrest and differentiation blocks affecting lymphoid and erythroid precursors.

Introduction

A knockout mouse model of deoxycytidine kinase (dCK) was previously generated to investigate the role played by this deoxyribonucleoside (dN) salvage kinase in hematopoietic development (1). We showed that *dCK*$^{-/-}$ mice display severe defects in T cell, B cell, and erythroid development. The causes of these defects remained, until now, unknown. Data in the literature point to several potential scenarios that may explain the observed developmental defects affecting the *dCK*$^{-/-}$ mice. Genetic mutations in enzymes of nucleotide metabolism cause immunodeficiency syndromes similar to that observed in the *dCK*$^{-/-}$ mice (2-6). Syndromes such as deficiencies in adenosine deaminase (ADA) and purine nucleoside phosphorylase (PNP) cause developing lymphocytes to be eliminated because of cell non-autonomous mechanisms of metabolic dysfunctions in non-hematopoietic tissues (5, 7). Therefore, it is important to test the cell autonomous versus cell non-autonomous nature of the *dCK*$^{-/-}$ phenotype in order to gain insight into the observed hematopoietic phenotypes.

Another mechanism by which the absence of dCK may cause defective lymphoid development is related to a possible role for dCK in supporting DNA damage repair during the recombination of T cell and B cell antigen receptor genes (8, 9). Variable, Diverse, Joining (V(D)J) gene segment recombination is the process by which antigenic diversity is first created in developing T cells and B cells (8, 9). The process depends upon the induction of DNA double-strand breaks (DSBs) at antigen receptor gene loci by the recombination activating genes 1 and 2 (*RAG1* and *RAG2*) (10). These DSBs are then repaired by non-homologous end joining (NHEJ) mechanisms to generate unique DNA sequences at antigen receptor loci (8). Failure to repair the DNA damage induced

during V(D)J recombination causes arrested lymphocyte development in various genetic models (8, 9). dCK has previously been implicated as functioning in DNA damage repair pathways (11-13). It is therefore possible that the arrested lymphocyte development in *dCK*$^{-/-}$ mice might be caused by defective V(D)J recombination in developing T and B cells.

An established experimental method to rescue defective T cell development and B cell development caused by impaired V(D)J recombination is to transgenically express fully rearranged antigen receptor genes (14-17). Therefore, the generation of *dCK*$^{-/-}$ mice that transgenically express fully rearranged T cell receptor (TCR) genes or B cell receptor (BCR) genes could help answer questions regarding defective lymphocyte development in *dCK*$^{-/-}$ mice.

Alternatively, hematopoietic defects in the *dCK*$^{-/-}$ mice may reflect a limited capability of developing T cells, B cells, and erythroid cells to synthesize and maintain sufficient dNTP pools. Since nucleotide pool imbalances are known to cause DNA synthesis defects and DNA replication stress (18-20), analyses of dNTP pool levels, DNA synthesis *in vivo*, and the possible presence of replication stress markers in highly proliferative lymphoid and erythroid progenitors might also yield insights into the biological function of dCK *in vivo*.

To investigate these and other possibilities, we determined whether abnormal hematopoiesis in *dCK*$^{-/-}$ mice was cell autonomous to bone marrow-derived cells. We also investigated a potential requirement for dCK in DNA damage repair during V(D)J recombination in developing thymocytes by generating *dCK*$^{-/-}$ mice that express a fully rearranged transgenic TCR. We quantified dNTP pools in developing lymphoid and

erythroid cells from WT and *dCK*$^{-/-}$ mice, and we examined cell cycle kinetics and activation of the DNA replication stress response pathway in highly proliferative subpopulations.

Material and Methods

Mice

Pmel-1 transgenic mice (Strain: *B6.Cg Thy1*^{a}*-Tg(TcraTcrb)8Rest/J*; Stock: 005023) and *CreERT2* transgenic mice (Strain *B6.Cg-Tg(UBC-cre/ERT2)1Ejb/J*; Stock 008085) were purchased from The Jackson Laboratory (Bar Harbor, ME). *Pmel-1* mice were genotyped using Touchdown PCR conditions (21) with primers oIMR3388 (5'-GGT CCT GTG GCT CCA GTT TAA T-3') and oIMR3389 (5'-CTG CTT AAC CTG TCC CTC ATG T-3') to amplify the transgenic TCRα chain; and oIMR3390 (5'- CTG GGC AGT GTT CTG TCT CC-3') and oIMR3391 (5'-ACC ATG GTC ATC CAA CAC AG-3') to amplify the transgenic TCRβ chain. *CreERT2* mice were genotyped with oIMR1084 5'-GCG GTC TGG CAG TAA AAA CTA TC-3' and oIMR1085 (5'-GTG AAA CAG CAT TGC TGT CAC TT-3') to identify the CreERT2 transgene. *dCK*$^{flox/flox}$ mice were genotyped with primer FLP Forward (5'-CAG AAG AGG GCA CCA GAT CC-3') and FLP Reverse (5'-TTT TGT TAT TGT GGG TTT TTC C-3') to differentiate between *dCK*^{flox} and *dCK*$^{+}$ alleles. *dCK*$^{-/-}$ mice containing the Neomycin resistance cassette were identified using primers Long Arm Forward (5'-AAC TGC TGA GCC ATC TCT CC-3') and Cre Reverse (5'-GGG CTC TAT GGC TTC TGA GG-3') to identify the *dCK*$^{-}$ allele.

Bone marrow transplant experiments

Mice receiving bone marrow transplant were 6-8 weeks old at time of irradiation. Recipient mice received 950 rad of dose, and were then injected with 10^6 whole bone marrow cells. Mice were subsequently maintained on a regimen of acidified water supplemented with trimethoprim-sulfamethoxazole antibiotic for 4 weeks post-irradiation. Hematopoietic reconstitution was allowed to proceed for 6 weeks before analysis.

Tissue preparation

Single-cell suspensions were prepared from bone marrow by flushing femur, tibia and humerus bones with DMEM supplemented with 2% FBS using 25 G needles, followed by 70 μm filtration. For bone marrow fraction purification, whole bone marrow was depleted of mature red blood cells by overlaying cell suspensions on a solution of 16% iodixanol (Sigma-Aldrich, D1556), 0.63% NaCl, 10 mM HEPES (pH 7.4), and 0.1% NaN_3, followed by centrifugation at 900*g* for 15 minutes. The mononuclear cell-containing supernatant was transferred and washed twice prior to antibody staining or dNTP extraction. Single-cell suspensions of thymus were prepared by mechanical dissociation using frosted glass slides in DMEM supplemented with 2% FBS and 50 μg/mL DNaseI (Roche) and passed through 70 μm sterile filters. $CD4^-/CD8^-$ thymocytes were purified from whole thymocyte suspensions using combined CD4 and CD8 negative selection kits (Invitrogen) to deplete $CD4^+$ and $CD8^+$ populations.

Intracellular dNTP pool measurements

Purified hematopoietic cell populations were counted and pelleted. Pellets were then suspended in 1 mL of ice-cold 60% methanol, vortexed for 1 min and stored overnight at -20°C. The following day, the lysates were boiled for 3 min and then centrifuged for 15 min at 17,000*g* at 4°C. Supernatants were evaporated overnight in a SVC100H SpeedVac Concentrator (Savant). Dry pellets were resuspended in 100 µL of ddH_2O, vortexed and centrifuged for 15 min at 17,000 *g* at 4°C to clear insoluble debris. 5 µL of concentrated lysate was used in a 25 µL reaction volume. Reactions were carried out for 2 hrs according to published conditions and reagents (22)**.**

DNA content staining and intracellular detection of BrdU and pH2A.X

BrdU (1 milligram) was administered by intraperitoneal injection. Tissues were collected, antibody-stained for surface antigens to identify DN3b thymocytes, Hardy Fraction B-C, and bone marrow EryA populations as described in Chapter 2. Surface-stained cells were then fixed and permeabilized for intracellular detection of BrdU and pH2A.X using a BrdU-FITC kit staining protocol and reagents (BD Biosciences). Cells were then intracellularly stained with BrdU-FITC and/or pH2A.X antibodies conjugated to FITC (Millipore, Clone JBW301) or Alexa647 (BD Biosciences, Clone N1-431). The total DNA content was assessed by staining with DAPI (Roche) at 1 µg/mL final concentration in PBS containing 2% FBS.

Western blots

Purified hematopoietic cell populations were lysed in 1X RIPA buffer containing 1X Halt Protease/Phosphatase Inhibitor (Pierce, 78440); supernatants were isolated after centrifugation at 17,000*g* for 15 min. Lysates were mixed with 1X Laemmli-SDS loading buffer, boiled, electrophoresed, and transferred to nitrocellulose membranes for immunoblotting. Monoclonal rabbit anti-Phospho-CHK1 (Ser345) (Clone 133D3); monoclonal mouse anti-CHK1 (clone 2G1D5) was purchased from Cell Signaling Technology**.**

Tamoxifen-induced deletion of dCK

Tamoxifen (Sigma-Aldrich, T5648) was dissolved in vegetable oil at 20 mg/mL and aliquots were stored at -20°C. 100 µL of tamoxifen solution was administered once a day for 4 days by intraperitoneal injection.

Results

The dCK$^{-/-}$ phenotype is cell autonomous to bone marrow-derived cells.

Bone marrow transplant (BMT) experiments were performed to determine whether the *dCK*$^{-/-}$ phenotype is autonomous to hematopoietic cells. WT recipient mice were lethally irradiated and reconstituted with whole bone marrow from WT and *dCK*$^{-/-}$ donor mice. Six weeks post-BMT, recipient mice were imaged by mPET/CT using ^{18}F-FAC to determine relative WT or *dCK*$^{-/-}$ bone marrow engraftment. Mice transplanted with WT marrow exhibited normal ^{18}F-FAC retention in bone marrow, thymus, and

spleen, while mice transplanted with *dCK*$^{-/-}$ marrow displayed ^{18}F-FAC uptake only in the gastrointestinal tract (Figure 3.1, A). The mPET/CT imaging data indicated that the *dCK*$^{-/-}$ donor bone marrow had successfully engrafted in the WT recipients.

Analyses of the BMT mice yielded the following findings: WT mice transplanted with *dCK*$^{-/-}$ marrow displayed hematopoietic characteristics similar to germline *dCK*$^{-/-}$ mice. Mice transplanted with *dCK*$^{-/-}$ bone marrow displayed massive splenomegaly (Figure 3.1, B and C; N=6 mice/recipient group; $P<0.0001$), indicating that the abnormal erythroid phenotype of germline *dCK*$^{-/-}$ mice was transferred to the WT recipient mice. Furthermore, the thymic hypoplasia phenotype of germline *dCK*$^{-/-}$ mice was also transferred to WT recipient mice. Thus, mice transplanted with *dCK*$^{-/-}$ bone marrow averaged $5x10^6$ viable thymocytes, while mice transplanted with WT bone marrow averaged $100x10^6$ viable thymocytes (Figure 3.1, D; N=6 mice/recipient group; $P<0.0001$). The thymic hypoplasia of mice transplanted with *dCK*$^{-/-}$ bone marrow was accompanied by a dramatic skewing of thymocyte differentiation towards the DN stage (Figure 3.1, E), identical to the phenotype observed in the germline *dCK*$^{-/-}$ mice. Based on the results from the BMT experiments, we conclude that the *dCK*$^{-/-}$ phenotype can be transplanted into WT recipients even though the recipient mice retain dCK activity in non-hematopoietic tissues.

Next, we determined if WT bone marrow cells can rescue the *dCK*$^{-/-}$ phenotype. Prior to transplantation (pre-BMT), germline *dCK*$^{-/-}$ mice were scanned by mPET/CT using the dCK-specific probe ^{18}F-FAC. The ^{18}F-FAC PET scans documented the lack of dCK activity in hematopoietic tissues from designated recipient *dCK*$^{-/-}$ mice (Figure 3.2, A). These mice were then lethally irradiated and transplanted with bone marrow from

WT donor mice. Six weeks after transplant (post-BMT), ^{18}F-FAC mPET/CT scans of the *dCK*$^{-/-}$ mice transplanted with WT bone marrow showed functional dCK activity in the bone marrow, thymus, and spleen (Figure 3.2, A). These imaging results thus indicated that the WT marrow successfully engrafted in *dCK*$^{-/-}$ mice and likely restored normal hematopoiesis in the 6 weeks since transplantation.

Analyses of germline *dCK*$^{-/-}$ mice transplanted with WT bone marrow revealed normal hematopoiesis that was undistinguishable from that observed in WT mice transplanted with WT marrow. Moreover, *dCK*$^{-/-}$ recipient mice had spleen sizes and weights that were statistically indistinguishable from spleens retrieved from WT recipient mice (Figure 3.2, B and C). These results indicated that the erythroid abnormalities previously present in *dCK*$^{-/-}$ mice were corrected by the BMT transplant. Additionally, *dCK*$^{-/-}$ recipient mice averaged numbers of total viable thymocytes that were statistically indistinguishable from those from WT recipient mice (Figure 3.2, D). Furthermore, thymocytes from *dCK*$^{-/-}$ recipient mice also had DN and DP thymocyte differentiation profiles that were indistinguishable from those observed in thymocytes from WT recipient mice (Figure 3.2, E). The findings from both sets of BMT experiments therefore demonstrated that the *dCK*$^{-/-}$ phenotype can be transplanted into normal mice and that it can be rescued through the transplantation of WT bone marrow.

Forced expression of a transgenic TCR does not rescue the dCK$^{-/-}$ *thymocyte phenotype*

To address the possibility that the T cell developmental phenotype in *dCK*$^{-/-}$ mice was caused by defective V(D)J recombination, we generated *dCK*$^{-/-}$ mice that

transgenically express a fully rearranged TCR. We chose to use mice that express the *Pmel-1* transgenic TCR (*Pmel*^{Tg}) that recognizes a mouse melanocyte epitope presented on MHC-I H-2D^{b} molecules (23). The MHC-I H-2D^{b} molecules of *Pmel*^{Tg} mice are also expressed in C57Bl/6-129Sv/J hybrid mice like those of the *dCK*$^{-/-}$ line (24), thus making the transgenic TCR compatible to stimulate the differentiation of transgenic CD8^{+} thymocytes in the *dCK*$^{-/-}$ background. We first intercrossed *dCK*$^{+/+}$ *Pmel*^{Tg} mice with *dCK*$^{-/-}$ *Pmel*^{Neg} mice to produce *dCK*$^{+/-}$ *Pmel*^{Tg} progeny. *dCK*$^{+/-}$ *Pmel*^{Tg} mice were then crossed to *dCK*$^{-/-}$ *Pmel*^{Neg} mice to yield *dCK*$^{+/-}$ *Pmel*^{Tg} and *dCK*$^{-/-}$ *Pmel*^{Tg} littermates for developmental analysis.

Thymocytes from *dCK*$^{+/-}$ *Pmel*^{Tg} and *dCK*$^{-/-}$ *Pmel*^{Tg} littermates were analyzed for the expression of TCR Vβ13, the TCRβ chain subtype that constitutes half of the *Pmel-1* TCR (23). CD8^{+} thymocyte populations from transgenic *dCK*$^{+/-}$ and *dCK*$^{-/-}$ mice each averaged having 85% of cells being positive for TCR Vβ13 expression (Figure 3.3, A). This indicated that expression of the transgenic TCR was equivalent between the genetic lines and thus made direct comparison of the transgenic TCR's effects upon differentiation possible. However, despite successful expression of the rearranged TCR in *dCK*$^{-/-}$ mice, total thymocyte cellularity was not rescued in transgenic *dCK*$^{-/-}$ mice when compared to transgenic *dCK*$^{+/-}$ mice. Whereas *dCK*$^{+/-}$ *Pmel*^{Tg} mice averaged 12x10^{7} viable thymocytes, *dCK*$^{-/-}$ *Pmel*^{Tg} mice possessed significantly fewer viable thymocytes with an average of 2x10^{7} cells per mouse (Figure 3.3, B; N=4 mice/genotype; P<0.0001). Staining whole thymocytes for CD4 and CD8 to identify DN and DP thymocyte populations revealed that DN to DP proportion abnormalities were not rescued in *dCK*$^{-/-}$ *Pmel*^{Tg} mice (Figure 3.3, C). While the percentages of DN

thymocytes between transgenic *dCK*$^{+/-}$ and *dCK*$^{-/-}$ mice did not differ in a statistically significant manner, the percentage of DP thymocytes between these two genotypes did differ significantly (Figure 3.3, D; N=3 mice/genotype; $P<0.004$). Thus, the failure of the transgenic TCR to rescue thymocyte development in transgenic *dCK*$^{-/-}$ mice indicated that defective V(D)J recombination was likely not responsible for the block in the development of *dCK*$^{-/-}$ T cells.

***dCK*$^{-/-}$ hematopoietic lineages have drastically depleted intracellular dCTP pools.**

Because dCK is capable of supplying cells with all four dNTPs needed for DNA replication and repair (25), we quantified dNTP pools in hematopoietic lineages affected by dCK inactivation. We purified DN thymocytes, whole bone marrow B cells, and nucleated bone marrow erythroblasts and assayed their intracellular dNTP pools. In each affected lineage, dCTP pools were significantly reduced in *dCK*$^{-/-}$ cells relative to WT cells, averaging 2.7 to 7.9-times lower dCTP concentrations in *dCK*$^{-/-}$ cells (Figure 3.4; $P<0.001$ to 0.03). In contrast, we could not demonstrate statistically significant differences in dTTP, dATP and dGTP pools in *dCK*$^{-/-}$ cells. These data indicate that, despite dCK's ability to help provide all four dNTPs, the enzyme appears to primarily supply dCTP to developing lymphocytes and erythroid cells.

***Proliferating dCK*$^{-/-}$ hematopoietic cells undergo S-phase arrest**

Having determined that *dCK*$^{-/-}$ hematopoietic progenitors experience dCTP pool deficiency, we next analyzed the ability of these cells to replicate their DNA. We therefore analyzed the cell cycle profiles generated by total DNA content staining in

highly proliferative DN3b thymocytes, Hardy Fraction B-C cells, and bone marrow EryA erythroblast subpopulations. While the percentages of *dCK*$^{-/-}$ DN3b and Hardy B-C cells in S-phase appeared normal, the distribution of these cells in the S-phase appeared to be shifted towards early S-phase rather than being evenly distributed throughout S-phase as was observed in WT cells (Figure 3.5, A). Unlike the comparable S-phase percentages observed between WT and *dCK*$^{-/-}$ developing lymphocytes, *dCK*$^{-/-}$ EryA cells averaged approximately 1.8-times as many cells in S-phase cells than were observed for WT EryA cells (Figure 3.5, A; N=3 mice/genotype; $P<0.01$). Furthermore, *dCK*$^{-/-}$ EryA S-phase cells had a pronounced early S-phase shift. While these findings strongly suggest that *dCK*$^{-/-}$ cells have abnormal early S-phase kinetics, these data alone do not show unequivocally that *dCK*$^{-/-}$ cells proliferate abnormally *in vivo*.

In order to determine the actual *in situ* S-phase kinetics of the proliferating subpopulations, we performed *in vivo* DNA replication assays using bromodeoxyuridine (BrdU). BrdU labels all cells that are in S-phase by the virtue of its incorporation into newly synthesized DNA (26). We pulsed WT and *dCK*$^{-/-}$ mice with BrdU by intraperitoneal injection and then isolated thymus and bone marrow cells 1 hour post-injection in order to determine BrdU incorporation in DN3b thymocytes, Hardy Fraction B-C cells, and EryA erythroblasts. Surprisingly, unlike the S-phase percentages generated by total DNA content staining alone, the BrdU assay indicated that significantly more *dCK*$^{-/-}$ cells from each of the three probed lineages were in active S-phase (i.e. BrdU^{+}) than were WT cells (Figure 3.5, B-D). These results indicated that *dCK*$^{-/-}$ cells are hyperproliferative relative to WT cells.

However, despite the fact that *dCK*$^{-/-}$ populations averaged more BrdU^{+} cells than WT populations, *dCK*$^{-/-}$ cells displayed clear and reproducible abnormalities in BrdU incorporation. BrdU^{+} *dCK*$^{-/-}$ cells were in fact primarily in early S-phase rather than being distributed evenly throughout S-phase as was observed in BrdU^{+} WT cells (Figure 3.5, B-D). Furthermore, overlaying matched WT and *dCK*$^{-/-}$ populations to compare BrdU incorporation revealed that BrdU^{+} WT cells had approximately 4-fold greater BrdU fluorescence than BrdU^{+} *dCK*$^{-/-}$ cells (Figure 3.5, E-G; N=4 mice/genotype; $P<0.001$ to 0.01). Since the relative fluorescence of BrdU incorporation into the DNA is directly proportional to the amount of newly synthesized DNA in the proliferating cells, we concluded that *dCK*$^{-/-}$ cells in S-phase synthesize one-fourth the amount of DNA as observed in S-phase WT cells.

The results of the 1 hour BrdU pulse experiment were intriguing and warranted further analyses using pulse-chase conditions to more precisely determine the kinetics of DNA synthesis by the BrdU^{+} *dCK*$^{-/-}$ cells. Free circulating BrdU is rapidly eliminated from the body of a mouse over a 1 hour period, creating natural “chase” conditions at time points following 1 hour (27, 28). It is during the chase period that BrdU^{+} cells’ progression through S-phase and into G_2/M can be traced for 5 to 8 hours (28). Successful progression through S-phase creates a characteristic BrdU “Chase Gap” as BrdU^{+} cells move forward with DNA synthesis in the absence of new BrdU incorporation (28). Additionally, cells entering S-phase in the absence of BrdU can be visualized by flow cytometry because they are BrdU^{-} but have a DNA content that is greater than G_1 cells (BrdU^{-} S-phase).

We pulsed mice with BrdU by intraperitoneal injection and then isolated bone marrow and thymus cells 4 and 6 hours post-injection, thereby creating approximate 3 and 5 hour chase conditions, respectively. Whereas $BrdU^+$ WT cells generated characteristic BrdU Chase Gaps at 3 and 5 hours of BrdU chase, significantly more *dCK*$^{-/-}$ cells resided in the Chase Gap gates, thereby indicating arrested DNA synthesis (Figure 3.6, A-C; N=4 mice/condition; $P<0.01$ to 0.001). Furthermore, *dCK*$^{-/-}$ cells failed to generate $BrdU^-$ S-phase populations during the chase (Figure 3.6, A-C), thereby indicating abnormal early S-phase kinetics. These BrdU pulse-chase experiments thus demonstrated that *dCK*$^{-/-}$ DN3b thymocytes, Hardy Fraction B-C cells, and EryA erythroblasts experience early S-phase arrest *in vivo*.

Proliferating dCK$^{-/-}$ *hematopoietic cells activate the Replication Stress Response pathway*

Since *dCK*$^{-/-}$ hematopoietic progenitors experience both dCTP pool deficiency and early S-phase arrest, it is likely that these cells activate the replication stress response (RSR) pathway (29, 30). The RSR pathway is activated by DNA lesions during S-phase and is primarily modulated through an ATR and checkpoint kinases 1 (Chk1) signaling pathway to induce cell cycle arrest and DNA repair (31). The RSR pathway is essential for preserving genomic integrity and the proliferative capacity of dividing cells (32). To determine if there was evidence of RSR pathway activation in *dCK*$^{-/-}$ hematopoietic progenitors, we purified DN thymocytes, total bone marrow B cells, and bone marrow erythroblasts and immunoblotted for Chk1 phosphorylated on Ser345 (pChk1), which is an activated form of Chk1 found during RSR pathway activation (33).

We found elevated levels of pChk1 in *dCK*$^{-/-}$ lysates from all three cell types (Figure 3.7, A-C), indicating activation of the RSR pathway in *dCK*$^{-/-}$ cells *in vivo*.

We then sought to determine if markers of the RSR pathway are present in proliferating subsets of *dCK*$^{-/-}$ hematopoietic progenitors. We therefore stained WT and *dCK*$^{-/-}$ DN3b thymocytes, Hardy Fraction B-C cells, and bone marrow EryA cells for H2A.X phosphorylated on Ser139 (pH2A.X), another key marker of an activated RSR pathway (33-35). *dCK*$^{-/-}$ cells had 55 to 77-times more cells staining positive for pH2A.X than WT cells (Figure 3.6, D-F; N=7 mice/genotype; $P<0.0001$). Furthermore, pH2A.X^{+} cells were primarily located in early S-phase (Figure 3.6, D-F), consistent with the previously identified S-phase arrest phenotypes in *dCK*$^{-/-}$ lymphoid and erythroid progenitors (Figure 3.5). We therefore concluded that the RSR pathway is likely activated in early S-phase in *dCK*$^{-/-}$ cells to induce *in vivo* cell cycle arrest that is responsible for the observed hematopoietic defects associated with dCK deletion.

RSR responses in dCK$^{-/-}$ hematopoietic cells are intrinsic to adult progenitors

Although global *dCK*$^{-/-}$ mice demonstrated reproducible transplantation of their hematopoietic defects into WT mice, one caveat that had to be addressed was the possibility that the observed hematopoietic development defects in adult mice were the result of permanent defects caused in *dCK*$^{-/-}$ hematopoietic stem cells (HSCs) during embryogenesis. Defects incurred in *dCK*$^{-/-}$ HSCs during embryogenesis could thus result in defective adult hematopoiesis regardless of whether dCK is expressed in adult tissues. To address this possibility, we generated conditional knockout mice in which dCK can be inactivated during adulthood by the administration of the estrogen receptor

antagonist tamoxifen. For this, we crossed *dCK*$^{flox/flox}$ mice (*Cre*^{Neg}) to mice that ubiquitously express the *CreERT2* transgene (36) to produce *dCK*$^{flox/flox}$ *CreERT2*^{Tg} (*Cre*^{Tg}) conditional knockout mice. CreERT2 is a fusion of Cre recombinase and an estrogen receptor mutant (ERT2) that enters the nucleus to target *flox* alleles only when 4-hydroxytamoxifen binds to the ERT2 portion of CreERT2 to promote nuclear translocation (37). Therefore, conditional knockout mice should develop normally with dCK activity intact until the administration of tamoxifen induces genetic deletion of *dCK* in adult mice.

Cre^{Tg} mice were scanned by mPET/CT with ^{18}F-FAC to confirm functional activity of dCK prior to administration of tamoxifen (Pre-TAM). These scans demonstrated that ^{18}F-FAC probe retention in the hematopoietic tissues of *Cre*^{Tg} mice was indistinguishable from WT mice, indicating that *dCK*^{flox} allele did not significantly affect dCK activity. *Cre*^{Tg} mice were then treated with 4 doses of tamoxifen by intraperintoneal injection over 4 days, and then were scanned again by ^{18}F-FAC mPET/CT, one day following the last injection of tamoxifen (Post-TAM) (Figure 3.8, A). The results from these scans demonstrated that tamoxifen treatment drastically reduced dCK activity throughout the bodies of *Cre*^{Tg} mice.

After demonstrating successful post-developmental inactivation of dCK activity in *Cre*^{Tg} mice, we sought to determine if the absence of dCK in treated *Cre*^{Tg} mice induces DNA replication defects and pH2A.X upregulation over treated *Cre*^{Neg} control mice. As a baseline control, some *Cre*^{Neg} and *Cre*^{Tg} were mock treated by injecting vegetable oil vehicle for 4 days and were then immunophenotyped to see if mock treatment caused *Cre*^{Tg} mice to display any differentiation defects or pH2A.X upregulation. We stained

whole thymocytes from mock treated *Cre*^{Neg} and *Cre*^{Tg} mice for CD4 and CD8 markers and found no differences in DN and DP proportions between the two genotypes (Figure 3.8, B). Nor did we detect any significant presence of pH2A.X in DN3b thymocytes from mock treated *Cre*^{Tg} mice (Figure 3.8, C). We concluded from these control measurements that untreated or mock treated *Cre*^{Tg} mice have normal hematopoietic development that lacks significant RSR activation.

We then deleted dCK in *Cre*^{Tg} mice and performed 3 hour BrdU chase studies. We found that *Cre*^{Tg} mice treated with tamoxifen had 2 to 6-times more DN3b thymocytes, Hardy Fraction B-C cells, and bone marrow EryA cells present in the BrdU Chase Gaps than did cells from tamoxifen-treated *Cre*^{Neg} mice (Figure 3.8, D-F, Top panels; N=2 mice/genotype). The failure of *Cre*^{Tg} cells to progress through early S-phase indicated that they were arrested in early S-phase in a manner similar to that observed in the global *dCK*$^{-/-}$ cells which undergo cell cycle arrest. Furthermore, 19 to 36-times more DN3b thymocytes, Hardy B-C cells, and bone marrow EryA cells from *Cre*^{Tg} mice stained positive for pH2A.X than did *Cre*^{Neg} cells (Figure 3.8, D-F, Bottom panels; N=4 mice/genotype). Similar to the pH2A.X staining patterns in *dCK*$^{-/-}$ cells, pH2A.X staining in *Cre*^{Tg} cells was also mainly found in cells in early S-phase. The recapitulation of cell cycle arrest and apparent RSR pathway activation in conditional knockout lymphoid and erythroid cells led us to conclude that the global *dCK*$^{-/-}$ phenotype is specifically caused by the absence of intrinsic dCK activity in adult hematopoietic progenitor cells.

Discussion

Studies presented in this chapter allowed us to draw the following conclusions: (i), the *dCK*$^{-/-}$ phenotype is cell autonomous to bone marrow-derived cells, indicating that hematopoietic progenitors need intrinsic dCK activity to support development; (ii), hematopoietic progenitor populations from *dCK*$^{-/-}$ mice suffer from severe dCTP deficiency; (iii), *dCK*$^{-/-}$ DN3b thymocytes, Hardy Fraction B-C cells, and bone marrow EryA cells exhibit significant S-phase arrest phenotypes; (iv), the early S-phase arrest phenotypes are directly associated with the expression of activated RSR pathway markers of pChk1 and pH2A.X. Together, these data indicate that the developmental defects observed in *dCK*$^{-/-}$ lymphoid and erythroid progenitors likely reflect DNA replication stress and cell cycle arrest caused by dCTP pool deficiency.

In this chapter, we have laid down the foundation for future studies to understand exactly why developing lymphoid and erythroid progenitors critically require dCK activity to prevent the dCTP pool deficiency, replication stress and early S-phase arrest *in vivo*. A potential explanation for these defects may be that developing lymphoid and erythroid cells have a limited ability to produce dCTP through the *de novo* pathway of nucleotide biosynthesis and therefore must rely upon dCK to supplement this essential dNTP pool. Microenvironmental conditions in the bone marrow and thymus might impair RNR's activity such that this critical regulator of *de novo* synthesis pathway can only efficiently contribute to dTTP, dATP, and dGTP pools in developing lymphoid and erythroid cells. Further studies into the mechanisms of RNR regulation in developing T cells, B cells, and erythroid cells would thus provide valuable insight why these cells depend upon dN salvage through dCK to supplement their dCTP pools.

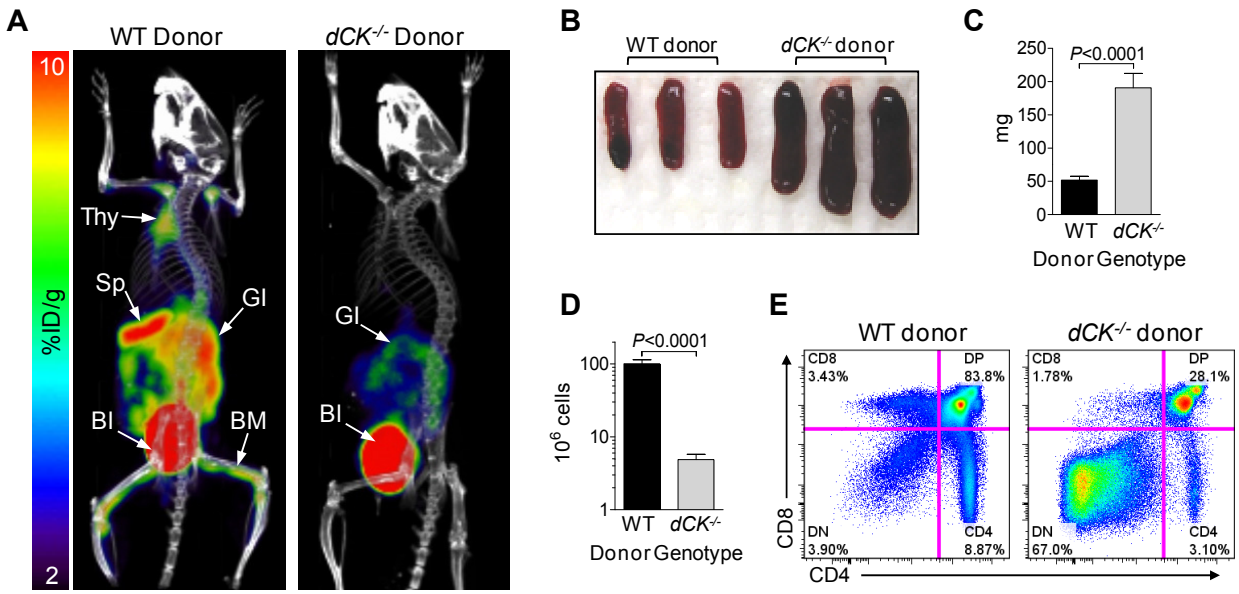


Figure 3.1. *dCK*$^{-/-}$ hematopoietic defects are transplantable into WT mice. (**A**) WT mice were scanned with ^{18}F-FAC mPET/CT 6 weeks after lethal irradiation followed by bone marrow transplantation with cells from WT or *dCK*$^{-/-}$ donor mice. Images scaled 2-10% of injected dose/gram of tissue (%ID/g). BM-bone marrow; Thy-Thymus; Sp-Spleen; GI-Gastrointestinal tract; Bl-Bladder. (**B-C**) Gross sizes (**B**), and weights (**C**), of spleens recovered from WT mice transplanted with WT or *dCK*$^{-/-}$ donor bone marrow. Graphs are average values + SEM (N=6 mice/donor genotype; $P<0.0001$). (**D-E**) Total viable thymocytes recovered (**D**), and CD4/CD8 staining of whole thymocytes (**E**), from thymi from WT mice transplanted with WT or *dCK*$^{-/-}$ donor bone marrow. Graphs are average values + SEM (N=6 per donor genotype; $P<0.0001$).

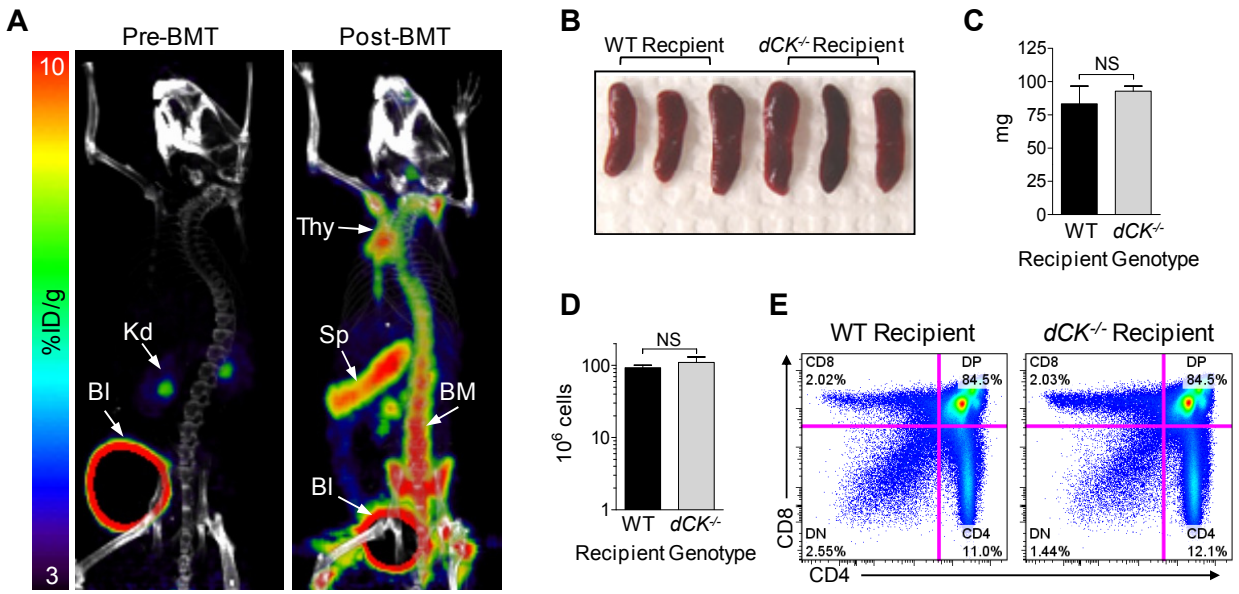


Figure 3.2. *dCK*$^{-/-}$ hematopoietic defects are rescued by bone marrow transplantation with WT cells. (**A**) A *dCK*$^{-/-}$ mouse scanned with ^{18}F-FAC mPET/CT prior to lethal irradiation and bone marrow transplant (Pre-BMT), and 6 weeks after bone marrow transplantation using cells from a WT donor mouse (Post-BMT). Images scaled 3-10% of injected dose/gram of tissue (%ID/g). BM-bone marrow; Thy-Thymus; Sp-Spleen; Kd-Kidney; Bl-Bladder. (**B-C**) Gross sizes (**B**), and weights (**C**), of spleens recovered from WT and *dCK*$^{-/-}$ recipient mice transplanted with WT donor bone marrow. Graphs are average values + SEM (N=3 mice/recipient genotype; NS-Not statistically significant). (**D-E**) Total viable thymocytes recovered (**D**), and CD4/CD8 staining of whole thymocytes (**E**), from thymi from WT and *dCK*$^{-/-}$ recipient mice transplanted with WT donor bone marrow. Graphs are average values + SEM (N=3 mice/recipient genotype; NS-Not statistically significant).

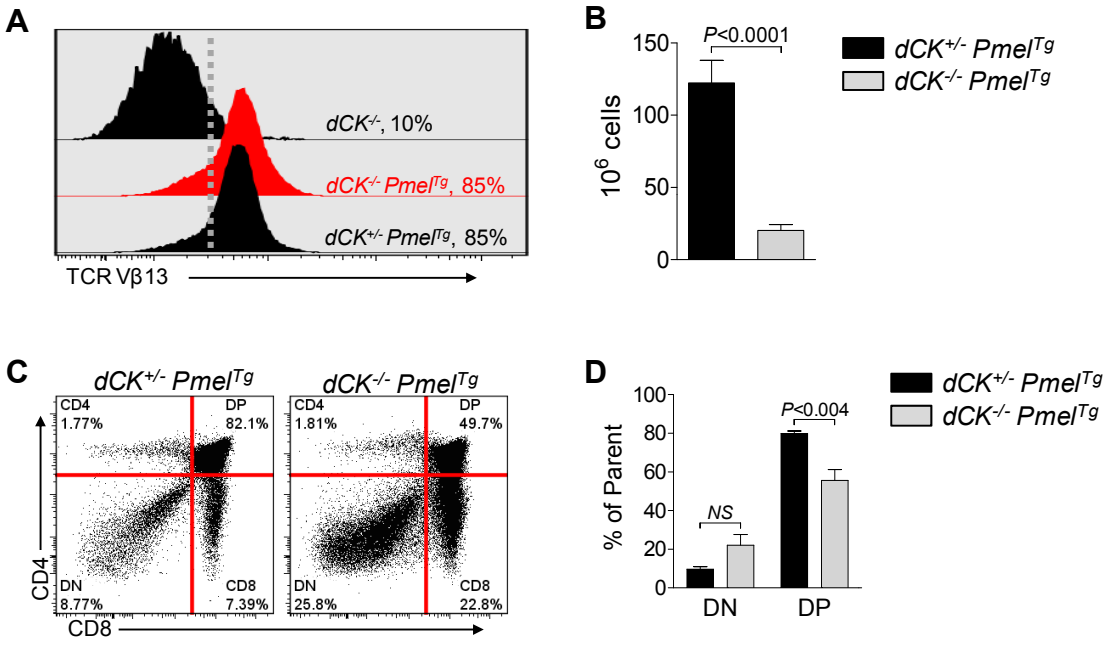


Figure 3.3. Expression of a transgenic TCR fails to rescue *dCK*$^{-/-}$ thymocyte development. (**A**) TCR Vβ13 expression analysis on CD8^{+} thymocytes from *dCK*$^{-/-}$ (Top curve), *dCK*$^{+/-}$*Pmel*^{Tg} (Middle curve), and *dCK*$^{-/-}$ *Pmel*^{Tg} (Bottom curve) mice. Percentages of cells staining positive for Vβ13 are indicated next to genotypes. (**B-C**) Total viable thymocytes recovered (**B**), and CD4/CD8 staining of whole thymocytes (**C**), from *dCK*$^{+/-}$*Pmel*^{Tg}, and *dCK*$^{-/-}$ *Pmel*^{Tg} mice. Graphs are average values + SEM (N=4 mice/genotype; *P*<0.0001). (**D**) Quantification of percentages of whole thymocytes *dCK*$^{+/-}$*Pmel*^{Tg} (Black bars) and *dCK*$^{-/-}$ *Pmel*^{Tg} mice (Grey bars) that are in DN or DP stages of differentiation. Graphs are average values + SEM (N=3 mice/genotype; *NS*=Not Statistically Significant; *P*<0.004).

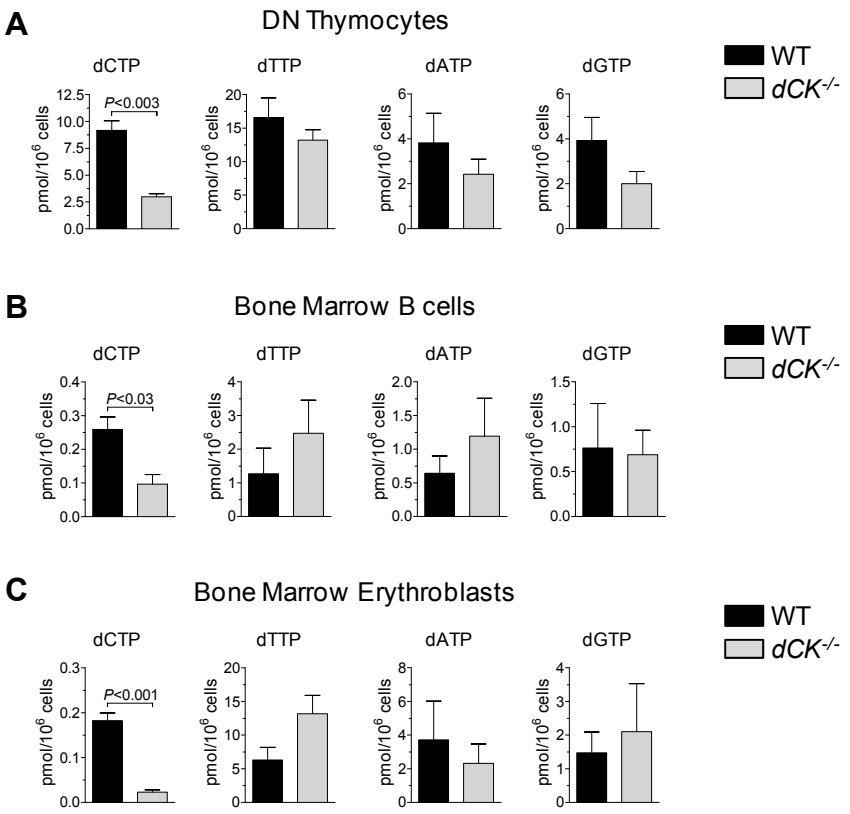


Figure 3.4. dCTP pool deficiency in *dCK*$^{-/-}$ lymphoid and erythroid progenitor populations. (**A-C**) dCTP, dTTP, dATP, and dGTP pools measured in DN thymocytes (**A**), bone marrow B cells (**B**), and bone marrow erythroblast populations (**C**), from WT (Black bars) and *dCK*$^{-/-}$ (Grey bars) mice. Graphs are average values + SEM from 3 independent measurements. Each measurement was generated using pooled progenitor populations from 4 mice per genotype per experiment (P<0.001 to 0.03).

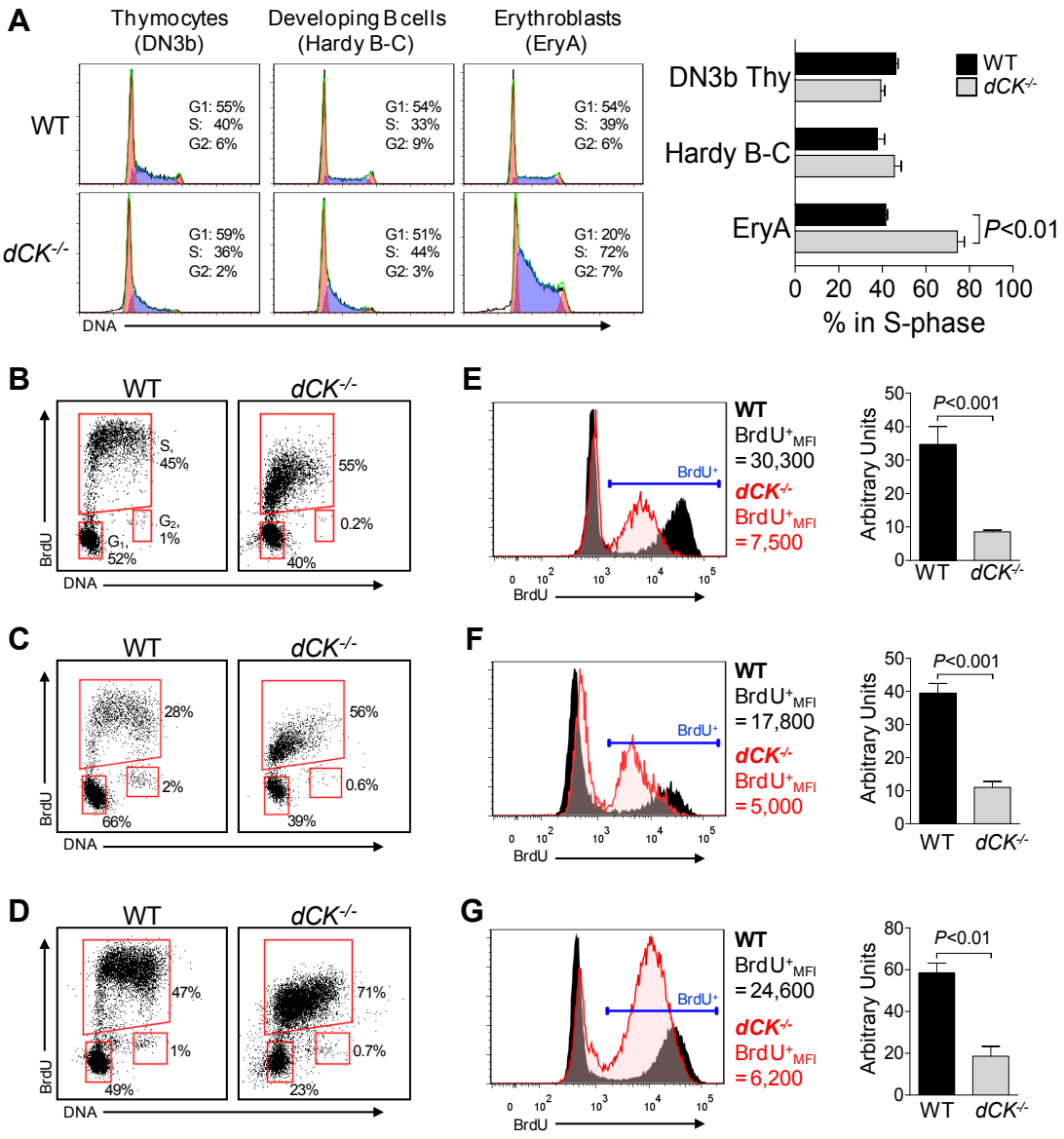


Figure 3.5. Abnormal S-phase profiles in *dCK*$^{-/-}$ hematopoietic progenitors. (**A**) Total DNA content and cell cycle phase determinations in WT and *dCK*$^{-/-}$ DN3b thymocytes, Hardy Fraction B-C cells, and bone marrow EryA cells. Quantification of percentages of WT (Black bars) and *dCK*$^{-/-}$ (Grey bars) cells found in S-phase are shown on the right. Graphs are average values + SEM (N=3 mice/genotype; $P<0.01$). (**B-D**) Representative flow cytometry plots of BrdU incorporation versus total DNA

content from DN3b thymocytes (**B**), Hardy Fraction B-C cells (**C**), and bone marrow EryA cells (**D**), from WT and *dCK*$^{-/-}$ mice pulsed with BrdU for 1 hour. Cell cycle phases determined by BrdU and DNA content are indicated (N=4 mice/genotype). (**E-G**) Overlays of BrdU incorporation profiles and calculation of relative BrdU incorporation per BrdU^{+} cell from DN3b thymocytes (**E**), Hardy Fraction B-C cells (**F**), and bone marrow EryA cells (**G**), from WT and *dCK*$^{-/-}$ mice. Blue gates on BrdU overlays indicate cells that are BrdU^{+}. Mean fluorescent values (MFI) of BrdU-FITC fluorescence for BrdU^{+} (BrdU$^{+}_{MFI}$) cells from each genotype are indicated next to the BrdU overlay plots. Relative BrdU incorporation values were calculated by taking BrdU$^{+}_{MFI}$ and dividing it by the MFI of BrdU-FITC fluorescence for BrdU^{-} cells. Graphs are average values + SEM (N=4 mice per genotype; P<0.001 to 0.01).

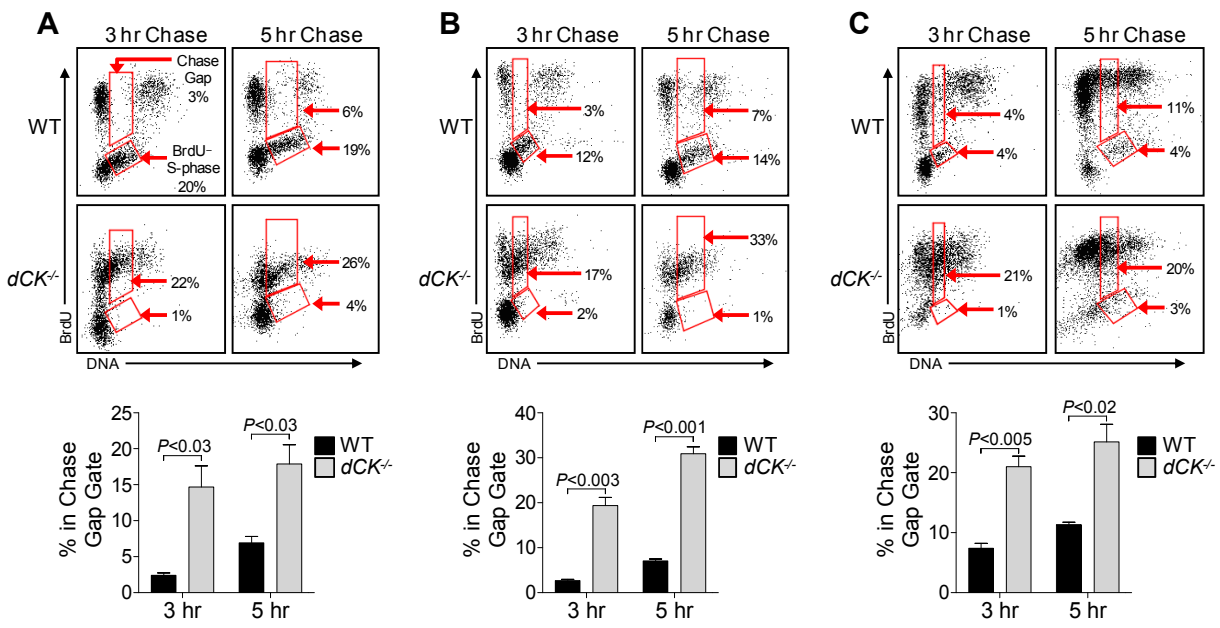


Figure 3.6. *dCK*$^{-/-}$ hematopoietic progenitors are arrested in early S-phase *in vivo*. (**A-C**) Representative flow cytometry plots of BrdU and total DNA content detection during 3 and 5 hr BrdU chase conditions in DN3b thymocytes (**A**), Hardy Fraction B-C cells (**B**), and bone marrow EryA cells (**C**). BrdU Chase Gaps (top gate in each plot) and BrdU^{-} S-phase cells (bottom gate in each plot) are depicted and the percentages of cells found in each gate are depicted. Quantifications of percentages of WT (Black bars) and *dCK*$^{-/-}$ (Grey bars) cells found in BrdU Chase Gap gates during 3 hr and 5 hr BrdU Chase conditions are provided below the flow cytometry plots. Graphs are average values + SEM (N=4 mice/genotype; P<0.001 to 0.03).

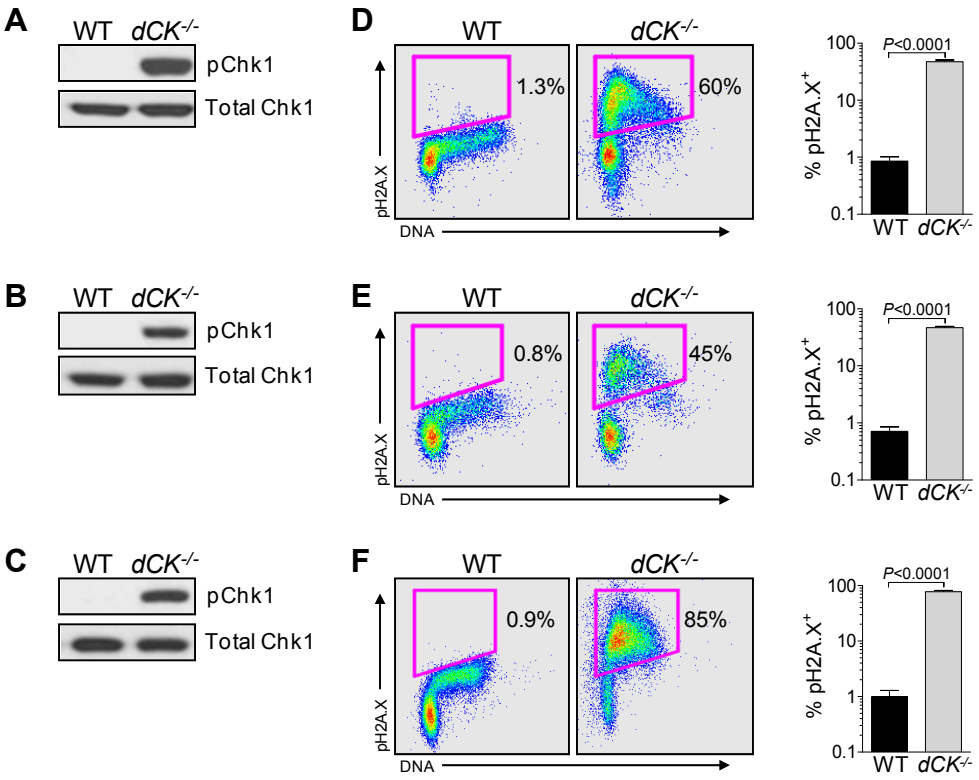


Figure 3.7. *dCK*$^{-/-}$ hematopoietic progenitors undergo replication stress responses *in vivo*. (**A-C**) Western blot analysis probing for Chk1 phosphorylated on Ser345 (pChk1) and total Chk1 present in WT and *dCK*$^{-/-}$ lysates of DN thymocytes (**A**), bone marrow B cells (**B**), and bone marrow erythroblasts (**C**). (**D-F**) Representative examples of flow cytometry detection of H2A.X phosphorylated in Ser139 (pH2A.X) and total DNA content from WT and *dCK*$^{-/-}$ DN3b thymocytes (**D**), Hardy Fraction B-C cells (**E**), and bone marrow EryA cells (**F**). Quantification of percentages of WT (Black bars) and *dCK*$^{-/-}$ (Grey bars) cells from each subpopulation staining positive for pH2AX are provided to the right of the flow cytometry plots. Graphs are average values + SEM (N=7 mice/genotype; *P*<0.0001).

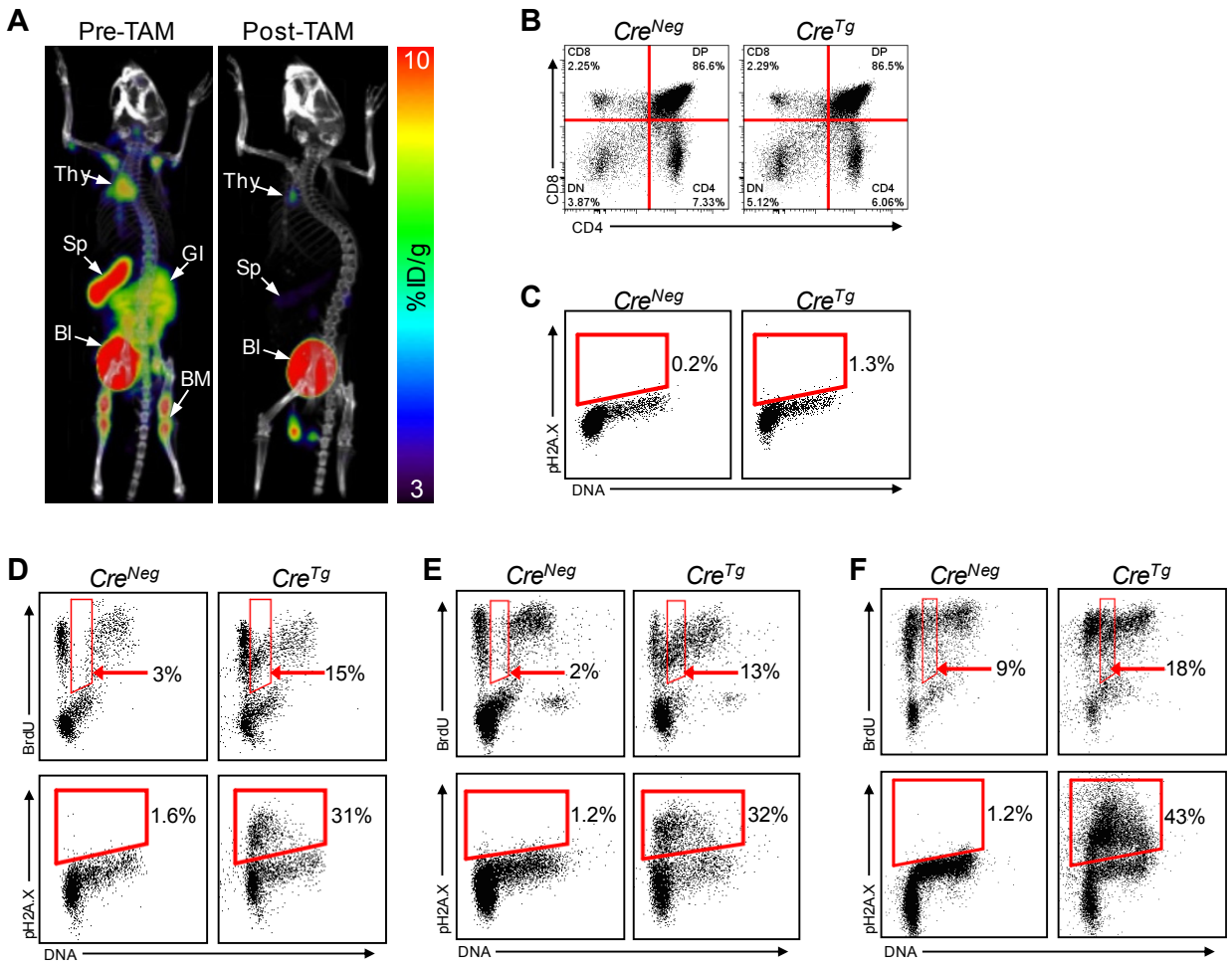


Figure 3.8. Conditional deletion of dCK in adult mice recapitulates the cell cycle defects and RSR pathway activation phenotypes characteristic of germline *dCK*$^{-/-}$ mice. (**A**) ^{18}F-FAC mPET/CT scans of a *dCK*$^{flox/flox}$ *CreERT*^{Tg} (*Cre*^{Tg}) mouse one day before (Pre-TAM) and one day after (Post-TAM) 4 days of single doses of tamoxifen by intraperintoneal injection. Images are scaled from 10-3% of injected dose/gram of tissue (%ID/g). BM-bone marrow; Thy-Thymus; Sp-Spleen; GI-Gastrointestinal tract; Bl-Bladder. (**B-C**) CD4/CD8 staining of whole thymocytes (**B**), and pH2A.X staining of DN3b thymocytes (**C**), from *dCK*$^{flox/flox}$ (*Cre*^{Neg}) and *Cre*^{Tg} after 4 days of intraperintoneal injection of vegetable oil (vehicle). N=2 mice/genotype. (**D-F, Top Panels**)

Representative flow cytometry plots of BrdU and total DNA content detection during 3 hr BrdU chase conditions in DN3b thymocytes (**D**), Hardy Fraction B-C cells (**E**), and bone marrow EryA cells (**F**), from Cre^{Neg} and Cre^{Tg} mice treated with tamoxifen for 4 days immediately prior to analysis. Percentages of cells found in BrdU Chase Gap gate are depicted on each plot (N=2 mice/genotype). (**D-F, Bottom Panels**) Representative flow cytometry plots of pH2A.X and total DNA content detection in DN3b thymocytes, Hardy Fraction B-C cells, and bone marrow EryA cells from Cre^{Neg} and Cre^{Tg} mice treated with tamoxifen for 4 days immediately prior to analysis. Percentages of cells staining positive for pH2A.X are depicted on each plot (N=4 mice/genotype).

References

1. Toy, G., W.R. Austin, H.I. Liao, D. Cheng, A. Singh, D.O. Campbell, T.O. Ishikawa, L.W. Lehmann, N. Satyamurthy, M.E. Phelps, H.R. Herschman, J. Czernin, O.N. Witte, and C.G. Radu. 2010. Requirement for deoxycytidine kinase in T and B lymphocyte development. *Proceedings of the National Academy of Sciences of the United States of America* 107:5551-5556.

2. Arpaia, E., P. Benveniste, A. Di Cristofano, Y. Gu, I. Dalal, S. Kelly, M. Hershfield, P.P. Pandolfi, C.M. Roifman, and A. Cohen. 2000. Mitochondrial basis for immune deficiency. Evidence from purine nucleoside phosphorylase-deficient mice. *The Journal of experimental medicine* 191:2197-2208.

3. Papinazath, T., W. Min, S. Sujiththa, A. Cohen, C. Ackerley, C.M. Roifman, and E. Grunebaum. 2011. Effects of purine nucleoside phosphorylase deficiency on thymocyte development. *The Journal of allergy and clinical immunology*

4. Nyhan, W.L. 2005. Disorders of purine and pyrimidine metabolism. *Molecular genetics and metabolism* 86:25-33.

5. Carbonaro, D.A., X. Jin, D. Cotoi, T. Mi, X.J. Yu, D.C. Skelton, F. Dorey, R.E. Kellems, M.R. Blackburn, and D.B. Kohn. 2008. Neonatal bone marrow transplantation of ADA-deficient SCID mice results in immunologic reconstitution despite low levels of engraftment and an absence of selective donor T lymphoid expansion. *Blood* 111:5745-5754.

6. Carbonaro, D.A., X. Jin, D. Petersen, X. Wang, F. Dorey, K.S. Kil, M. Aldrich, M.R. Blackburn, R.E. Kellems, and D.B. Kohn. 2006. In vivo transduction by intravenous injection of a lentiviral vector expressing human ADA into neonatal ADA gene knockout mice: a novel form of enzyme replacement therapy for ADA deficiency. *Mol Ther* 13:1110-1120.

7. Toro, A., and E. Grunebaum. 2006. TAT-mediated intracellular delivery of purine nucleoside phosphorylase corrects its deficiency in mice. *The Journal of clinical investigation* 116:2717-2726.

8. Schatz, D.G., and P.C. Swanson. 2011. V(D)J recombination: mechanisms of initiation. *Annual review of genetics* 45:167-202.

9. Jung, D., C. Giallourakis, R. Mostoslavsky, and F.W. Alt. 2006. Mechanism and control of V(D)J recombination at the immunoglobulin heavy chain locus. *Annual review of immunology* 24:541-570.

10. Akamatsu, Y., and M.A. Oettinger. 1998. Distinct roles of RAG1 and RAG2 in binding the V(D)J recombination signal sequences. *Molecular and cellular biology* 18:4670-4678.

11. Matsuoka, S., B.A. Ballif, A. Smogorzewska, E.R. McDonald, 3rd, K.E. Hurov, J. Luo, C.E. Bakalarski, Z. Zhao, N. Solimini, Y. Lerenthal, Y. Shiloh, S.P. Gygi, and S.J. Elledge. 2007. ATM and ATR substrate analysis reveals extensive protein networks responsive to DNA damage. *Science (New York, N.Y* 316:1160-1166.

12. Csapo, Z., G. Keszler, G. Safrany, T. Spasokoukotskaja, I. Talianidis, M. Staub, and M. Sasvari-Szekely. 2003. Activation of deoxycytidine kinase by gamma-irradiation and inactivation by hyperosmotic shock in human lymphocytes. *Biochemical pharmacology* 65:2031-2039.

13. Haveman, J., J. Sigmond, C. van Bree, N.A. Franken, C. Koedooder, and G.J. Peters. 2006. Time course of enhanced activity of deoxycytidine kinase and thymidine kinase 1 and 2 in cultured human squamous lung carcinoma cells, SW-1573, induced by gamma-irradiation. *Oncology reports* 16:901-905.

14. Herzog, S., M. Reth, and H. Jumaa. 2009. Regulation of B-cell proliferation and differentiation by pre-B-cell receptor signalling. *Nat Rev Immunol* 9:195-205.

15. Ciofani, M., and J.C. Zuniga-Pflucker. 2010. Determining gammadelta versus alphass T cell development. *Nat Rev Immunol* 10:657-663.

16. Reichman-Fried, M., R.R. Hardy, and M.J. Bosma. 1990. Development of B-lineage cells in the bone marrow of scid/scid mice following the introduction of functionally rearranged immunoglobulin transgenes. *Proceedings of the National Academy of Sciences of the United States of America* 87:2730-2734.

17. Chang, Y., G.C. Bosma, and M.J. Bosma. 1995. Development of B cells in scid mice with immunoglobulin transgenes: implications for the control of V(D)J recombination. *Immunity* 2:607-616.

18. Rampazzo, C., C. Miazzi, E. Franzolin, G. Pontarin, P. Ferraro, M. Frangini, P. Reichard, and V. Bianchi. 2010. Regulation by degradation, a cellular defense against deoxyribonucleotide pool imbalances. *Mutation research* 703:2-10.

19. Poli, J., O. Tsaponina, L. Crabbe, A. Keszthelyi, V. Pantesco, A. Chabes, A. Lengronne, and P. Pasero. 2012. dNTP pools determine fork progression and origin usage under replication stress. *The EMBO journal* 31:883-894.

20. Davidson, M.B., Y. Katou, A. Keszthelyi, T.L. Sing, T. Xia, J. Ou, J.A. Vaisica, N. Thevakumaran, L. Marjavaara, C.L. Myers, A. Chabes, K. Shirahige, and G.W. Brown. 2012. Endogenous DNA replication stress results in expansion of dNTP pools and a mutator phenotype. *The EMBO journal* 31:895-907.

21. Korbie, D.J., and J.S. Mattick. 2008. Touchdown PCR for increased specificity and sensitivity in PCR amplification. *Nature protocols* 3:1452-1456.

22. Mathews, C.K., and L.J. Wheeler. 2009. Measuring DNA precursor pools in mitochondria. *Methods in molecular biology (Clifton, N.J* 554:371-381.

23. Overwijk, W.W., A. Tsung, K.R. Irvine, M.R. Parkhurst, T.J. Goletz, K. Tsung, M.W. Carroll, C. Liu, B. Moss, S.A. Rosenberg, and N.P. Restifo. 1998. gp100/pmel 17 is a murine tumor rejection antigen: induction of "self"-reactive, tumoricidal T cells using high-affinity, altered peptide ligand. *The Journal of experimental medicine* 188:277-286.

24. Fischer Lindahl, K. 1997. On naming H2 haplotypes: functional significance of MHC class Ib alleles. *Immunogenetics* 46:53-62.

25. Arner, E.S., and S. Eriksson. 1995. Mammalian deoxyribonucleoside kinases. *Pharmacology & therapeutics* 67:155-186.

26. Dolbeare, F., H. Gratzner, M.G. Pallavicini, and J.W. Gray. 1983. Flow cytometric measurement of total DNA content and incorporated bromodeoxyuridine. *Proceedings of the National Academy of Sciences of the United States of America* 80:5573-5577.

27. Kriss, J.P., and L. Revesz. 1962. The distribution and fate of bromodeoxyuridine and bromodeoxycytidine in the mouse and rat. *Cancer research* 22:254-265.

28. Terry, N.H., and R.A. White. 2006. Flow cytometry after bromodeoxyuridine labeling to measure S and G2+M phase durations plus doubling times in vitro and in vivo. *Nature protocols* 1:859-869.

29. Gagou, M.E., P. Zuazua-Villar, and M. Meuth. 2010. Enhanced H2AX phosphorylation, DNA replication fork arrest, and cell death in the absence of Chk1. *Molecular biology of the cell* 21:739-752.

30. Halazonetis, T.D., V.G. Gorgoulis, and J. Bartek. 2008. An oncogene-induced DNA damage model for cancer development. *Science (New York, N.Y* 319:1352-1355.

31. Toledo, L.I., M. Murga, and O. Fernandez-Capetillo. 2011. Targeting ATR and Chk1 kinases for cancer treatment: a new model for new (and old) drugs. *Molecular oncology* 5:368-373.

32. Bartkova, J., Z. Horejsi, K. Koed, A. Kramer, F. Tort, K. Zieger, P. Guldberg, M. Sehested, J.M. Nesland, C. Lukas, T. Orntoft, J. Lukas, and J. Bartek. 2005. DNA damage response as a candidate anti-cancer barrier in early human tumorigenesis. *Nature* 434:864-870.

33. Branzei, D., and M. Foiani. 2008. Regulation of DNA repair throughout the cell cycle. *Nat Rev Mol Cell Biol* 9:297-308.

34. Bonner, W.M., C.E. Redon, J.S. Dickey, A.J. Nakamura, O.A. Sedelnikova, S. Solier, and Y. Pommier. 2008. GammaH2AX and cancer. *Nature reviews* 8:957-967.

35. Ward, I.M., and J. Chen. 2001. Histone H2AX is phosphorylated in an ATR-dependent manner in response to replicational stress. *The Journal of biological chemistry* 276:47759-47762.

36. Ruzankina, Y., C. Pinzon-Guzman, A. Asare, T. Ong, L. Pontano, G. Cotsarelis, V.P. Zediak, M. Velez, A. Bhandoola, and E.J. Brown. 2007. Deletion of the developmentally essential gene ATR in adult mice leads to age-related phenotypes and stem cell loss. *Cell stem cell* 1:113-126.

37. Feil, R., J. Wagner, D. Metzger, and P. Chambon. 1997. Regulation of Cre recombinase activity by mutated estrogen receptor ligand-binding domains. *Biochemical and biophysical research communications* 237:752-757.

CHAPTER 4

Deoxycytidine Kinase Counteracts DNA Replication Stress Induced by Thymidine Kinase 1 Activity *In Vivo*

Abstract

Nucleotide deprivation is known to induce replication stress (RS) and DNA damage in dividing cells. However, the mechanism by which nucleotide biosynthesis is regulated *in vivo* to prevent such deleterious effects remains unknown. In Chapter 4 we investigate a functional link between nucleotide deficiency, RS and the deoxyribonucleoside (dN) salvage pathway enzymes deoxycytidine kinase (dCK) and thymidine kinase (TK1). We show that lymphoid and erythroid precursor cells differentiate and proliferate *in vivo* in tissue environments that contain high levels of thymidine. To test thymidine's role in producing RS in *dCK*$^{-/-}$ T cell precursors, we performed *in vitro* proliferation assays to demonstrate that the salvage of thymidine in *dCK*$^{-/-}$ cells selectively and acutely causes proliferation arrest due to RS induction. To further explore thymidine's impact upon T cell, B cell, and erythroid development in *dCK*$^{-/-}$ mice, we generated *dCK/TK1* double-knockout (DKO) mice. Characterizing hematopoietic development in these DKO mice revealed that DKO hematopoietic cells have restored dCTP pools, improved differentiation, and overall reduced RS *in vivo,* as compared to *dCK*$^{-/-}$ mice. These results thus identify a previously unrecognized biological activity of endogenous thymidine as a strong inducer of RS *in vivo* through TK1-mediated dCTP pool depletion. We propose a model explaining how kinases of the deoxyribonucleoside salvage pathway "tune" nucleotide biosynthesis to both induce and resolve endogenous RS in hematopoietic precursor cells.

Introduction

Replication stress (RS) is a common source of endogenous DNA damage induced by accumulation of single-stranded DNA (ssDNA) at stalled replication forks and processed double-stranded DNA breaks (DSBs) (1). These lesions activate the ATR and CHK1 checkpoint kinases, which orchestrate a complex signal transduction network termed the Replication Stress Response (RSR) pathway (2). The RSR pathway is essential for preserving genomic integrity and the proliferative capacity of dividing cells (3). While significant progress has been made in mapping the RSR pathway and elucidating its biological relevance, less is known about endogenous causes of RS.

Genetic and pharmacological approaches point to deoxyribonucleotide triphosphate (dNTP) pool deficiency as a strong inducer of RS (4-6). Ectopic expression of oncogenes such as *ras, myc, cyclin E, mos, cdc25A,* and *E2F1* will elicit RS and induce genomic instability (3, 7-9). The underlying mechanism of oncogene-triggered RS is the forced, unregulated entry into the cell cycle of quiescent cells that lack a sufficient supply of DNA precursors to fully execute genome replication (1). Pharmacological interventions can also induce RS. Such interventions typically use inhibitors like hydroxyurea (HU) or 5-fluorouracil (5-FU) to interrupt dNTP synthesis in S-phase cells (10, 11). These genetic and pharmacologic studies raise the question of whether *endogenous factors* could also induce RS by inhibiting dNTP synthesis. If endogenous RS inducers do exist, it is possible that (i) they will exert their functions by interfering with critical nodes of the dNTP metabolism network, and (ii) the resulting alterations in metabolism could modulate both normal and pathological biological pathways.

In mammalian cells, dNTPs can be synthesized either *de novo* or by recycling nucleosides via the cytosolic nucleoside salvage pathways (12). *De novo* synthesis utilizes glucose and amino acids to generate ribonucleotide precursors of RNA (13). A fraction of the *de novo* synthesized ribonucleotides are converted into deoxyribonucleotides by the rate-limiting ribonucleotide reductase (RNR) enzyme complex (14). In addition to *de novo* synthesis, cells can also utilize cytosolic nucleoside salvage pathways to produce dNTPs from previously formed deoxyribonucleosides (dNs) (15). The rate-limiting enzymes of the salvage pathway are deoxycytidine kinase (dCK) and thymidine kinase (TK1). dCK converts deoxycytidine, deoxyadenosine, and deoxyguanosine into deoxyribonucleotide monophosphate (dNMP) precursors of dNTPs (16). TK1 phosphorylates thymidine and deoxyuridine to generate dNMP precursors of thymidine triphosphate (dTTP) pools (15).

While drugs like HU and 5-FU induce RS by inhibiting the generation of dNTPs through the *de novo* pathway (17, 18), putative endogenous inducers of dNTP insufficiency that cause RS may exert their actions through these kinases that regulate the critical first steps of the nucleoside salvage pathways. It is well established from cell culture studies that exposure to high thymidine levels during cell division can induce S-phase arrest (11, 19, 20). This effect is mediated by the triphosphate form of thymidine, dTTP, a strong allosteric inhibitor of RNR's affinity for its pyrimidine ribonucleotide substrates cytidine diphosphate (CDP) and uridine diphosphate (UDP) (21). The inhibition of CDP conversion to deoxycytidine diphosphate (dCDP) causes dCTP pool deficiencies that result in S-phase arrest (21, 22). This phenomenon forms the biochemical basis of a widely used experimental approach for synchronizing cells in S-

phase known as “the thymidine block” (23). However, the millimolar thymidine concentrations typically used to induce S-phase arrest and RS are likely non-physiological (24). Nonetheless, such *in vitro* demonstrations of nucleoside salvage pathway-mediated induction of RS suggest that nucleoside kinases may indeed provide a functional link between nucleotide metabolism and RS *in vivo*. In support of this hypothesis, dCK has been recently identified as a direct target of the DNA damage sensor kinases ATM and ATR, providing evidence that the salvage pathway may be directly involved in RS and DNA damage responses (25).

In this chapter, we investigated the role that thymidine salvage plays in generating the RS phenotypes observed in *dCK*$^{-/-}$ mice. We performed *in vitro* proliferation assays using *dCK*$^{-/-}$ thymocytes to demonstrate that proliferation in the absence of the high thymidine concentrations present *in vivo* alleviates much of the RS phenotype in *dCK*$^{-/-}$ cells. Additionally, we show that addition of low amounts of thymidine to cultures of proliferating thymocytes selectively blocks *dCK*$^{-/-}$ cell proliferation by inducing acute RSR activation. To further test the role that thymidine salvage plays in generating RS in the absence of dCK activity, we generated *dCK/TK1* double-knockout (DKO) mice to analyze RS induction *in vivo*. Despite the complete absence of cytosolic dN salvage activity in DKO hematopoietic precursors, DKO status restored dCTP pool levels in DKO bone marrow cells to that of WT levels and ameliorated, rather than aggravated, hematopoiesis in DKO mice relative to the defects observed in *dCK*$^{-/-}$ mice. Collectively, these *in vitro* and *in vivo* studies show that thymidine itself is a major inducer of endogenous RS in proliferating hematopoietic progenitors. Our results demonstrate an antagonistic functional relationship between

dCK and TK1 in regulating dCTP pools *in vivo,* and reveal a previously unappreciated role for endogenous thymidine as a biologically active metabolite linked to the induction of endogenous RS in the hematopoietic niches of the bone marrow and the thymus

Material and Methods

Mice

TK1$^{-/-}$ mice were re-derived from cryopreserved embryonic stem cells stored at the UC Davis Repository (Stock VG18248) and genotyped as previously described (26). *dCK/TK1* double-knockout (DKO) mice were generated by first intercrossing *dCK*$^{+/-}$ mice to *TK1*$^{+/-}$ mice to generate *dCK*$^{+/-}$ *TK1*$^{+/-}$ progeny. *dCK*$^{+/-}$ *TK1*$^{+/-}$ mice were then intercrossed together to generate *dCK/TK1* double-knockout mice at potential 1:16 frequency.

Whole tissue nucleoside concentration measurements

Solid tissues were homogenized at 4°C using the BulletBlender Tissue Homogenizer (NextAdvance) according to the manufacturer's specifications. Homogenization buffer was acetonitrile:methanol (9:1). BM cells were flushed using ice-cold PBS, filtered into single-cell suspensions, pelleted and resuspended in homogenization buffer. Whole blood was collected in heparinized tubes and then centrifuged to separate plasma and blood cells. Both fractions were extracted directly with the homogenization buffer. Extracted samples were dried using a SpeedVac Concentrator and then resuspended in ddH_2O. Thymidine concentrations were then

determined by liquid chromatography-tandem mass spectrometry (LC-MS/MS) using an Agilent 64060 Triple Quad LC/MS system. The stationary phase was a Thermo Fisher Hypercarb column (2.1 x 100 mM) with 0.1% formic acid in ddH_2O and 0.1% formic acid in acetonitrile as the mobile phases.

CTV labeling of thymocytes

Single-cell suspensions of thymocytes were resuspended in PBS containing 0.5% FBS at a cell density of $50x10^6$ cells/mL. 5 mM stocks of CTV dye (Invitrogen) dissolved in DMSO were diluted to 50 µM in PBS/0.5% FBS and then added at a dilution of 1:10 to the cell suspension (5 µM final concentration). Cells were mixed well, incubated at 37°C for 20 min, and then washed twice with 40 mL of PBS/5% FBS. Cells were then stained with fluorescent antibodies to identify DN3a thymocytes and purified via FACS.

OP9-DL1 co-cultures

OP9 cells were purchased from ATCC (CRL-2749) and transduced by retroviral infection with Delta-like Ligand 1 vector (DL1), kindly provided by Dr. Juan Carlos Zúñiga-Pflücker, and FACS-sorted based on their GFP fluorescence. OP9-DL1 cells were maintained in Minimum Essential Medium, Alpha Modification (Sigma-Aldrich, M4526) supplemented with 20% FBS, 100 U/mL penicillin, 100 µg/mL streptomycin. Thymocyte/OP9-DL1 co-cultures were initiated by plating $50x10^3$ OP9-DL1 cells in 250 µL of media/well in 48-well tissue culture dishes at Day -1. On Day 0, DN3a thymocytes were FACS purified and resuspended in OP9-DL1 media supplemented with 10 ng/mL

Flt3-L (Peprotech, 250-31L) and 10 ng/mL IL-7 (Peprotech, 217-17) at a cell density of 10^5 cells/mL. 250 µL of thymocyte suspensions were then plated atop OP9-DL1 monolayers ($25x10^3$ cells, 5 ng/mL final concentrations of Flt3-L and IL-7 in 500 µL total volume). Co-cultures were incubated for 2 or 4 days. Thymocytes were harvested by forceful pipetting, surface stained for developmental markers and analyzed by flow cytometry. Total cell counting was achieved by adding 10 µL of homogenized 7.66 µm AccuCount Blank particles (Spherotech, ACBP-70-10) solution (~10^4 beads/tube) to stained cell suspensions just prior to acquisition on the flow cytometer. Total cell counts per well were back-calculated using the following equation: [total viable cells acquired] ÷ [total beads acquired] x [10^4 beads/tube].

Results

Hematopoietic progenitors proliferate in the presence of high thymidine levels

An established approach to deplete dCTP pools and induce RSR pathway activation in transformed cancer cells grown in culture is to exogenously add millimolar amounts of thymidine to the cell culture medium (11, 19, 20). In many cell types, salvage of exogenous thymidine by TK1 leads to the generation of excess dTTP pools that allosterically inhibit RNR from reducing CDP into dCDP, thereby depleting intracellular dCTP pools (12, 22). The ultimate outcome of acutely depleting dCTP pools is S-phase arrest mediated by RSR pathway activation (11). Because of the apparent similarities between thymidine-induced S-phase arrest in cultured cells and the *in vivo*

S-phase arrest we found in *dCK*$^{-/-}$ hematopoietic progenitors, we hypothesized that perhaps thymidine played a major role in generating the *dCK*$^{-/-}$ phenotype.

To start investigating a potential role for thymidine as an inducer of RS in hematopoietic progenitors, we first sought to quantify endogenous levels of this nucleoside in various tissues in C57Bl/6 mice. We extracted nucleosides from whole tissue homogenates and determined the relative abundance of thymidine (in µmol per milligram of tissue) using mass spectrometry. Thymidine levels were highest in the bone marrow and thymus (Figure 4.1, A). The high concentrations of thymidine in these tissues could mean that developing lymphoid and erythroid cells proliferating in their normal *in vivo* environments may be subjected to thymidine-induced replication stress.

Next, we sought to experimentally determine if removing developing *dCK*$^{-/-}$ lymphocytes from these environments would relieve their RS-induced S-phase arrest. To test this assumption, we used the OP9-DL1 co-culture system that supports the proliferation and differentiation of DN thymocytes into DP thymocytes (27). Using mass spectrometry, we first determined that normal OP9 cell culture medium contained sub-micromolar levels of thymidine (Figure 4.1, B). These concentrations are likely much lower than what developing thymocytes are exposed to *in vivo*. We therefore proceeded with testing the proliferative capacity of *dCK*$^{-/-}$ thymocytes in the low-thymidine environment of the OP9-DL1 co-culture system.

Thymidine specifically inhibits dCK$^{-/-}$ *thymocyte proliferation*

To measure thymocyte proliferation *in vitro*, we used CellTrace Violet (CTV) (28), a fluorescent dye that allows tracking at the single cell level of mitotic events executed

by thymocytes in the OP9-DL1 co-culture system. The CTV dye covalently labels primary amines in intracellular proteins, thereby conferring violet fluorescence to cells. Upon cell division, fluorescently-labeled intracellular proteins are evenly distributed between daughter cells, which now have a fluorescent intensity that is one-half of the fluorescent intensity of parent cells. Fluorescent peaks of diminishing intensity are therefore a direct readout of the number of times that the cells in each peak have divided, starting from 0 divisions and going up to as many as 8 divisions (Figure 4.2, A).

In this model we chose to study DN3a thymocytes from WT and *dCK*$^{-/-}$ mice because DN3a cells are primarily G_1-synchronized (80-90% in G_1) (Figure 4.2, B), and *dCK*$^{-/-}$ DN3a cells have about one-third as many pH2A.X-positive cells as compared *dCK*$^{-/-}$ DN3b cells (Figure 4.2, C). These two qualities of DN3a cells would thus enable better interpretation of environmentally-induced RS between the WT and *dCK*$^{-/-}$ genotypes. We anticipated that *dCK*$^{-/-}$ DN3a thymocytes would proliferate normally in the OP9-DL1 system because their ability to salvage thymidine would likely be significantly reduced compared to the *in vivo* conditions.

We cultured CTV-labeled DN3a cells with OP9-DL1 stroma for 4 days and then measured proliferation over this period by CTV dye dilution. Mock treated *dCK*$^{-/-}$ thymocytes (i.e. no thymidine supplement) were able to proliferate robustly as evidenced by equal numbers of cell divisions (Figure 4.2, D, First row) and comparable numbers of total viable thymocytes remaining in culture after 4 days of incubation when compared to WT cells (Figure 4.2, E). However, addition of thymidine (20 μM) significantly and specifically inhibited the proliferation of *dCK*$^{-/-}$ thymocytes as evidenced by the reduction of division peaks and reduced total viable cell counts amongst *dCK*$^{-/-}$

cells (Figure 4.2, D, Second row; Figure 4.2, E). Higher concentrations of thymidine (50 and 100 μM) completely blocked the proliferation of *dCK*$^{-/-}$ thymocytes (Figure 4.2, D, Third and Fourth rows). Therefore, in contrast to the *in vivo* phenotype, *dCK*$^{-/-}$ thymocytes proliferate normally in cell culture. However, these cells are acutely sensitive to thymidine-induced proliferation block *in vitro*.

Thymidine specifically induces RS and cell death in proliferating dCK$^{-/-}$ thymocytes

We sought to determine if the thymidine-induced blockade of *dCK*$^{-/-}$ thymocyte proliferation *in vitro* was associated with RS induction in S-phase. We therefore stained for the RS marker of pH2A.X in WT and *dCK*$^{-/-}$ DN3a thymocytes cultured on OP9-DL1 stroma for 2 days. In absence of added thymidine (Mock treatment), *dCK*$^{-/-}$ thymocytes had low pH2A.X staining (2% positive), which was comparable to the background staining in WT thymocytes (0.5% positive) (Figure. 4.3, A, First row). However, addition of low amounts of thymidine (20 μM) induced a 10-fold increase the percentage of *dCK*$^{-/-}$ thymocytes staining positive for pH2A.X staining (20%), while WT thymocytes failed to induce increases in pH2A.X staining (Figure 4.3, A, Second row). Furthermore, the induction of pH2A.X in *dCK*$^{-/-}$ thymocytes was specific to cells that were in S-phase, as determined by total DNA content staining. Increasing the thymidine concentration to 100 μM induced WT thymocytes to be 20% positive for pH2A.X, but with low mean fluorescent staining intensity of pH2A.X within the pH2A.X-positive cells, thus indicating lower levels of RS (29) than the 20% positive pH2A.X staining seen in *dCK*$^{-/-}$ thymocytes treated with 20 μM thymidine (Figure 4.3, A, Second and Third rows).

Lastly, while *dCK*$^{-/-}$ thymocytes treated with 100 μM thymidine showed reduced numbers of pH2A.X-positive cells (6% positive), this reduction in pH2A.X-positive cells was associated with a decrease in *dCK*$^{-/-}$ thymocytes in S-phase. This observation indicated that the higher levels of RS induced in *dCK*$^{-/-}$ thymocytes by 100 μM thymidine were perhaps preventing the in *dCK*$^{-/-}$ cells from entering or progressing further through S-phase.

We next determined whether the thymidine-induced RS was also triggering cell death in *dCK*$^{-/-}$ thymocytes over 2 days of *in vitro* culturing. Total DNA content staining was used to identify dead cells via Sub-G_1 DNA content, a marker of apoptosis-induced DNA fragmentation (30). Mock-treated *dCK*$^{-/-}$ thymocytes had statistically higher basal percentages of cells with Sub-G_1 DNA content than did WT cells (N=3; P<0.04), but overall cell cycle profiles were comparable between WT and *dCK*$^{-/-}$ cells (Figure 4.3, B, First row). 20 μM thymidine increased the percentages of Sub-G_1 *dCK*$^{-/-}$ thymocytes, but had no effect upon WT cells (Figure 4.3, B, Second row). 100 μM thymidine triggered a dramatic 4-fold increase in Sub-G_1 *dCK*$^{-/-}$ thymocytes over mock-treated cells, while again no effect was seen in WT cells (Figure 4.3, B, Third row). Thymidine addition thus had a selective dose-dependent killing effect upon *dCK*$^{-/-}$ thymocytes (Figure 4.3, C; N=3 independent measurements; P<0.001 to 0.04). The OP9-DL1 co-culture experiments allowed us to conclude that thymidine specifically prevents the proliferation of *dCK*$^{-/-}$ thymocytes by inducing RS in S-phase cells that can lead to selective cell death in *dCK*$^{-/-}$ thymocytes at concentrations that have little effect upon WT thymocytes.

Hematopoietic development in TK1-deficient mice

The observation that exogenously added thymidine induced RS and cell death in proliferating *dCK*$^{-/-}$ thymocytes warranted further investigations of the mechanism by which thymidine could cause such acute proliferation defects. Since thymidine induces RS in proliferating cells via TK1-mediated salvage (12), we sought to directly test the role of TK1 in generating the *dCK*$^{-/-}$ hematopoietic phenotype. TK1-deficient mice have been reported previously, but the only hematopoietic defects described in these mice were the presence of slightly abnormal secondary lymphoid structures and elevated levels of micronucleated erythrocytes (26, 31). We therefore sought to carefully characterize hematopoietic development, dNTP pools, and RS phenotypes in *TK1*$^{-/-}$ mice. Our ultimate goal was to generate *dCK/TK1* double-knockout mice directly test the role that salvage of thymidine via TK1 plays in generating the *in vivo* RS phenotypes we observed in *dCK*$^{-/-}$ mice.

Our analysis revealed that thymi from 5-week old *TK1*$^{-/-}$ mice were reduced in size by ~20% compared to WT littermates (Figure 4.4, A). However, CD4 and CD8 staining of total thymocytes to identify DN and DP populations revealed that thymocyte development in *TK1*$^{-/-}$ mice was, in fact, normal (Figure 4.4, B). Consistent with the absence of any overt defects in T cell development in the *TK1*$^{-/-}$ mice, we did not observe any obvious defects in cell cycle kinetics of *TK1*$^{-/-}$ DN3b thymocytes *in vivo* (Figure 4.4, C).

Analyses of Hardy Fraction A-D and Hardy Fraction E-F populations of developing B cells in the bone marrow of *TK1*$^{-/-}$ mice also did not reveal any obvious developmental defects (Figure 4.4, D). Additionally, no cell cycle defects were observed

in highly proliferative Hardy Fraction B-C cells from *TK1*$^{-/-}$ mice (Figure 4.4, E). Surface staining for erythroid developmental markers in *TK1*$^{-/-}$ mice did not reveal any abnormalities in EryA, EryB, and EryC populations (Figure 4.4, F). We did, however, observe an increase in the percentage of *TK1*$^{-/-}$ EryA cells found in S-phase (average 50% in S-phase), as compared to WT controls (average 43% in S-phase) (Figure 4.4, G), but this difference did not achieve statistical significance (Figure 4.4, H). We thus concluded from our hematopoietic developmental phenotyping and cell cycle phase determinations that proliferating hematopoietic progenitors largely do not require TK1 activity to support differentiation.

dNTP pool imbalances and RS induction in TK1*$^{-/-}$ *hematopoietic progenitors

Despite the absence of severe developmental defects in *TK1*$^{-/-}$ hematopoietic progenitors, it was important to determine whether TK1 deletion altered dNTP pools in developing hematopoietic cells. We therefore assayed dNTP pools in DN thymocytes, bone marrow-resident B cells, and bone marrow-resident erythroid progenitors from WT and *TK1*$^{-/-}$ littermates.

TK1$^{-/-}$ DN thymocytes did not display any depletions in dNTP pools (Figure 4.5, A). In contrast, bone marrow-resident developing B cells from *TK1*$^{-/-}$ mice demonstrated significantly decreased dTTP concentrations; the other three dNTP pools appeared unaffected (Figure 4.5, B; $P<0.005$). Bone marrow-resident developing erythroblasts also showed significantly decreased concentrations of dTTP in *TK1*$^{-/-}$ mice (Figure 4.5, C; $P<0.002$). Interestingly, *TK1*$^{-/-}$ BM erythroblasts concurrently displayed a significant increase in dCTP pools (Figure 4.5, C; $P<0.05$). The dNTP measurements allowed us to

conclude that TK1 deletion significantly influences dTTP pools in bone marrow-resident hematopoietic progenitors, but its absence does not significantly affect dTTP pools in DN thymocytes. The inconsistency in dTTP pool perturbations between developing T cells, B cells, and erythroid cells could be the result of an *in vivo* compensatory mechanisms present in the thymus but not in the bone marrow. We plan to further investigate this possibility by performing *in vivo* labeling studies using nucleosides labeled with stable isotopes followed by LC/MS analyses of the size and origin of intracellular dNTP pools.

Bone marrow-resident TK1$^{-/-}$ hematopoietic progenitors experience RS in vivo

The dramatic dTTP pool deficiency present in bone marrow-resident *TK1$^{-/-}$* developing B cells, and erythroid cells indicated that these populations may undergo RS *in vivo*. We therefore purified DN thymocytes, bone marrow-resident B cells, and bone marrow-resident erythroid progenitors to probe for the presence of the RS marker of Chk1 phosphorylated on Ser345 (pChk1) by western blot.

We did not detect any elevation of pChk1 in *TK1$^{-/-}$* DN thymocytes versus WT controls (Figure 4.6, A), consistent with the absence of significant dTTP depletions in *TK1$^{-/-}$* DN thymocytes (Figure 4.5, A). In contrast, we did detect significantly elevated levels of pChk1 in *TK1$^{-/-}$* developing B cells (Figure 4.6, B), and in *TK1$^{-/-}$* erythroid progenitors (Figure 4.6, C). These findings indicated that *TK1$^{-/-}$* developing B cells and erythroid cells were indeed subject to RS *in vivo*. Whether the degree of RS in proliferating *TK1$^{-/-}$* cells was comparable to that experienced by *dCK$^{-/-}$* cells remained to be determined. To enable more direct comparisons of RS we performed flow cytometry

analysis to detect pH2A.X in proliferating DN3b thymocytes, Hardy Fraction B-C cells, and EryA cells from *TK1*$^{-/-}$ mice. We found slightly elevated levels of pH2A.X staining in *TK1*$^{-/-}$ DN3b thymocytes (Figure 4.6, D), Hardy Fraction B-C cells (Figure 4.6, E), and EryA cells (Figure 4.6, F), versus WT controls. However, only the pH2A.X increases in *TK1*$^{-/-}$ EryA cells achieved statistical significance (Figure 4.6, G; N=4 mice; $P<0.03$). The pH2A.X analyses allowed us to conclude that EryA cells have the highest degree of RS in *TK1*$^{-/-}$ mice amongst T cell, B cell and erythroid progenitor cells. Nonetheless, the degree of RS induction in *TK1*$^{-/-}$ cells was far less than that observed in *dCK*$^{-/-}$ EryA cells (Figure 3.7, F).

Generation of dCK/TK1 double-knockout mice to test development in the absence of cytosolic dN salvage activity

Next, we sought to test whether inactivation of thymidine salvage *in vivo* would rescue the defects in hematopoietic development observed in *dCK*$^{-/-}$ mice. We therefore intercrossed the *dCK*$^{-/-}$ and *TK1*$^{-/-}$ mouse lines to generate *dCK/TK1* double-knockout (DKO) mice. These mice should lack all cytosolic dN salvage activity and would have to rely entirely on the *de novo* synthesis pathway to generate cytosolic pyrimidine dNTPs.

dCK$^{+/-}$ *TK1*$^{+/-}$ double-heterozygous mice were first generated and then intercrossed to generate DKO mice at an expected 1:16 Mendelian frequency. However, DKO mice were generated at sub-Mendelian frequencies with a hazard ratio of approximately 1.85. DKO mice demonstrated overall slower growth as 5 week old DKO mice weighed approximately 30% less than WT, *TK1*$^{-/-}$, and *dCK*$^{-/-}$ littermates (Figure 4.7, A; N=7 mice/genotype; $P<0.0001$). The sub-Mendelian rate of DKO

generation and the apparent growth retardation in DKO mice indicated that the absence of all cytosolic dN salvage had deleterious effects upon overall development. Nonetheless, we found that dCTP pools from DKO whole bone marrow cells were on average 2.7-times higher than dCTP pool levels in *dCK*$^{-/-}$ cells (Figure 4.7, B; N=4 mice/genotype; P<0.0004). Additionally, dTTP pools from DKO whole bone marrow cells averaged approximately 90% reduced relative to concentrations found in *dCK*$^{-/-}$ cells (Figure 4.7, C; N=4 mice/genotype; P<0.0001). These results indicated that inactivating TK1 in *dCK*$^{-/-}$ mice prevents dCTP pool deficiency induced by thymidine salvage via TK1 in hematopoietic tissues.

Inactivation of TK1 dramatically improves the thymic T cell development in the dCK$^{-/-}$ mice

Investigating hematopoietic development in DKO mice yielded surprising results. DKO thymi were smaller than WT and *TK1*$^{-/-}$ thymi, but significantly larger than *dCK*$^{-/-}$ thymi (Figure 4.8, A; N=7 mice/genotype; P<0.0001). The increase in overall thymic cellularity in DKO thymi versus *dCK*$^{-/-}$ thymi indicated that that inactivation of TK1 normalized thymic T cell development. To further characterize T cell development in the DKO mice, we performed flow cytometric analysis using thymocyte development markers.

Staining WT, *TK1*$^{-/-}$, *dCK*$^{-/-}$, and DKO thymi with CD4 and CD8 to identify DN and DP populations showed that DKO thymi had DP to DN proportions that were virtually indistinguishable from WT and *TK1*$^{-/-}$ thymi (Figure 4.8, B). This observation indicated that DKO DN thymocytes were rescued from the proliferation block that is present in

dCK$^{-/-}$ DN thymocytes. The DN thymocyte population was further characterized by CD25 and CD44 staining to identify the DN1-4 populations. This analysis revealed that the apparent block in *dCK*$^{-/-}$ DN differentiation during the DN3 stage was largely relieved in DKO DN thymocytes as evidenced by the reduction in the percentage of DN3 cells relative to the other DN subpopulations (Figure 4.8, C). Lastly, staining the DN3 populations for CD27 to discriminate between DN3a and DN3b thymocytes revealed that DKO thymi had a significant restoration of the proportion of DN3b thymocytes relative to *dCK*$^{-/-}$ DN3b cells (Figure 4.8, D). The cell surface phenotyping data indicated that the proliferative defects present in *dCK*$^{-/-}$ thymocytes were largely rescued in DKO mice.

We next investigated whether the improved T cell development in DKO mice versus *dCK*$^{-/-}$ mice was associated with a reduction in RS markers. We probed DN thymocytes from WT, *TK1*$^{-/-}$, *dCK*$^{-/-}$, and DKO mice by western blot for the presence of the RS markers of pChk1 and the Chk2 kinase phosphorylated on Thr68 (pChk2). We found significantly lower levels of pChk1 and pChk2 in lysates from DKO DN thymocytes versus *dCK*$^{-/-}$ DN thymocytes (Figure 4.8, E), thus indicating that DKO DN thymocytes experience less RS *in vivo* than *dCK*$^{-/-}$ DN thymocytes. We further probed for the presence of the RS marker of pH2A.X with respect to cell cycle position in the highly proliferative DN3b thymocyte population. We found significantly less pH2A.X in DKO DN3b thymocytes than in *dCK*$^{-/-}$ DN3b thymocytes (Figure 4.8, F). The pH2A.X staining that was present in DKO DN3b thymocytes appeared to be in the G_1 phase of the cell cycle rather than the S-phase. These data indicated to us that DKO DN3b

thymocytes were largely relieved of the RS present in early S-phase that affects *dCK*$^{-/-}$ DN3b thymocytes *in vivo*.

DKO thymocytes are resistant to thymidine-induced proliferation block

To confirm that the improved differentiation of DKO thymocytes versus *dCK*$^{-/-}$ thymocytes was accompanied by increased resistance to thymidine-induced proliferation block, we stimulated CTV-labeled WT, *TK1*$^{-/-}$, *dCK*$^{-/-}$, and DKO DN3a thymocytes on OP9-DL1 stroma and measured proliferation in the presence of increasing concentration of thymidine. While *dCK*$^{-/-}$ thymocyte proliferation was again severely inhibited by 20 μM thymidine—and completely inhibited by 100 μM thymidine—DKO thymocytes were completely resistant to thymidine induced proliferation block at both concentrations (Figure 4.9). We therefore concluded that the resistance of DKO thymocytes to thymidine-induced RS likely enables T cell development to proceed much more efficiently than in dCK single-knockout mice.

Inactivation of TK1 improves B cell development in dCK$^{-/-}$ *mice*

Next, we investigated whether B lymphocyte development was improved in DKO mice over the defective development observed in *dCK*$^{-/-}$ mice. Staining whole bone marrow cells to identify Hardy Fraction A-D and E-F populations revealed significant increases in both DKO Hardy Fraction A-D and E-F populations over *dCK*$^{-/-}$ mice (Figure 4.10, A). Further analyzing the Hardy A-D population to identify Hardy Fraction A, B-C, and D populations demonstrated that DKO mice had a large restoration of the Hardy

Fraction D population over *dCK*$^{-/-}$ mice (Figure 4.10, B). These results indicated that the proliferative defects observed in the preceding differentiation stage (Hardy Fraction B-C) were corrected relative to *dCK*$^{-/-}$ cells.

We therefore stained Hardy Fraction B-C cells for total DNA content to directly determine their cell cycle state *in vivo*. DKO Hardy Fraction B-C cells appeared to have normal cell cycle distributions with an absence of the early S-phase arrest profile observed in *dCK*$^{-/-}$ cells (Figure 4.10, C). Concurrent with the normalization of cell cycle profiles in Hardy Fraction B-C cells in DKO mice was a reduction in pH2A.X staining DKO S-phase cells (Figure 4.10, D). These data indicated that, similar to developing T cells, developing B cells in DKO mice were subject to less RS *in vivo* than their *dCK*$^{-/-}$ counterparts because of the absence of TK1-mediated salvage of thymidine. This reduction in RS likely allows the developing DKO B cells to proliferate and differentiate *in vivo* more easily than developing *dCK*$^{-/-}$ B cells.

Inactivation of TK1 relieves early S-phase arrest in erythroid progenitors

Lastly, we sought to determine the effect that inactivation of both dCK and TK1 had upon erythroid development. We stained whole bone marrow cells to identify EryA, EryB, and EryC stages of erythroid development and found a large proportion of EryA cells with high FSC profiles in DKO bone marrow (Figure 4.11, A). The identification of this population in DKO mice indicated that DKO EryA cells were still arrested in cell cycle because their large cell size correlates with greater proportions of cells being in the S-, G_2-, or M-phases of the cell cycle (32).

We therefore analyzed total DNA content in EryA cells from WT, *TK1*$^{-/-}$, *dCK*$^{-/-}$, and DKO mice to determine if the early S-phase arrest present in *dCK*$^{-/-}$ EryA cells was rescued. We found that DKO EryA cells were in fact relieved of the early S-phase arrest observed in *dCK*$^{-/-}$ EryA cells (Figure 4.11, B). However, unlike the rescues we observed in DKO DN3b thymocytes and Hardy B-C cells, DKO EryA cells retained a significant late S-phase arrest profile (Figure 4.11, B). To determine if the late S-phase arrest was associated with RSR activation in DKO cells, we assayed pH2A.X levels. We found a strong correlation between strong pH2A.X staining in late S-phase with cells that displayed an arrest DNA profile (Figure 4.11, C). These results indicated that while DKO EryA cells were still subject to significant RS *in vivo*, RS appears to primarily occur in late S-phase rather than in the early S-phase seen in *dCK*$^{-/-}$ EryA cells.

Discussion

A functional interplay between dCK and TK1 regulates dNTP pools and prevents RS during hematopoietic development

Using genetic models of individual and combined deficiencies in the cytosolic dN kinases dCK and TK1 (Figure 4.12), we demonstrate that the dN salvage pathways contribute to both induction and prevention of RS during hematopoietic development. We also show that endogenous thymidine itself is a highly active metabolite that induces RS *in vivo*. Concerning the latter finding, it is important to emphasize the biochemical similarities between our observations *in vivo* and a widely used *in vitro*

experimental approach for synchronizing cultured cells in cell cycle known as the "thymidine block" (23).

Despite its frequent use by many groups and for many decades, the thymidine block approach has been thought of exclusively as an *in vitro* "laboratory tool" (33) with little if any relevance to *in vivo* conditions. Our data challenge this assumption by establishing thymidine block as a metabolically relevant phenomenon *in vivo*, which has profound consequences for the development of major hematopoietic lineages. In the course of a typical thymidine block experiment, cultured cells exposed to high concentrations of thymidine undergo S-phase arrest through a TK1-dependent mechanism (11). It is through the kinase action of TK1 that exogenously added thymidine is trapped in cells, thus enabling its conversion to dTTP in the cytosol. dTTP is not only a precursor of DNA but also a strong allosteric inhibitor of RNR's affinity for the pyrimidine ribonucleotide substrates cytidine diphosphate (CDP) and uridine diphosphate (UDP) (21). dTTP-mediated inhibition of CDP conversion to dCDP depletes dCTP pools and consequently causes S-phase arrest (21, 22). Here we show that, in the absence of dCK activity, physiological concentrations of thymidine present in the hematopoietic niches of the bone marrow and thymus are sufficient to induce dCTP deprivation and severe RS in proliferating cells belonging to several major hematopoietic lineages (i.e., T cells, B cells, and erythroid precursors). By enabling deoxycytidine salvage in these cells, dCK replenishes dCTP pools depleted by dTTP produced from thymidine via TK1, thereby playing an essential role in hematopoiesis.

The two cytosolic dN salvage kinases thus play paradoxically opposing roles; TK1 in the absence of dCK induces RS, while dCK functions to prevent RS in TK1-expressing cells exposed to elevated levels of endogenous thymidine.

The biological significance of the deoxyribonucleoside salvage pathway

Proliferating hematopoietic progenitors express high levels of dCK and TK1 (34). However, since the dN salvage pathways appear to be largely dispensable in DKO hematopoietic lineages, it indicates that the *de novo* synthesis pathway can maintain dNTP pools at levels that are sufficient to support hematopoietic proliferation. In contrast, the fact that DKO mice are born at sub-Mendelian frequencies and surviving animals display growth retardation indicates that the dN salvage pathway is important to support overall growth. It is possible that the growth defects present in DKO mice may result from increased stress forced upon other biosynthetic pathways in the absence of cytosolic dN salvage activity. The utilization of dN salvage for dNTP synthesis requires significantly less ATP and NADPH than does *de novo* synthesis (35). For example, *de novo* synthesis of 1 mole of dCTP or dTTP starting from glucose, glutamine, aspartate, and bicarbonate requires 6 moles of ATP each, while the same amount can be generated via salvage at a cost of 3 moles of ATP (36). ATP and NADPH savings afforded by utilizing pyrimidine salvage instead of *de novo* synthesis could then be spent by cells to generate other essential biomass, such as proteins and phospholipids. An alternative explanation for the growth defects in the DKO mice involves mitochondrial dysfunction due to imbalances in the dNTP pools in this organelle. Defects in mitochondrially compartmentalized dNTP synthesis have been shown to

cause severe developmental abnormalities (37-40). Since mitochondrial dNTP pools in cycling cells correlate linearly with the cytoplasmic pools (41), imbalances in cytosolic dNTP pools resulting from defective dN salvage metabolism may impair mitochondrial DNA synthesis and thus trigger mitochondrial stress manifested by embryonic lethality and neonatal growth retardation.

Sources of nucleosides in hematopoietic niches

The nucleoside substrates of the salvage pathway likely arise from normal cellular turnover occurring in bone marrow and thymus (42). Genomic DNA originating from apoptotic lymphocytes or from the extruded nuclei of maturing erythrocytes (43) could provide the salvage pathway with its substrates. Phagocytic cells residing at hematopoietic niches promote nucleic acid degradation and subsequently excrete the constituent dNs into the extracellular milieu (44, 45). Hematopoietic progenitors undergoing rapid division in such thymidine-rich environments would benefit from the availability of this essential precursor of DNA. The ability to produce dTTP from salvaged thymidine would reduce the need to produce this essential nucleotide via the *de novo* pathway. However, since rapidly proliferating hematopoietic cells appear to lack a mechanism to control excessive accumulation of dTTP pools derived from thymidine salvage, they have instead evolved a way to counteract dTTP-mediated depletion of dCTP pools. We propose that dCK fills this critical role by supplementing dCTP pools produced by the *de novo* pathway, and thus playing a critical role in preventing endogenous RS and DNA damage during hematopoietic development.

Differential requirements for dCTP and dTTP in early and late S-phase

Intracellular dNTP pools are at the limit of detection in quiescent mammalian cells and even S-phase cells only have pools that are sufficient for a few minutes of DNA synthesis (17). Significant differences in the magnitude and timing of RS induction between *dCK*$^{-/-}$ and *TK1*$^{-/-}$ hematopoietic cells as they progress through S-phase indicate a differential susceptibility to depletion of dCTP and dTTP pools at different time points during DNA synthesis. Areas surrounding the sequences of DNA at which replication is initiated on chromosomes (i.e., origins of replication) are typically GC rich in mammalian cells (46). Therefore, earlier DNA replication events in these areas may require higher dCTP pools than would DNA replication towards the end of the S-phase. Furthermore, dCTP pools turnover more rapidly in early S-phase than do dTTP pools (47), an observation that is consistent with the distinct RS induction profiles documented in our dCK and TK1 knockout models. The rapid utilization of dCTP for DNA synthesis in early S-phase would thus require rapid replenishment through combined *de novo* and salvage pathways in order to allow DNA synthesis to continue. Similarly, the demand for dTTP may increase towards late S-phase and this could be the reason for which we do not observe RS induction in *TK1*$^{-/-}$ and DKO mice until late phases of DNA replication.

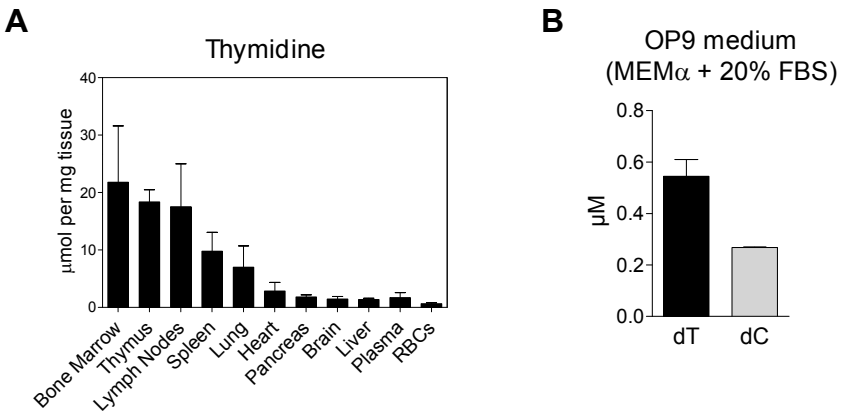


Figure 4.1. High thymidine concentrations in hematopoietic and lymphopoietic tissues in mice. (**A**) Relative thymidine abundance in various tissues from C57Bl/6 mice in µmol of nucleoside per milligram of homogenized tissue. (**B**) Thymidine (dT) and deoxycytidine (dC) concentrations (in µM) found in OP9 medium (MEMα supplemented with 20% FBS).

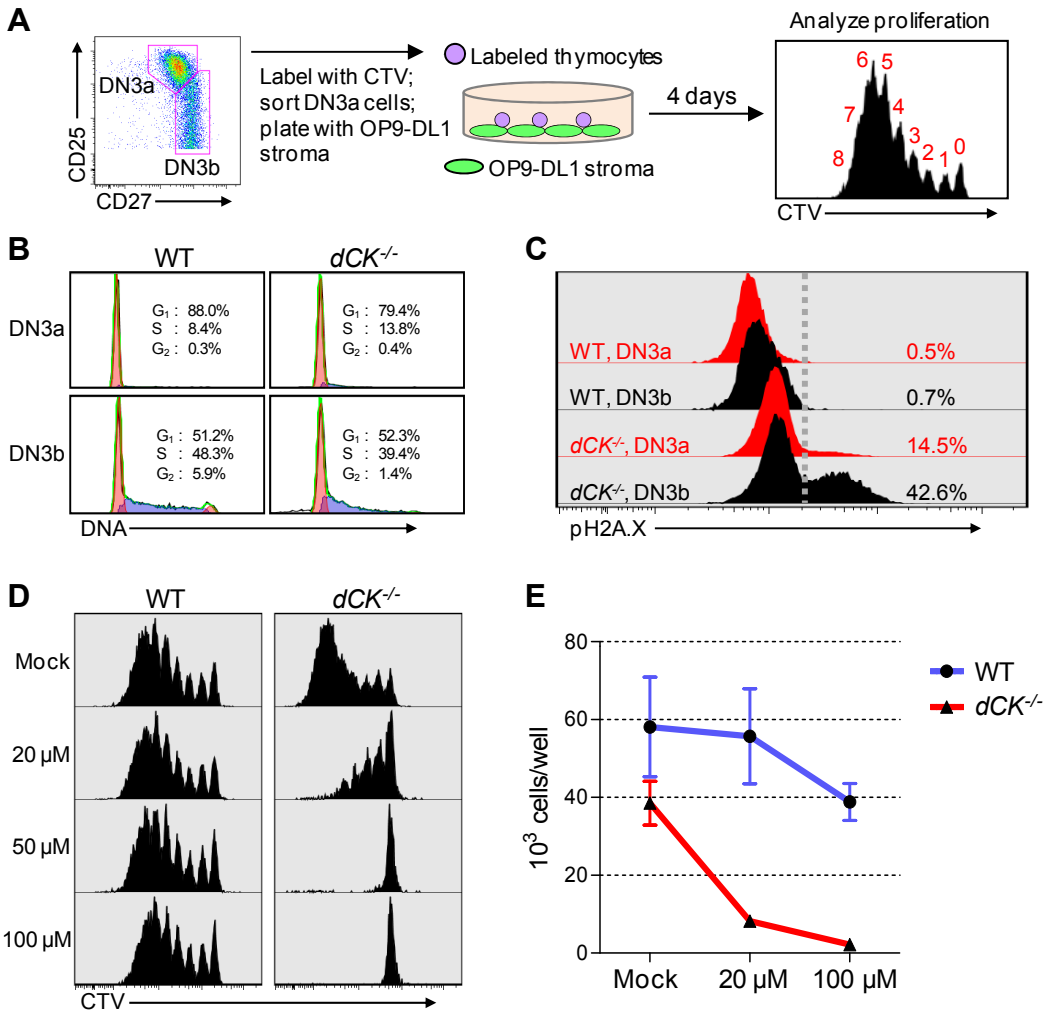


Figure 4.2. *In vitro* thymidine salvage selectively blocks the proliferation of *dCK*$^{-/-}$ thymocytes. (**A**) Schematic of the OP9-DL1 co-culture system for *in vitro* proliferation of DN3a thymocytes. Numbers in the schematic flow cytometry analysis reflect the total number of completed cell divisions as determined by the generation of CellTrace Violet (CTV) peaks of diluted dye intensity. (**B-C**) Total DNA content determined by DAPI staining and cell cycle phase discrimination (**B**), and pH2A.X detection (**C**), in DN3a and DN3b thymocytes from WT and *dCK*$^{-/-}$ mice. Percentages of cells with pH2A.X detection fluorescence above the threshold cutoff (dotted grey line) are indicated for respective genotypes/cell type pairs on the right side of pH2A.X histogram plot. (**D-E**) CTV dye

dilution curves (**D**), and total viable thymocytes recovered per well (**E**), from WT and *dCK*$^{-/-}$ DN3a thymocytes stimulated on OP9-DL1 stroma in 48-well plates for 4 days in the absence (Mock) or presence (20, 50, and 100 μM) of exogenously added thymidine in the culture medium.

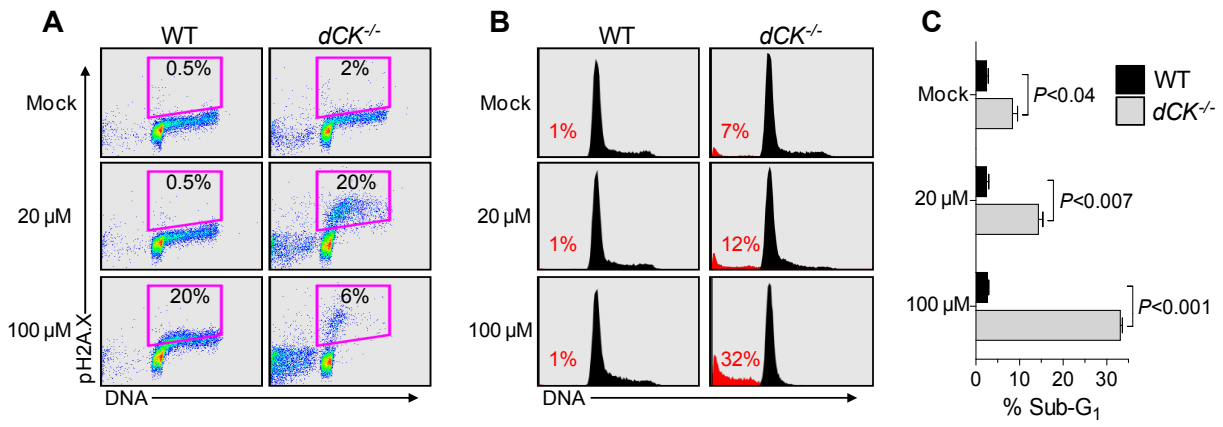


Figure 4.3. *In vitro* thymidine salvage selectively induces RS and cell death in *dCK*$^{-/-}$ thymocytes. (**A**) pH2A.X and total DNA content detection in WT and *dCK*$^{-/-}$ DN3a thymocytes after 48 hours of stimulation in the absence (Mock) or presence (20 and 100 μM) of added thymidine. (**B-C**) Detection of Sub-G_1 dead cells (red curves) (**B**), and quantification of Sub-G_1 dead cells (**C**), as determined by total DNA content staining of WT (Black bars) and *dCK*$^{-/-}$ (Grey bars) DN3a thymocytes stimulated on OP9-DL1 stroma for 48 hours in increasing concentrations of thymidine. Graphs are average values + SEM (N = 3/genotype; P<0.001 to 0.04).

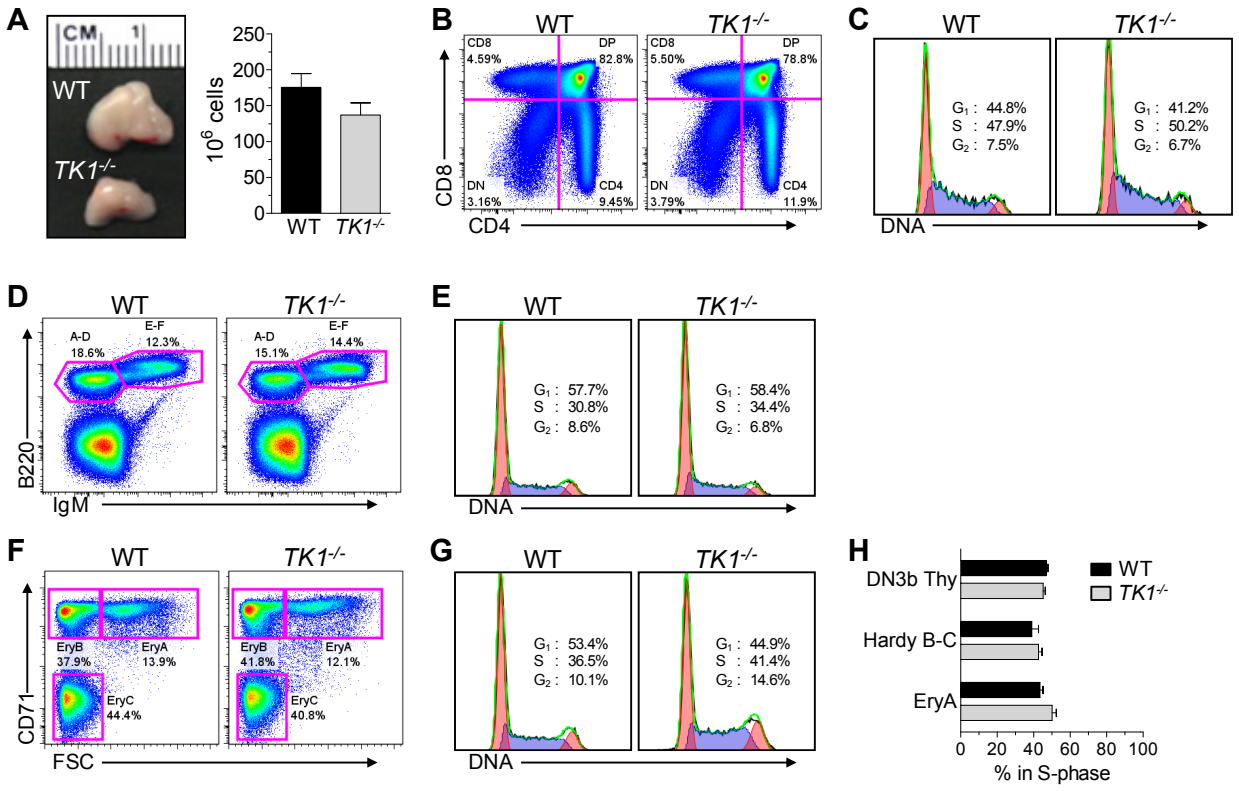


Figure 4.4. Lymphoid and erythroid development in *TK1*$^{-/-}$ mice. (**A**) Gross size and total viable thymocytes recovered from 5-week old WT and *TK1*$^{-/-}$ mice. (**B-C**) CD4 and CD8 staining of whole thymocytes to identify DN and DP thymocyte populations (**B**), and total DNA content staining to determine cell cycle phases in DN3b thymocytes (**C**), from WT and *TK1*$^{-/-}$ mice. (**D-E**) IgM and B220 staining of whole bone marrow cells to identify Hardy Fraction A-D and E-F populations (**D**), and total DNA content staining to determine cell cycle phases in Hardy Fraction B-C cells (**E**), from WT and *TK1*$^{-/-}$ mice. (**F-G**) CD71 and forward scatter (FSC) profiles of Ter119^{+} cells to identify EryA, EryB, and EryC populations (**F**), and total DNA content staining to determine cell cycle phases in EryA cells (**G**), from WT and *TK1*$^{-/-}$ mice. (**H**) Quantification of S-phase cells from DN3b thymocytes, Hardy Fraction B-C cells, and EryA cells from WT (Black bars) and *TK1*$^{-/-}$ (Grey bars) mice. Graphs are average values + SEM (N=3 mice/genotype).

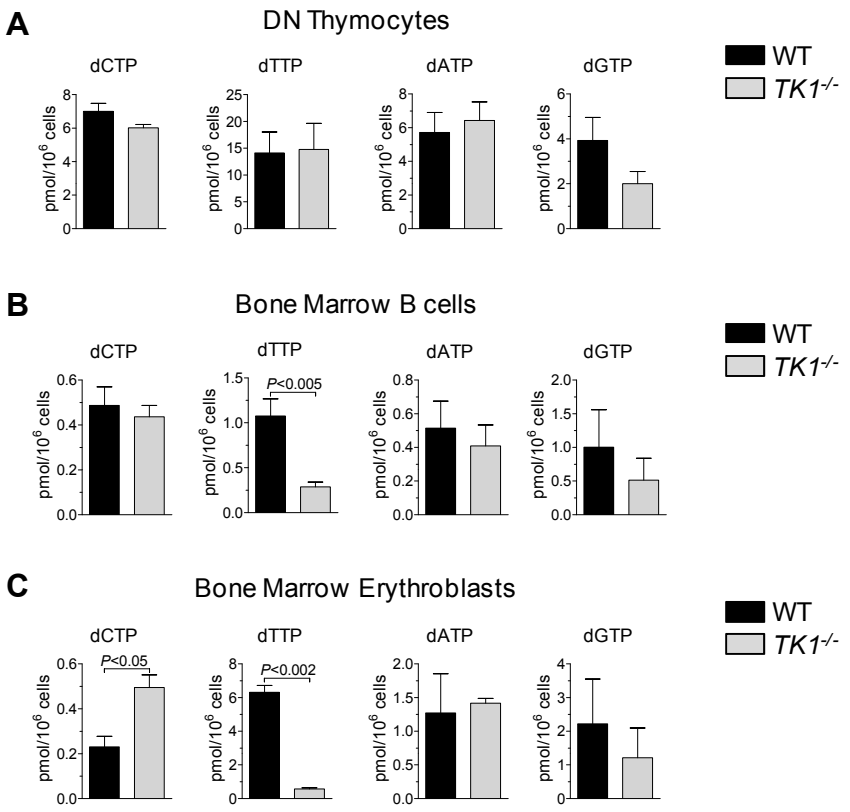


Figure 4.5. *TK1*$^{-/-}$ hematopoietic progenitors from the bone marrow have dTTP pool depletions. (**A-C**) dCTP, dTTP, dATP, and dGTP pools measured in DN thymocytes (**A**), bone marrow B cells (**B**), and bone marrow erythroblast populations (**C**), from WT (Black bars) and *TK1*$^{-/-}$ (Grey bars) mice. Graphs are average values + SEM from 3 independent measurements. Each measurement was generated using pooled progenitor populations from 4 mice per genotype per experiment (P<0.002 to 0.05).

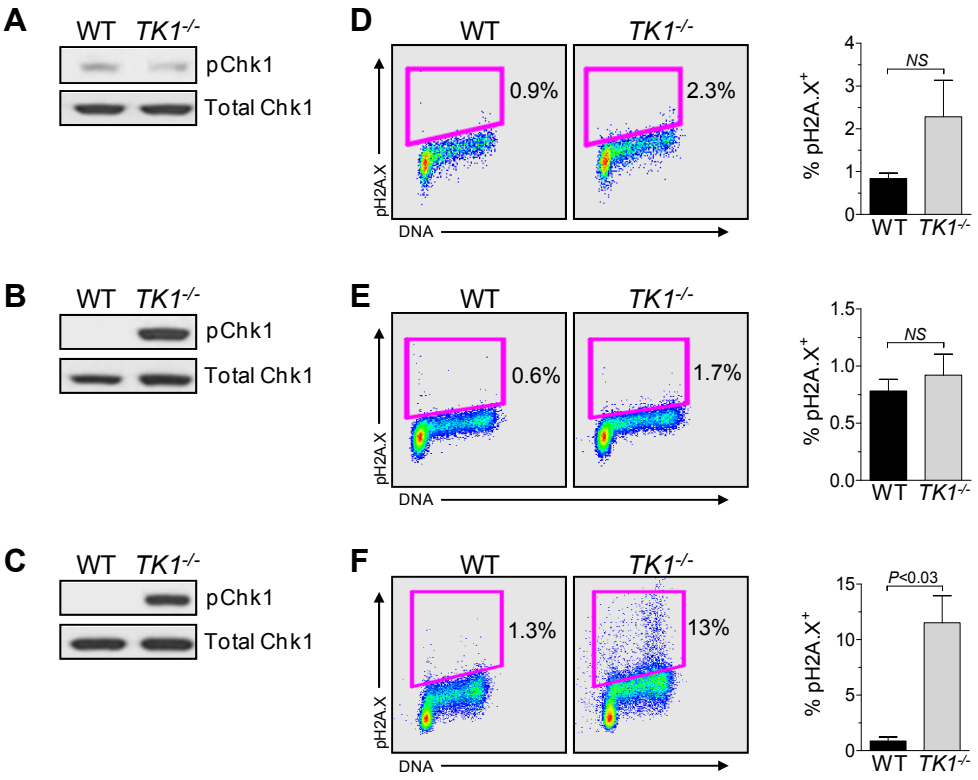


Figure 4.6. *TK1*$^{-/-}$ hematopoietic progenitors undergo replication stress *in vivo*. (**A-C**) Western blot analysis probing for Chk1 phosphorylated on Ser345 (pChk1) and total Chk1 present in WT and *TK1*$^{-/-}$ lysates of DN thymocytes (**A**), bone marrow B cells (**B**), and bone marrow erythroblasts (**C**). (**D-F**) Representative examples of flow cytometry detection of pH2A.X and total DNA content from WT and *TK1*$^{-/-}$ DN3b thymocytes (**D**), Hardy Fraction B-C cells (**E**), and bone marrow EryA cells (**F**). Quantification of percentages of WT (Black bars) and *TK1*$^{-/-}$ (Grey bars) cells from each subpopulation staining positive for pH2A.X are provided to the right of the flow cytometry plots. Graphs are average + SEM (N=4 mice/genotype; *NS* = Not statistically significant; *P*<0.03).

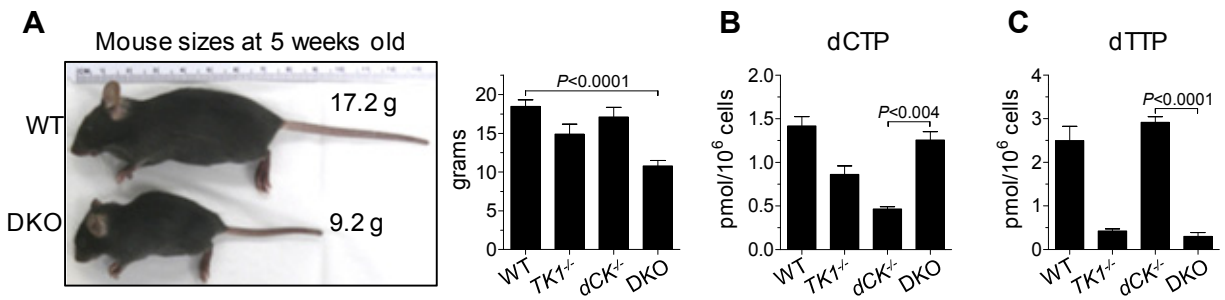


Figure 4.7. Gross sizes and pyrimidine dNTP pools from *dCK/TK1* double-knockout (DKO) mice. (**A**) Gross size and weights of WT, *TK1*$^{-/-}$, *dCK*$^{-/-}$, and DKO mice at 5 weeks of age. Graphs are average values + SEM (N=7 mice/genotype; *P*<0.0001). (**B-C**) dCTP pools (**B**), and dTTP pools (**C**), from whole bone marrow cells from WT, *TK1*$^{-/-}$, *dCK*$^{-/-}$, and DKO mice at 5 weeks of age. Graphs are average values + SEM (N=4 mice/genotype; *P*<0.0001 to 0.004).

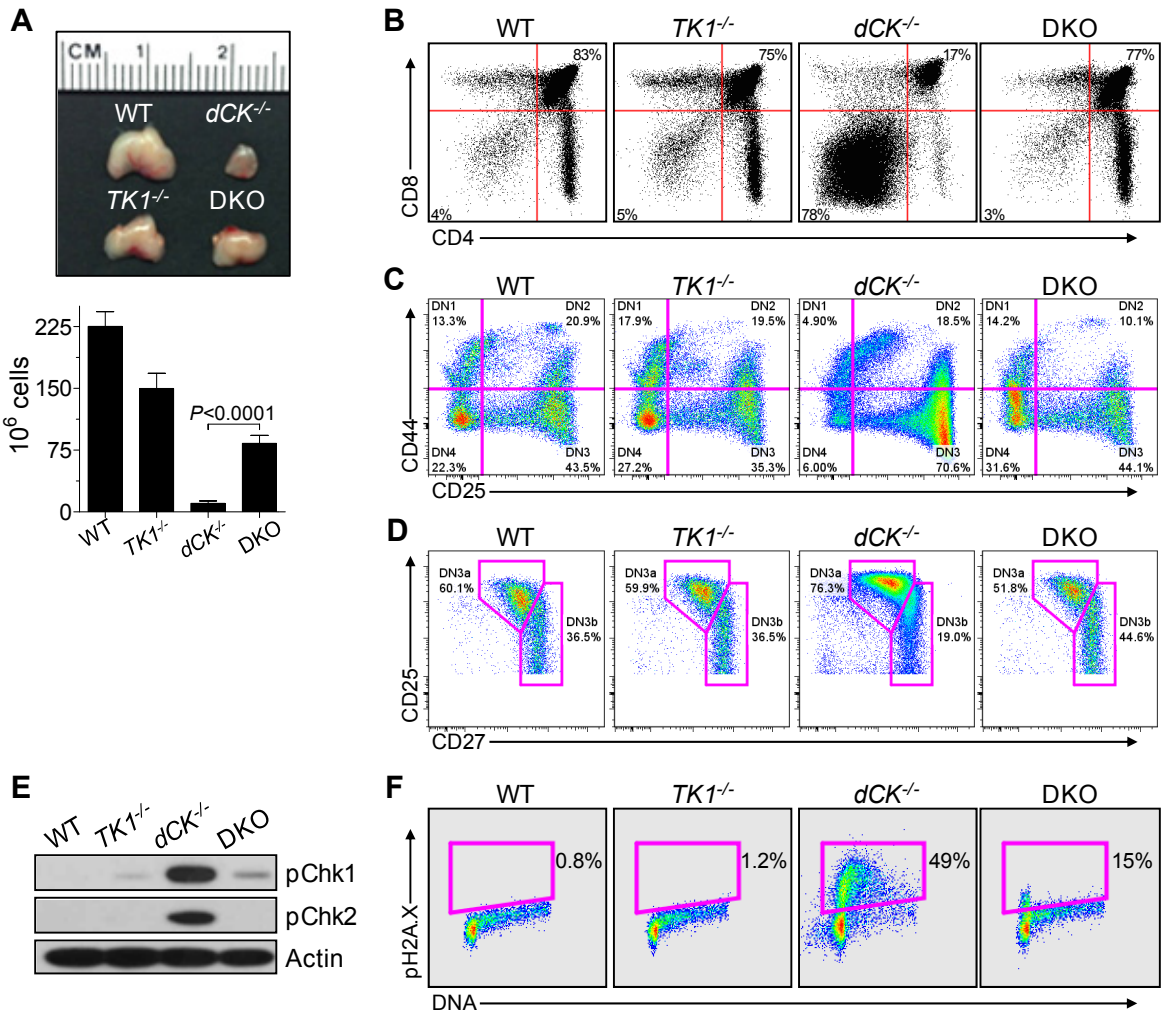


Figure 4.8. TK1 inactivation largely rescues thymic T cell development in *dCK*$^{-/-}$ mice. (**A-B**) Gross thymus size (**A**), and total viable thymocytes recovered (**B**), from WT, *TK1*$^{-/-}$, *dCK*$^{-/-}$, and DKO mice. Graphs are average values + SEM (N=7 mice/genotype; *P*<0.0001). (**B-D**) CD4 and CD8 staining of total thymocytes (**B**), CD25 and CD44 staining of DN thymocytes (**C**), and CD25 and CD27 staining of DN3 thymocytes (**D**), from WT, *TK1*$^{-/-}$, *dCK*$^{-/-}$, and DKO mice. (**E**) Western blots probing for pChk1 and pChk2 in DN thymocytes. Actin was used as a loading control. (**F**) pH2A.X and total DNA content detection in DN3b thymocytes from WT, *TK1*$^{-/-}$, *dCK*$^{-/-}$, and DKO mice.

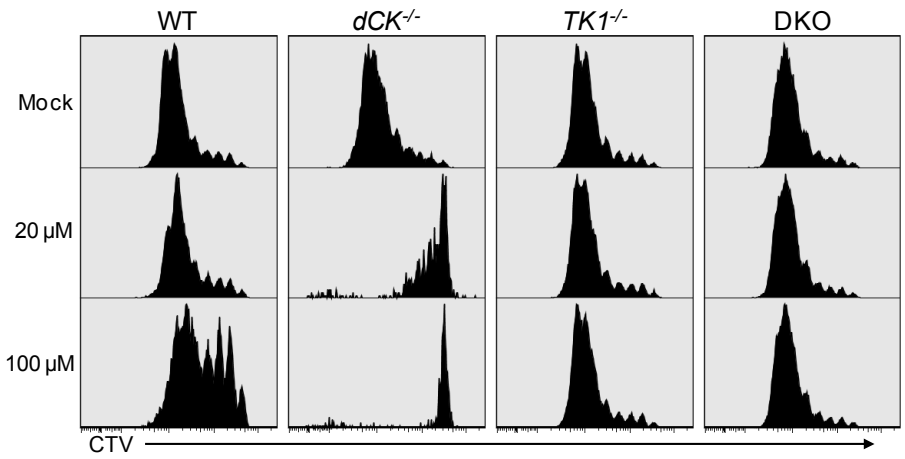


Figure 4.9. DKO thymocytes are resistant to thymidine-induced proliferation block *in vitro*. CTV dye dilution curves from WT, *dCK*$^{-/-}$, *TK1*$^{-/-}$, and DKO DN3a thymocytes stimulated on OP9-DL1 stroma for 4 days in the absence (Mock) or presence (20 and 100 μM) of exogenously added thymidine in the culture medium

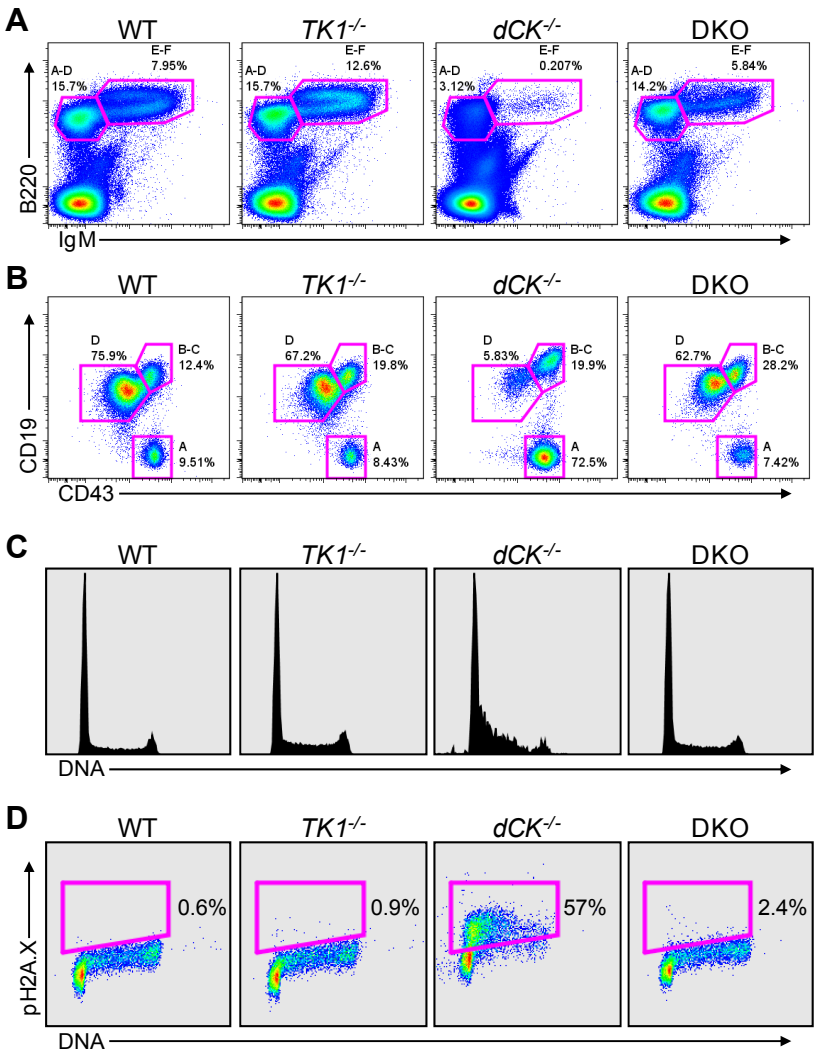


Figure 4.10. TK1 deletion largely rescues bone marrow B cell development in *dCK*$^{-/-}$ mice. (**A-B**) IgM and B220 staining of whole bone marrow cells to identify Hardy Fraction A-D and E-F populations (**A**), CD43 and CD19 staining of IgM^{-} B220^{+} cells to identify Hardy Fraction A, B-C, and D populations (**B**), from WT, *TK1*$^{-/-}$, *dCK*$^{-/-}$, and DKO mice. (**C-D**) Total DNA content (**C**), and pH2A.X detection (**D**), in Hardy B-C cells from WT, *TK1*$^{-/-}$, *dCK*$^{-/-}$, and DKO mice.

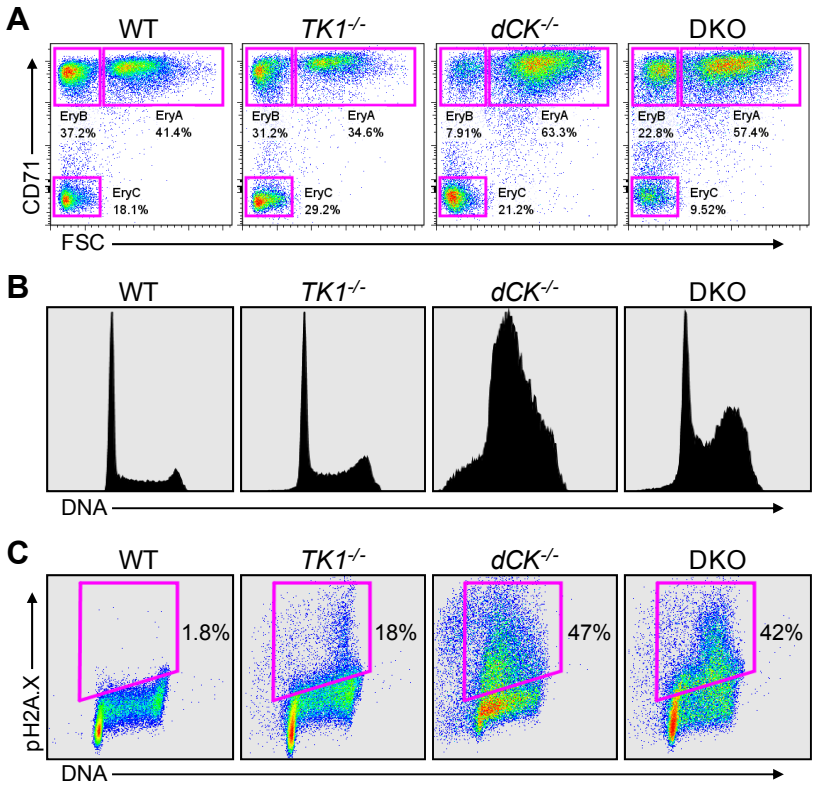


Figure 4.11. TK1 inactivation relieves the early S-phase arrest observed in erythroid precursors from *dCK*$^{-/-}$ mice. (**A**) CD71 and forward scatter (FSC) profiles of Ter119^{+} cells from whole bone marrow to identify EryA, EryB, and EryC populations from WT, *TK1*$^{-/-}$, *dCK*$^{-/-}$, and DKO mice. (**B-C**) Total DNA content (**B**), and pH2A.X detection (**C**), in bone marrow EryA cells from WT, *TK1*$^{-/-}$, *dCK*$^{-/-}$, and DKO mice.

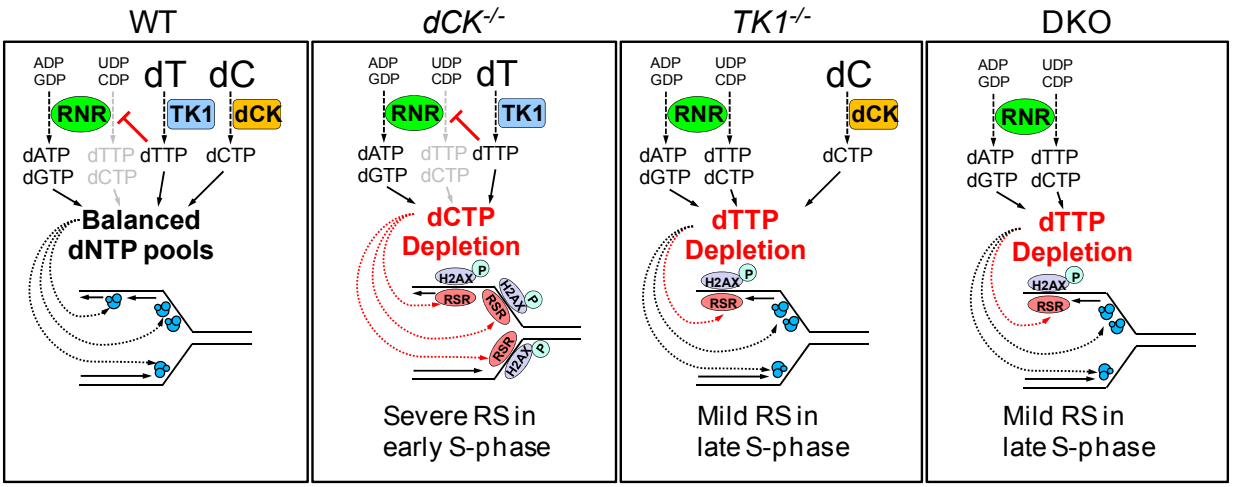


Figure 4.12. Deoxyribonucleoside salvage kinases induce and resolve replication stress (RS) during hematopoiesis. Model depicting how the *de novo* and salvage pathways interact to maintain dNTP pools and to prevent nucleotide deficiency and endogenous replication stress in rapidly dividing hematopoietic progenitors. Under normal conditions (WT panel), the ribonucleotide reductase (RNR) complex reduces purine ribonucleotide diphosphates (ADP, GDP) and pyrimidine ribonucleotide diphosphates (CDP, UDP) to contribute to dNTP pools (dATP, dGTP, dTTP, dCTP). While RNR appears to be solely responsible for producing the purine dNTP pools, the majority of dTTP pools are produced from salvaged thymidine, which is present in abundant amounts in thymus and bone marrow. The inability of hematopoietic cells to control the size of dTTP pools generated by the TK1 branch of the salvage pathway leads to a situation in which elevated dTTP levels prevent RNR from reducing CDP to dCDP via allosteric inhibition. To maintain the size of the dCTP pool, rapidly dividing hematopoietic cells must rely on the dCK branch of the salvage pathway. In the absence of dCK activity (*dCK*$^{-/-}$ panel), dCTP pools become insufficient, leading to DNA synthesis arrest in early S-phase, coupled with severe RS and strong activation of the

replication stress response (RSR) pathway. In the absence of TK1 activity (*TK1*$^{-/-}$ panel), dTTP pools are depleted, but residual levels of this nucleotide appear to be sufficient for maintaining DNA replication. Thus, only minor DNA synthesis defects occur and these selectively affect erythroid precursors, which display mild RS in late S-phase. In the absence of both dCK and TK1 (DKO panel), dTTP pools are depleted due to the inability to salvage thymidine. dTTP pool depletion is well tolerated by T and B lymphoid precursors but causes late S-phase RS in erythroid precursors. Importantly, residual dTTP pools in DKO cells are below the levels required to allosterically inhibit CDP and UDP reduction by RNR. RNR is therefore capable of maintaining dCTP pools in the absence of dCK. Switching both dCTP and dTTP production from the salvage pathway to the *de novo* pathway, enables quasi-normal hematopoietic development in the DKO mice. Solid arrows indicate single step processes; dashed arrows indicate multi-step processes with intermediates not named/depicted in the schematic.

References

1. Halazonetis, T.D., V.G. Gorgoulis, and J. Bartek. 2008. An oncogene-induced DNA damage model for cancer development. *Science (New York, N.Y* 319:1352-1355.

2. Toledo, L.I., M. Murga, and O. Fernandez-Capetillo. 2011. Targeting ATR and Chk1 kinases for cancer treatment: a new model for new (and old) drugs. *Molecular oncology* 5:368-373.

3. Bartkova, J., Z. Horejsi, K. Koed, A. Kramer, F. Tort, K. Zieger, P. Guldberg, M. Sehested, J.M. Nesland, C. Lukas, T. Orntoft, J. Lukas, and J. Bartek. 2005. DNA damage response as a candidate anti-cancer barrier in early human tumorigenesis. *Nature* 434:864-870.

4. Bester, A.C., M. Roniger, Y.S. Oren, M.M. Im, D. Sarni, M. Chaoat, A. Bensimon, G. Zamir, D.S. Shewach, and B. Kerem. 2011. Nucleotide deficiency promotes genomic instability in early stages of cancer development. *Cell* 145:435-446.

5. Davidson, M.B., Y. Katou, A. Keszthelyi, T.L. Sing, T. Xia, J. Ou, J.A. Vaisica, N. Thevakumaran, L. Marjavaara, C.L. Myers, A. Chabes, K. Shirahige, and G.W. Brown. 2012. Endogenous DNA replication stress results in expansion of dNTP pools and a mutator phenotype. *The EMBO journal* 31:895-907.

6. Poli, J., O. Tsaponina, L. Crabbe, A. Keszthelyi, V. Pantesco, A. Chabes, A. Lengronne, and P. Pasero. 2012. dNTP pools determine fork progression and origin usage under replication stress. *The EMBO journal* 31:883-894.

7. Denko, N.C., A.J. Giaccia, J.R. Stringer, and P.J. Stambrook. 1994. The human Ha-ras oncogene induces genomic instability in murine fibroblasts within one cell cycle. *Proceedings of the National Academy of Sciences of the United States of America* 91:5124-5128.

8. Bartkova, J., N. Rezaei, M. Liontos, P. Karakaidos, D. Kletsas, N. Issaeva, L.V. Vassiliou, E. Kolettas, K. Niforou, V.C. Zoumpourlis, M. Takaoka, H. Nakagawa, F. Tort, K. Fugger, F. Johansson, M. Sehested, C.L. Andersen, L. Dyrskjot, T. Orntoft, J. Lukas, C. Kittas, T. Helleday, T.D. Halazonetis, J. Bartek, and V.G. Gorgoulis. 2006. Oncogene-induced senescence is part of the tumorigenesis barrier imposed by DNA damage checkpoints. *Nature* 444:633-637.

9. Di Micco, R., M. Fumagalli, and F. d'Adda di Fagagna. 2007. Breaking news: high-speed race ends in arrest--how oncogenes induce senescence. *Trends in cell biology* 17:529-536.

10. Arlt, M.F., A.C. Ozdemir, S.R. Birkeland, T.E. Wilson, and T.W. Glover. 2011. Hydroxyurea induces de novo copy number variants in human cells. *Proceedings of the National Academy of Sciences of the United States of America* 108:17360-17365.

11. Gagou, M.E., P. Zuazua-Villar, and M. Meuth. 2010. Enhanced H2AX phosphorylation, DNA replication fork arrest, and cell death in the absence of Chk1. *Molecular biology of the cell* 21:739-752.

12. Reichard, P. 1988. Interactions between deoxyribonucleotide and DNA synthesis. *Annual review of biochemistry* 57:349-374.

13. Evans, D.R., and H.I. Guy. 2004. Mammalian pyrimidine biosynthesis: fresh insights into an ancient pathway. *The Journal of biological chemistry* 279:33035-33038.

14. Fairman, J.W., S.R. Wijerathna, M.F. Ahmad, H. Xu, R. Nakano, S. Jha, J. Prendergast, R.M. Welin, S. Flodin, A. Roos, P. Nordlund, Z. Li, T. Walz, and C.G. Dealwis. 2011. Structural basis for allosteric regulation of human ribonucleotide reductase by nucleotide-induced oligomerization. *Nature structural & molecular biology* 18:316-322.

15. Arner, E.S., and S. Eriksson. 1995. Mammalian deoxyribonucleoside kinases. *Pharmacology & therapeutics* 67:155-186.

16. Sabini, E., S. Hazra, S. Ort, M. Konrad, and A. Lavie. 2008. Structural basis for substrate promiscuity of dCK. *Journal of molecular biology* 378:607-621.

17. Bianchi, V., E. Pontis, and P. Reichard. 1986. Changes of deoxyribonucleoside triphosphate pools induced by hydroxyurea and their relation to DNA synthesis. *The Journal of biological chemistry* 261:16037-16042.

18. Van Triest, B., H.M. Pinedo, G. Giaccone, and G.J. Peters. 2000. Downstream molecular determinants of response to 5-fluorouracil and antifolate thymidylate synthase inhibitors. *Ann Oncol* 11:385-391.

19. Rodriguez, R., and M. Meuth. 2006. Chk1 and p21 cooperate to prevent apoptosis during DNA replication fork stress. *Molecular biology of the cell* 17:402-412.

20. Bolderson, E., J. Scorah, T. Helleday, C. Smythe, and M. Meuth. 2004. ATM is required for the cellular response to thymidine induced replication fork stress. *Human molecular genetics* 13:2937-2945.

21. Larsson, K.M., A. Jordan, R. Eliasson, P. Reichard, D.T. Logan, and P. Nordlund. 2004. Structural mechanism of allosteric substrate specificity regulation in a ribonucleotide reductase. *Nature structural & molecular biology* 11:1142-1149.

22. Bjursell, G., and P. Reichard. 1973. Effects of thymidine on deoxyribonucleoside triphosphate pools and deoxyribonucleic acid synthesis in Chinese hamster ovary cells. *The Journal of biological chemistry* 248:3904-3909.

23. Xeros, N. 1962. Deoxyriboside control and synchronization of mitosis. *Nature* 194:682-683.

24. Traut, T.W. 1994. Physiological concentrations of purines and pyrimidines. *Molecular and cellular biochemistry* 140:1-22.

25. Matsuoka, S., B.A. Ballif, A. Smogorzewska, E.R. McDonald, 3rd, K.E. Hurov, J. Luo, C.E. Bakalarski, Z. Zhao, N. Solimini, Y. Lerenthal, Y. Shiloh, S.P. Gygi, and S.J. Elledge. 2007. ATM and ATR substrate analysis reveals extensive protein networks responsive to DNA damage. *Science (New York, N.Y* 316:1160-1166.

26. Dobrovolsky, V.N., T. Bucci, R.H. Heflich, J. Desjardins, and F.C. Richardson. 2003. Mice deficient for cytosolic thymidine kinase gene develop fatal kidney disease. *Molecular genetics and metabolism* 78:1-10.

27. Taghon, T.N., E.S. David, J.C. Zuniga-Pflucker, and E.V. Rothenberg. 2005. Delayed, asynchronous, and reversible T-lineage specification induced by Notch/Delta signaling. *Genes & development* 19:965-978.

28. Quah, B.J., and C.R. Parish. 2012. New and improved methods for measuring lymphocyte proliferation in vitro and in vivo using CFSE-like fluorescent dyes. *Journal of immunological methods* 379:1-14.

29. Paris, L., E. Cordelli, P. Eleuteri, M.G. Grollino, E. Pasquali, R. Ranaldi, R. Meschini, and F. Pacchierotti. 2011. Kinetics of gamma-H2AX induction and removal in bone marrow and testicular cells of mice after X-ray irradiation. *Mutagenesis* 26:563-572.

30. Kajstura, M., H.D. Halicka, J. Pryjma, and Z. Darzynkiewicz. 2007. Discontinuous fragmentation of nuclear DNA during apoptosis revealed by discrete "sub-G1" peaks on DNA content histograms. *Cytometry A* 71:125-131.

31. Dobrovolsky, V.N., L.J. McGarrity, L.S. VonTungeln, R.A. Mittelstaedt, S.M. Morris, F.A. Beland, and R.H. Heflich. 2005. Micronucleated erythrocyte

frequency in control and azidothymidine-treated Tk+/+, Tk+/- and Tk-/- mice. *Mutation research* 570:227-235.

32. Coquelle, A., S. Mouhamad, M.O. Pequignot, T. Braun, G. Carvalho, S. Vivet, D. Metivier, M. Castedo, and G. Kroemer. 2006. Enrichment of non-synchronized cells in the G1, S and G2 phases of the cell cycle for the study of apoptosis. *Biochemical pharmacology* 72:1396-1404.

33. Gentry, G.A. 1992. Viral thymidine kinases and their relatives. *Pharmacology & therapeutics* 54:319-355.

34. Rylova, S.N., S. Mirzaee, F. Albertioni, and S. Eriksson. 2007. Expression of deoxynucleoside kinases and 5'-nucleotidases in mouse tissues: implications for mitochondrial toxicity. *Biochemical pharmacology* 74:169-175.

35. Lunt, S.Y., and M.G. Vander Heiden. 2011. Aerobic glycolysis: meeting the metabolic requirements of cell proliferation. *Annual review of cell and developmental biology* 27:441-464.

36. Voet, D., Voet J.G. 2004. Biochemistry. J. Wiley & Sons, Hoboken, NJ.

37. Eriksson, S., and L. Wang. 2008. Molecular mechanisms of mitochondrial DNA depletion diseases caused by deficiencies in enzymes in purine and pyrimidine metabolism. *Nucleosides, nucleotides & nucleic acids* 27:800-808.

38. Gonzalez-Vioque, E., J. Torres-Torronteras, A.L. Andreu, and R. Marti. 2011. Limited dCTP availability accounts for mitochondrial DNA depletion in mitochondrial neurogastrointestinal encephalomyopathy (MNGIE). *PLoS genetics* 7:e1002035.

39. Zhou, X., M. Johansson, N. Solaroli, B. Rozell, A. Grandien, and A. Karlsson. 2010. Hematopoiesis in the thymidine kinase 2 deficient mouse model of mitochondrial DNA depletion syndrome. *Journal of inherited metabolic disease* 33:231-236.

40. Zhou, X., N. Solaroli, M. Bjerke, J.B. Stewart, B. Rozell, M. Johansson, and A. Karlsson. 2008. Progressive loss of mitochondrial DNA in thymidine kinase 2-deficient mice. *Human molecular genetics* 17:2329-2335.

41. Gandhi, V.V., and D.C. Samuels. 2011. A review comparing deoxyribonucleoside triphosphate (dNTP) concentrations in the mitochondrial and cytoplasmic compartments of normal and transformed cells. *Nucleosides, nucleotides & nucleic acids* 30:317-339.

42. Sohn, S.J., J. Thompson, and A. Winoto. 2007. Apoptosis during negative selection of autoreactive thymocytes. *Current opinion in immunology* 19:510-515.

43. Chasis, J.A., and N. Mohandas. 2008. Erythroblastic islands: niches for erythropoiesis. *Blood* 112:470-478.

44. Hsu, C.L., W. Lin, D. Seshasayee, Y.H. Chen, X. Ding, Z. Lin, E. Suto, Z. Huang, W.P. Lee, H. Park, M. Xu, M. Sun, L. Rangell, J.L. Lutman, S. Ulufatu, E. Stefanich, C. Chalouni, M. Sagolla, L. Diehl, P. Fielder, B. Dean, M. Balazs, and F. Martin. 2012. Equilibrative nucleoside transporter 3 deficiency perturbs lysosome function and macrophage homeostasis. *Science (New York, N.Y* 335:89-92.

45. Qiu, L.B., H. Dickson, N. Hajibagheri, and P.R. Crocker. 1995. Extruded erythroblast nuclei are bound and phagocytosed by a novel macrophage receptor. *Blood* 85:1630-1639.

46. Schmegner, C., H. Hameister, W. Vogel, and G. Assum. 2007. Isochores and replication time zones: a perfect match. *Cytogenetic and genome research* 116:167-172.

47. Bianchi, V., S. Borella, C. Rampazzo, P. Ferraro, F. Calderazzo, L.C. Bianchi, S. Skog, and P. Reichard. 1997. Cell cycle-dependent metabolism of pyrimidine deoxynucleoside triphosphates in CEM cells. *The Journal of biological chemistry* 272:16118-16124.

CHAPTER 5:

Conclusions

A series of classic *in vivo* nucleic acid labeling experiments performed in the 1950s using ^{15}N-labeled nucleosides revealed that ribonucleosides are incorporated into both RNA and DNA, whereas deoxyribonucleosides are used exclusively for DNA synthesis (1, 2). Besides providing the first insights into the phenomenon of ribonucleotide reduction, these studies also showed that the nucleoside salvage pathway is active *in vivo*. Following these observations, the field of nucleoside salvage metabolism became an area of intense investigation in biochemistry. However, the biological significance of rate-limiting nucleoside salvage kinases such as dCK and TK1 has remained enigmatic. In certain ways, the studies presented in this dissertation were primed by findings that resembled the initial *in vivo* labeling work of Reichard and colleagues (1). In an attempt to non-invasively image immune system activation *in vivo,* Radu and colleagues injected mice with a deoxycytidine analog labeled with a positron emitter (^{18}F-FAC), and then quantified probe accumulation in tissues throughout the body using mPET/CT (3). mPET/CT imaging revealed a striking preferential accumulation of ^{18}F-FAC in thymus and bone marrow, thus prompting the development of genetic approaches to examine the role of dCK-mediated salvage metabolism in development (4).

Despite the intense biochemical characterization of nucleotide metabolism in the many decades since the identification of ribonucleotide reduction in mammals, there remain significant uncertainties as to how dNTPs are synthesized *in vivo* to support cellular proliferation. For example, recent publications either focus exclusively on the *de novo* pathway as the main mechanism to produce dNTPs (5), or suggest that hematopoietic cells lack *de novo* synthesis and thus must derive all their dNTPs from

salvage synthesis (6). These points of view appear to overemphasize the role of one biosynthetic pathway at the expense of the other. In contrast, the genetic and biochemical studies presented in this dissertation demonstrate that, *in vivo,* the *de novo* and salvage dNTP biosynthetic pathways are in fact inextricably linked through shared intermediates, products, and allosteric control mechanisms. Moreover, in response to certain stimuli or to changes in their environmental conditions, hematopoietic cells may have the ability to modulate their dNTP production between the two biosynthetic pathways. Therefore, we recommend that the *de novo* synthesis and the dN salvage pathways should be studied together rather than individually.

The findings presented in this dissertation also provide strong experimental evidence that dN salvage kinases significantly regulate RS dynamics during hematopoiesis. The model of nucleotide metabolism regulation *in vivo* emerging from our studies suggests that a complex functional interplay between salvage and *de novo* dNTP synthesis is required to prevent RS and endogenous DNA damage during hematopoiesis. Furthermore, the demonstration of a functional link between endogenous thymidine, dN kinases, nucleotide deficiency, and RS induction highlights a potential therapeutic strategy to induce RS overload, and ultimately cell death, in hyperproliferative diseases such as cancer.

Thymidine therapy has been attempted to treat tumor models in mice (7), and in leukemias and lymphomas in humans (8, 9), based on the ability of this nucleoside to induce S-phase arrest in cultured cancer cells by inhibiting their *de novo* dCTP synthesis (10, 11). Although well tolerated in patients, thymidine had limited efficacy when used as single agent therapy (8, 9). By demonstrating that dCK—which is

frequently overexpressed in hematological malignancies (12)—significantly contributes to dCTP pools *in vivo*, the results presented this dissertation may have revealed an important mechanism of resistance to thymidine and thus explain the failure of thymidine in initial clinical trials. We hypothesize that improving the therapeutic efficacy of thymidine in cancer will also require pharmacological inhibition of dCK activity to prevent dCK-mediated rescue of *in vivo* thymidine block. Whether an adequate therapeutic window exists for a combination therapy consisting of thymidine and a small molecule dCK inhibitor must be determined in future studies.

Many questions still remain regarding the role of dN salvage kinases in supporting dNTP pools in mature lymphocytes and in malignant hyperproliferative tissues. While we have demonstrated that dCK and TK1 make significant contributions to dNTP pools during hematopoietic development, it still remains unknown what contributions—if any—that dCK and TK1 make to dNTP pools in activated lymphocytes that are proliferating in secondary lymphoid organs. Future studies to determine the degree of immunocompetence of *dCK*$^{-/-}$ and *TK1*$^{-/-}$ mice through the use of lymphocyte-mediated models of viral infection rejection (13), autoimmune disorder induction (14), and tumor cell rejection (15), would be critical to answer these important immunological questions. Questions regarding the role of dCK and TK1 in supporting oncogenic disease initiation and progression could similarly be interrogated using genetic mouse models of inducible cancer (16-18). Following these avenues of research could potentially positively impact human health by generating important insights into how the fundamental processes of dNTP biosynthesis affect functional immunity and oncogenic transformation.

References

1. Reichard, P., and B. Estborn. 1951. Utilization of desoxyribosides in the synthesis of polynucleotides. *The Journal of biological chemistry* 188:839-846.

2. Hammarsten, E., Reichard, P. and Saluste, E. 1950. Pyrimidine nucleosides as precursors of pyrimidines in polynucleotides. *Journal of Biological Chemistry* 183:

3. Radu, C.G., C.J. Shu, E. Nair-Gill, S.M. Shelly, J.R. Barrio, N. Satyamurthy, M.E. Phelps, and O.N. Witte. 2008. Molecular imaging of lymphoid organs and immune activation by positron emission tomography with a new [18F]-labeled 2'-deoxycytidine analog. *Nature medicine* 14:783-788.

4. Toy, G., W.R. Austin, H.I. Liao, D. Cheng, A. Singh, D.O. Campbell, T.O. Ishikawa, L.W. Lehmann, N. Satyamurthy, M.E. Phelps, H.R. Herschman, J. Czernin, O.N. Witte, and C.G. Radu. 2010. Requirement for deoxycytidine kinase in T and B lymphocyte development. *Proceedings of the National Academy of Sciences of the United States of America* 107:5551-5556.

5. Lunt, S.Y., and M.G. Vander Heiden. 2011. Aerobic glycolysis: meeting the metabolic requirements of cell proliferation. *Annual review of cell and developmental biology* 27:441-464.

6. Hsu, C.L., W. Lin, D. Seshasayee, Y.H. Chen, X. Ding, Z. Lin, E. Suto, Z. Huang, W.P. Lee, H. Park, M. Xu, M. Sun, L. Rangell, J.L. Lutman, S. Ulufatu, E. Stefanich, C. Chalouni, M. Sagolla, L. Diehl, P. Fielder, B. Dean, M. Balazs, and F. Martin. 2012. Equilibrative nucleoside transporter 3 deficiency perturbs lysosome function and macrophage homeostasis. *Science (New York, N.Y* 335:89-92.

7. Lockshin, A., B.C. Giovanella, J.S. Stehlin, Jr., T. Kozielski, C. Quian, and R.W. Apperson. 1985. Antitumor activity and minimal toxicity of concentrated thymidine infused in nude mice. *Cancer research* 45:1797-1802.

8. Blumenreich, M.S., T.M. Woodcock, M. Andreeff, W. Hiddemann, T.C. Chou, K. Vale, M. O'Hehir, B.D. Clarkson, and C.W. Young. 1984. Effect of very high-dose thymidine infusions on leukemia and lymphoma patients. *Cancer research* 44:2203-2207.

9. Kufe, D.W., P. Beardsley, D. Karp, L. Parker, A. Rosowsky, G. Canellos, and E. Frei, 3rd. 1980. High-dose thymidine infusions in patients with leukemia and lymphoma. *Blood* 55:580-589.

10. Xeros, N. 1962. Deoxyriboside control and synchronization of mitosis. *Nature* 194:682-683.

11. Bjursell, G., and P. Reichard. 1973. Effects of thymidine on deoxyribonucleoside triphosphate pools and deoxyribonucleic acid synthesis in Chinese hamster ovary cells. *The Journal of biological chemistry* 248:3904-3909.

12. Hubeek, I., G.J. Peters, A.J. Broekhuizen, I. Talianidis, J. Sigmond, B.E. Gibson, U. Creutzig, G. Giaccone, and G.J. Kaspers. 2005. Immunocytochemical detection of deoxycytidine kinase in haematological malignancies and solid tumours. *Journal of clinical pathology* 58:695-699.

13. Schepers, K., M. Toebes, G. Sotthewes, F.A. Vyth-Dreese, T.A. Dellemijn, C.J. Melief, F. Ossendorp, and T.N. Schumacher. 2002. Differential kinetics of antigen-specific CD4+ and CD8+ T cell responses in the regression of retrovirus-induced sarcomas. *J Immunol* 169:3191-3199.

14. Gold, R., C. Linington, and H. Lassmann. 2006. Understanding pathogenesis and therapy of multiple sclerosis via animal models: 70 years of merits and culprits in experimental autoimmune encephalomyelitis research. *Brain* 129:1953-1971.

15. Overwijk, W.W., A. Tsung, K.R. Irvine, M.R. Parkhurst, T.J. Goletz, K. Tsung, M.W. Carroll, C. Liu, B. Moss, S.A. Rosenberg, and N.P. Restifo. 1998. gp100/pmel 17 is a murine tumor rejection antigen: induction of "self"-reactive, tumoricidal T cells using high-affinity, altered peptide ligand. *The Journal of experimental medicine* 188:277-286.

16. Tuveson, D.A., A.T. Shaw, N.A. Willis, D.P. Silver, E.L. Jackson, S. Chang, K.L. Mercer, R. Grochow, H. Hock, D. Crowley, S.R. Hingorani, T. Zaks, C. King, M.A. Jacobetz, L. Wang, R.T. Bronson, S.H. Orkin, R.A. DePinho, and T. Jacks. 2004. Endogenous oncogenic K-ras(G12D) stimulates proliferation and widespread neoplastic and developmental defects. *Cancer cell* 5:375-387.

17. Caulin, C., T. Nguyen, G.A. Lang, T.M. Goepfert, B.R. Brinkley, W.W. Cai, G. Lozano, and D.R. Roop. 2007. An inducible mouse model for skin cancer reveals distinct roles for gain- and loss-of-function p53 mutations. *The Journal of clinical investigation* 117:1893-1901.

18. van Miltenburg, M.H., and J. Jonkers. 2012. Using genetically engineered mouse models to validate candidate cancer genes and test new therapeutic approaches. *Current opinion in genetics & development* 22:21-27.